Strength and Ductility of Slitted

Reinforced Concrete Masonry Shear Wall

BY

Louis Lee Yaw

B.S.E. Civil (Walla Walla College, 1992)

THESIS

Submitted in partial satisfaction of the requirements for the degree of

MASTER OF SCIENCE

in

Engineering

in the

OFFICE OF GRADUATE STUDIES

of the

UNIVERSITY OF CALIFORNIA

DAVIS

Approved:

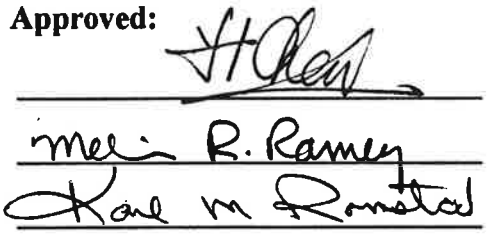

Committee in Charge

1996

Louis Lee Yaw

September 1996

M.S. Civil Engineering

Strength and Ductility of Slitted Reinforced Concrete Masonry Shear Wall

Abstract

For ductile design of perforated masonry shear walls, a large ductility demand may be imposed on the hinging regions of the wall. Previous experimental tests of masonry wall-piers have indicated that the conventional construction of these members may not provide an adequate ductility capacity in the wall to warrant the use of a large force reduction factor for design. In this thesis the technique for enhancing the in-plane lateral ductility capacity of reinforced concrete masonry walls, of low aspect ratios, by including vertical slits in the center region of the wall is investigated. The conventional construction of masonry walls using a running-bond pattern for masonry blocks is replaced by a stack-bonded layout in the middle of the wall where vertical separation joints are incorporated. The horizontal reinforcement is discontinued across the separations joints. Two fully grouted reinforced concrete masonry wall-piers (64" x 64"), one of conventional monolithic construction and the other of slitted construction, were tested under combined axial compression and in-plane large-amplitude reversed cyclic loading. Compared to the monolithic wall, the response of the slitted wall was characterized by a reduced lateral stiffness and strength as well as an increase in the ultimate drift capacity. The increase in ductility capacity of the slitted masonry wall, however, is smaller than the increase in ductility capacity of slitted reinforced concrete infill panels used for the stiffening of steel frame buildings in Japan. Test results presented in this thesis include the lateral force versus lateral drift response of the walls, as well as reinforcement strain distributions in the walls.

Acknowledgments

The study described in this paper was partially supported by the Concrete Masonry Association of California and Nevada. The assistance provided by Mr. Stuart Beavers is gratefully acknowledged. Masonry blocks for the project were provided by Basalite of Dixon, California, and the construction for one of the specimens was made by Townsend & Schmidt Masonry of Sacramento, California. My advisor, Professor Rob Chai, was very helpful during the construction and testing of the specimens in the laboratory. Without his help none of this would have been made possible and for this many thanks are in order. Much appreciation is due to my boss David A. Crane who has been very understanding and willing to lend advice during this process of my education. A great debt is also owed to my parents for their constant support and encouragement during this endeavor. Last, I express my thanks to God through which all things are possible.

LLY, 1996

Table of Contents

Chapter 1

INTRODUCTION

1.1 Previous Research

Extensive research has been conducted to establish the seismic characteristics of reinforced concrete masonry walls [2,3,4,7,8,9,10,11]. One major study tested masonry shear panels with aspect ratios of one and two [2,4]. These panels were subjected to a combination of in-plane reversed cyclic lateral load and in-plane axial compression. Test variables included horizontal and vertical steel ratios, types of block used, fully or partially grouted block, and axial load levels. The influence of these variables on the panel ultimate strength, stiffness degradation, energy dissipation, and ductility capacity has been reported [2,4].

Another study conducted under the TCCMAR program tested twenty 6'x6' reinforced masonry wall panels. In addition to reversed cyclic lateral load tests, a number of the wall panels were subjected to monotonic lateral loads [10,11]. Testing has indicated that masonry walls of low aspect ratios may exhibit three modes of failure depending on the amount of longitudinal and vertical reinforcement: (i) a ductile flexural failure involving yielding of vertical reinforcement, (ii) a brittle shear failure dominated by major diagonal tensile cracking, and (iii) an intermediate flexural/shear failure where limited yielding of the vertical steel and extensive diagonal tensile cracking occurs. Unless large amounts of horizontal steel are used, the wall response tends to be governed by a shear failure having relatively low ductility.

It was also found that the shear strength equation in the Uniform Building Code was conservative [12]. A more accurate method of determining shear strength which takes into account the effect of axial load has been proposed [11]. Although the flexural strength of the panel increases with axial force, the ductility capacity of the wall decreases

and brittle shear failure may occur in cases of high axial force with limited ductility.

The current approach to seismic design of structures is based on ductility (i.e. the ability of the structure to dissipate seismic energy). Ductility in masonry walls may be provided by promoting yielding of the vertical steel through the capacity design approach. This design approach ensures that a brittle failure due to shear, bond, or anchorage mechanisms will not occur [1,3].

In this report a method for enhancing the ductility of masonry shear panels, using slitted shear panels, is investigated. The basis of the new method and the experimental results are presented. Following a theoretical assessment of ductility demand on hinging shear panels, the proposed method of increasing ductility in masonry shear panels is presented.

1.2 Seismic Design of Building Structures

For a building structure to survive an earthquake an appropriate design methodology must be chosen. Although, the lateral force resisting elements of a building structure could be designed to stay within the elastic range for a given design earthquake so that no structural damage or permanent structural deformations occur, the elastic approach may not be economically feasible. Consequently, building structures are allowed by building codes to respond inelastically and sustain damage during the design level seismic event. The cyclic inelastic deformations of the building structure also involve dissipation of the earthquake ground motion energy. Buildings designed with adequate ductility and energy dissipation capacity are capable of surviving intense ground motion associated with major earthquakes. To this end, dependable assessment of the ductility capacity of critical members in a structural system is important. For structural systems with large ductility capacity, the corresponding design shear force may be accordingly reduced resulting in a more economical design [3,7].

The walls of low and medium story buildings are often used as the lateral resisting elements of a structural system. These walls can be used quite effectively in this capacity

if detailed correctly. However, walls are commonly interrupted by intermittent window or door openings as shown in Figure 1.1. The piers adjacent to these openings can be subjected to a combination of high axial, shear, and bending forces during an earthquake. Since the buildings are designed to withstand an earthquake force less than that required for an elastic response, plastic hinges will likely form in these piers on either side of the intermittent openings. Piers in the hinging regions must be designed carefully, and a good understanding of the pier ductility capacity must be established in order to benefit the entire building structure [3,7].

A careful study of potential failure mechanisms will reveal that the system ductility of a building structure is limited by the ductility of individual structural elements in the structural system. By increasing the ductility of individual piers it is possible to effectively increase a building's system ductility. This goal motivated the research presented in this report.

Consider the ductility demand on the hinging pier of a multistory masonry wall perforated by window and door openings as shown in Figure 1.1. The displacement ductility capacity of the wall is given by

$$\mu_{sys} \equiv \frac{\Delta_{ur}}{\Delta_{yr}} \tag{1.1}$$

where

Δ_{ur} = ultimate displacement at roof level

Δ_{yr} = yield displacement at roof level

Δ_p = plastic deflection of piers 1,2, and 3

μ_{sys} = system ductility

The ultimate displacement of the wall at the roof level may be written as

$$\Delta_{ur} = \Delta_{yr} + \Delta_p \tag{1.2}$$

Dividing equation (1.2) by Δ_{yr} gives

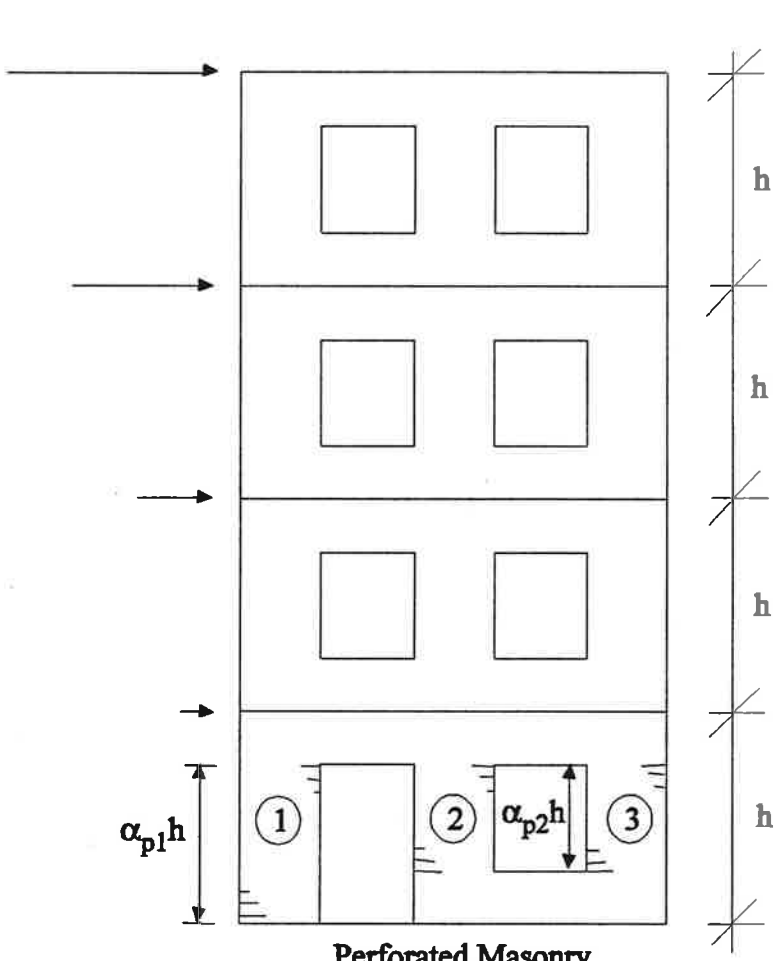

Perforated Masonry Wall With Different Size Openings In Bottom Story

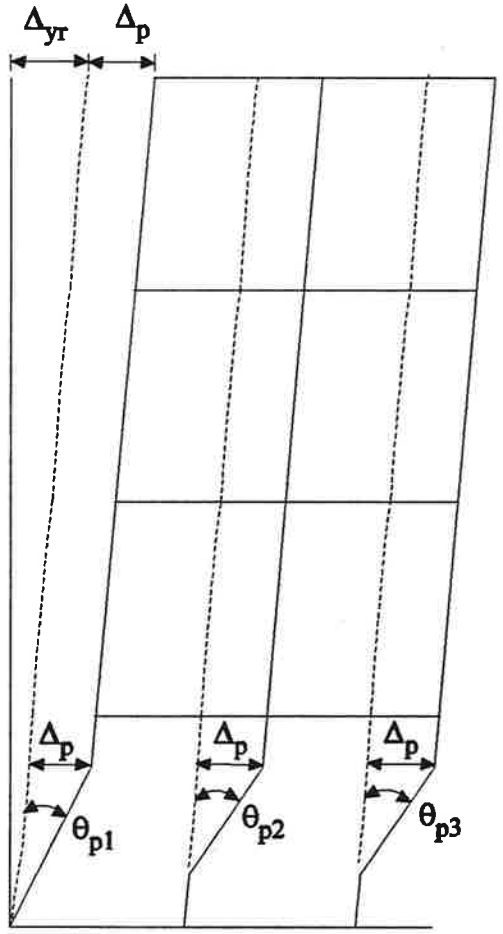

Failure Mechanism Pier Hinging In Bottom Story

Figure 1.1 Perforated Masonry Wall

$$\mu_{sys} = 1 + \frac{\Delta_p}{\Delta_{yr}} \tag{1.3}$$

Rearrangement of equation (1.4) gives,

$$\Delta_p = [\mu_{sys} - 1]\Delta_{yr} \tag{1.4}$$

Assuming the linear yield displacement profile [7] shown in Figure 1.1 yields the following equations for the yield displacements of piers 1, 2 and 3.

$$(\Delta_y)_{pier1} = \left(\frac{\Delta_{yr}}{nh}\right)\alpha_{p1}h = \left(\frac{\alpha_{p1}}{n}\right)\Delta_{yr} \tag{1.5a}$$

$$(\Delta_y)_{pier2} = (\Delta_y)_{pier3} = \left(\frac{\Delta_{yr}}{nh}\right)\alpha_{p2}h = \left(\frac{\alpha_{p2}}{n}\right)\Delta_{yr} \tag{1.5b}$$

where α_{pi} = pier height to story height ratio

Rearranging equation (1.5a),

$$\Delta_{yr} = \frac{n}{\alpha_{p1}}(\Delta_y)_{pier1} \tag{1.6}$$

and substituting equation (1.6) into equation (1.4) yields,

$$\Delta_p = [\mu_{sys} - 1]\frac{n}{\alpha_{p1}}(\Delta_y)_{pier1} \tag{1.7}$$

Hence, the plastic contribution to the ductility of pier 1.

$$\frac{\Delta_p}{(\Delta_y)_{pier1}} = [\mu_{sys} - 1]\frac{n}{\alpha_{p1}} \tag{1.8}$$

The ultimate displacement of the pier is the sum of the elasto-plastic yield displacement of the pier and the plastic displacement of the pier,

$$(\Delta_u)_{pier1} = (\Delta_y)_{pier1} + \Delta_p \tag{1.9}$$

Dividing equation 1.9 by the pier yield displacement produces the ductility demand at the pier.

$$(\mu)_{pier1} = \frac{(\Delta_u)_{pier1}}{(\Delta_y)_{pier1}} = 1 + \frac{\Delta_p}{(\Delta_y)_{pier1}} \tag{1.10}$$

Substituting equation (1.8) into equation (1.10) results in an expression for the ductility demand of pier 1.

$$(\mu)_{pier1} = 1 + [\mu_{sys} - 1]\frac{n}{\alpha_{p1}} \tag{1.11}$$

The ductility demand of piers 2 and 3 can be similarly expressed.

$$(\mu)_{pier2} = (\mu)_{pier3} = 1 + [\mu_{sys} - 1]\frac{n}{\alpha_{p2}} \tag{1.12}$$

Therefore, the individual pier ductilities are proportional to the system ductility.

$$\mu_{sys} \propto (\mu)_{pier\,n} \tag{1.13}$$

where n = 1,2,3, and vice versa.

Example

Consider a four story wall with bottom story hinging. Assume a bottom story height of 10 feet. A door results in a height of 9'-4" for pier 1, and a window causes piers 2 and 3 to be 4'-0" tall. The variables are summarized below.

$$\mu_{sys} = 1.25,\ n = 4.0,\ h = 10'$$

$$\alpha_{p1}h = 9'-4", \quad \Rightarrow \alpha_{p1} = 0.93\overline{3}$$

$$\alpha_{p2}h = 4'-0", \quad \Rightarrow \alpha_{p2} = 0.4$$

Using equation (1.11) and (1.12) with the above parameters yields

$$(\mu)_{pier1} = 1 + [1.25 - 1]\frac{4}{0.933} = \underline{\underline{2.07}}$$

$$(\mu)_{pier2} = (\mu)_{pier3} = 1 + [1.25 - 1]\frac{4}{0.4} = \underline{\underline{3.50}}$$

If the system ductility is increased to 2.0, the pier ductilities become

$$(\mu)_{pier1} = 5.29, \quad (\mu)_{pier2} = (\mu)_{pier3} = 11.0$$

Clearly an increase in system ductility requires increases in the individual pier ductility capacities. Thus it is important to investigate the means by which an increased ductility capacity of the pier may be achieved. Previous research on concrete shear panels provided insight on how one might increase the ductility of shear panels as individual structural elements [5,6].

1.3 Slitted Concrete Shear Panels

The need to limit the inter story drift of high-rise moment-resisting steel frame buildings under lateral loads often requires the addition of stiffening elements to the frame.

One approach involves the insertion of reinforced concrete infill panels into the openings of the frame at strategic locations [5]. An incompatible mode of deformations however exists between the stiff infill panels and the more flexible frame since the deformation of the infill panel is dominated primarily by shear as a result of low aspect ratio whereas the deformation of the frame is dominated by flexure. Consequently brittle shear failures may occur in the infill panels at relatively low lateral displacement prior to reaching the lateral strength of the frame. In order to overcome such difficulty, practice in Japan has incorporated vertical slits into the center region of reinforced concrete infill panels at regular spacing to reduce the stiffness of the panel and to provide a more compatible mode of deformation for the infill [5,6]. The discontinuity created by the vertical slits effectively reduces the panel into a sub assemblage of smaller and more slender piers interconnected by continuos beams at the top and bottom portion of the panel. The slits were formed by asbestos sheets or wooden planks, and the horizontal reinforcement was discontinued at the slits.

Comparative tests of monolithic reinforced concrete infill panels and slitted infill panels have indicated that, despite a reduction in lateral stiffness and strength, slitted infill panels exhibited a significant increase in the ultimate drift capacity when compared to monolithic infill panels. For monolithic panels, brittle shear failure occurred at a rather small ultimate drift ratio of about 0.005 after the formation of major diagonal cracking in the panel [5]. In contrast, however, the ductility capacity of slitted panels is improved with an ultimate drift ratio increased to a value of about 0.01 [5]. Figure 1.2 shows a typical slitted reinforced concrete infill panel. The hysteresis loops for the panels discussed above for a monolithic panel and a slitted panel are shown in Figure 1.3. The evolution of damage in slitted panels under reversed cyclic loading was characterized by the formation of well distributed flexural cracks at the ends of the smaller piers formed by the vertical slits. Although minor shear cracking was observed in the slitted regions of the panel, these cracks occurred at a later stage of loading than for flexural cracking and the

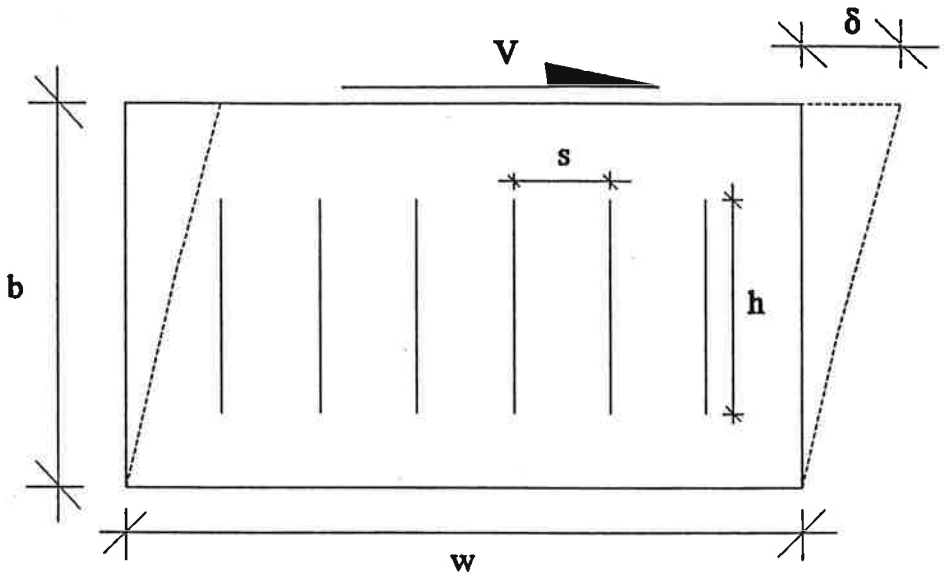

Figure 1.2 Slitted Concrete Shear Panel [5]

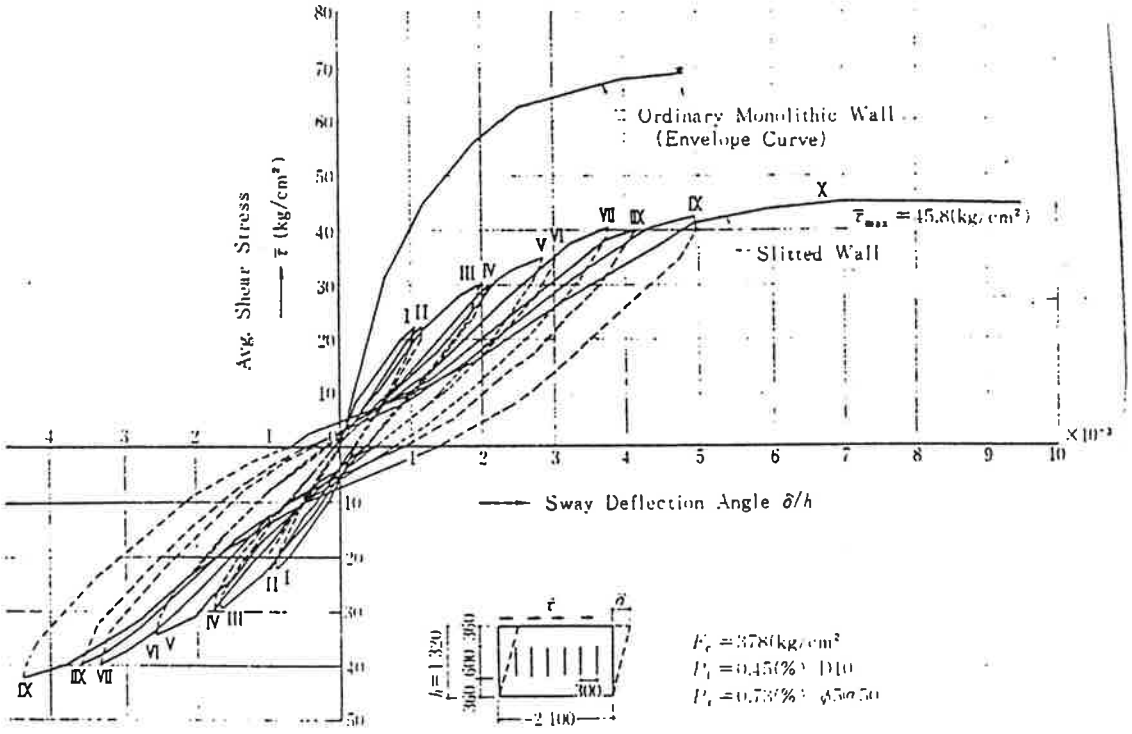

Figure 1.3 Shear Stress Versus Drift Angle For Monolithic and Slitted Concrete Shear Panels [5]

crack widths associated with shear cracking were relatively small.

1.4 Scope of Research

The improved ductility capacity of reinforced concrete infill panels by vertical slits motivated the research presented in this paper. The conventional construction of monolithic masonry piers using running-bond block layouts is replaced by stack-bonded units in the center of the pier. Soft filler material of the same thickness as the mortar joint is used to provide the separations in the pier and horizontal reinforcement is discontinued across the vertical separation joints.

Chapter 2

Reversed Cyclic Load Tests of Reinforced Concrete Masonry Wall Panels

2.1 General

A monolithic wall and a slitted wall were constructed to compare the difference in ductility between them. Figure 2.1 shows the dimensions of the monolithic and the slitted walls. The difference between the two walls is the slits and the difference in horizontal reinforcement. In the monolithic wall, horizontal reinforcement extended the full width of the wall. For the slitted wall, the reinforcement was continuous at the top two and bottom two courses of masonry blocks; however, the horizontal reinforcement was discontinued across the slits. The construction, setup, instrumentation, and loading of these test specimens is presented in the remainder of this chapter.

2.2 Test Specimens

The two walls were nominally 162.6 by 162.6 cm (64 by 64 inches) and 15.24 cm (6 inches) thick. Open end bond beam units of dimensions 15.2x20.3x40.6 cm (6x8x16 inches) were used for both walls. The half blocks used were 15.2x20.3x20.3 cm (6x8x8 inches). Walls of this thickness were chosen to limit the lateral strength of the wall to be less than the capacity of the horizontal hydraulic ram. The wall specimens were constructed by licensed masons. At each course, the horizontal reinforcing was placed as shown in Figure 2.2. Strain gage wires where necessary were routed through the mortar joints as the blocks were laid. Concave type mortar joints(type S mix) were used in both walls. For the monolithic wall, blocks were placed in a running bond pattern. For the slitted wall, the bottom two and top two courses were placed in a running bond pattern, while the middle four courses were stack bonded. The vertical separation joints were provided by polystyrene sheets reinforced with duct tape. The purpose of the polystyrene sheets, of same thickness as the mortar joints, was to maintain and fill the gap between the blocks during construction. These sheets were left in place during testing. Figure 2.1 illustrates the arrangement of the blocks for the two walls. Photos 2.1 and 2.2 illustrate

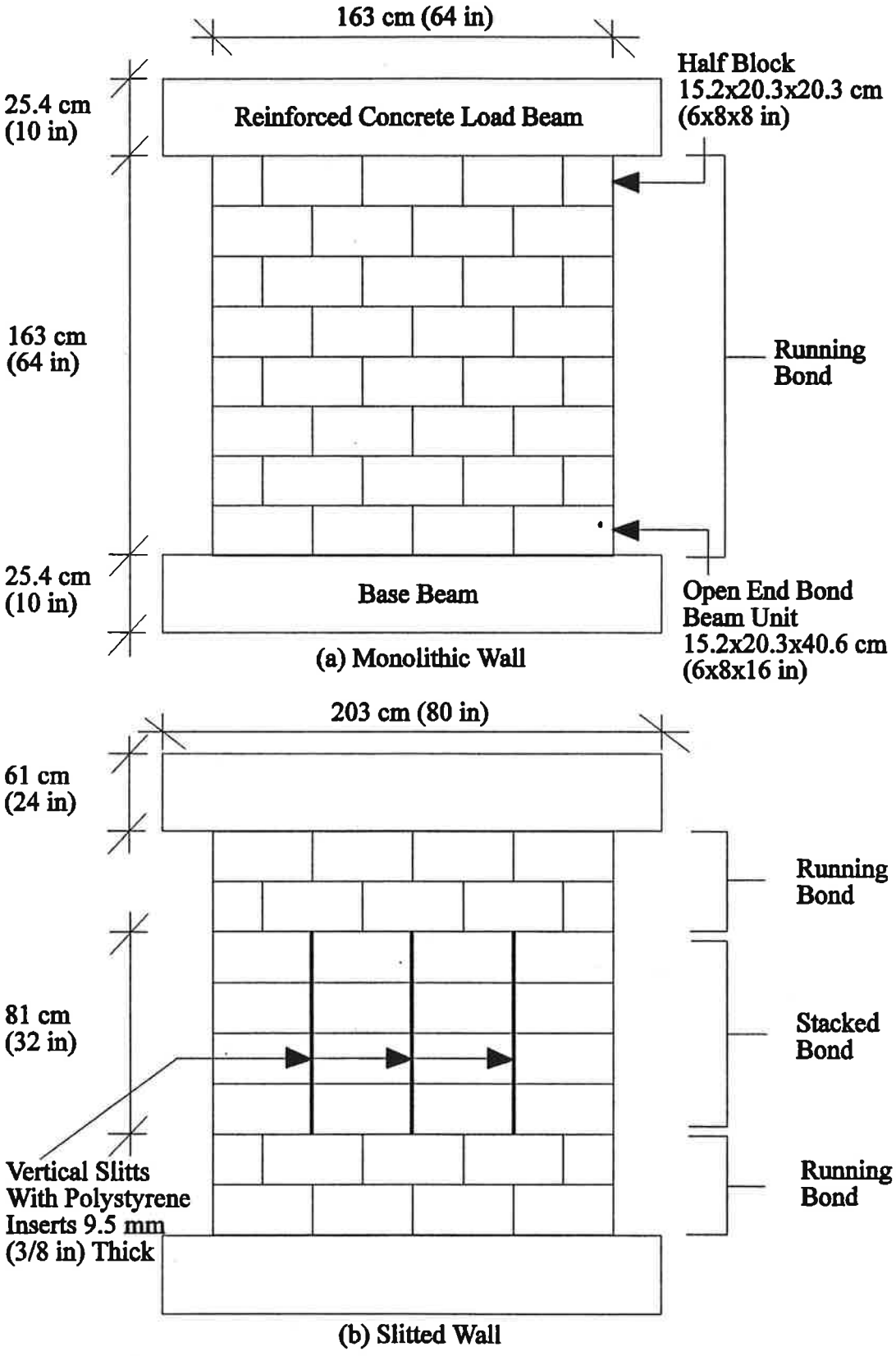

Figure 2.1 Block Stacking Patterns

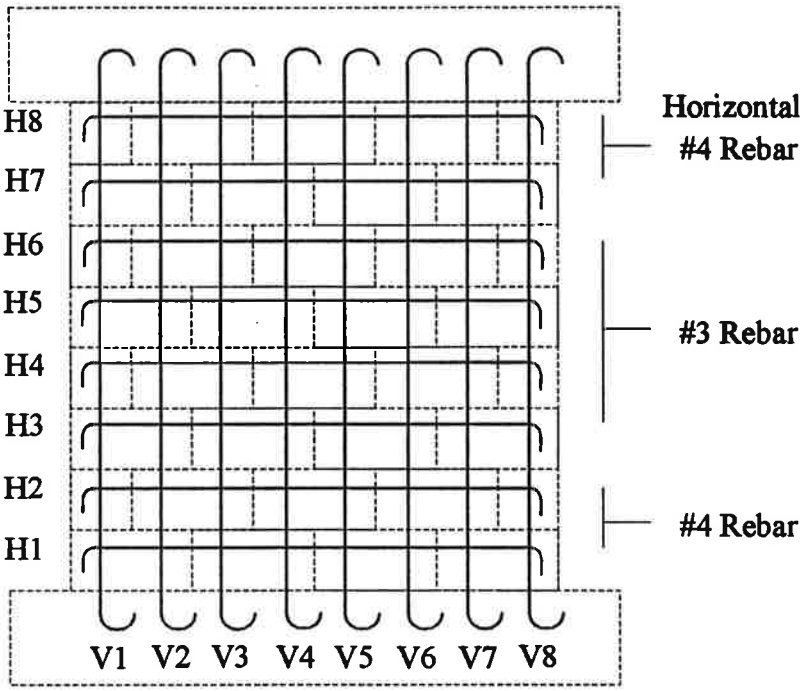

Note: All Vertical Bars Are #4

(a) Monolithic Wall

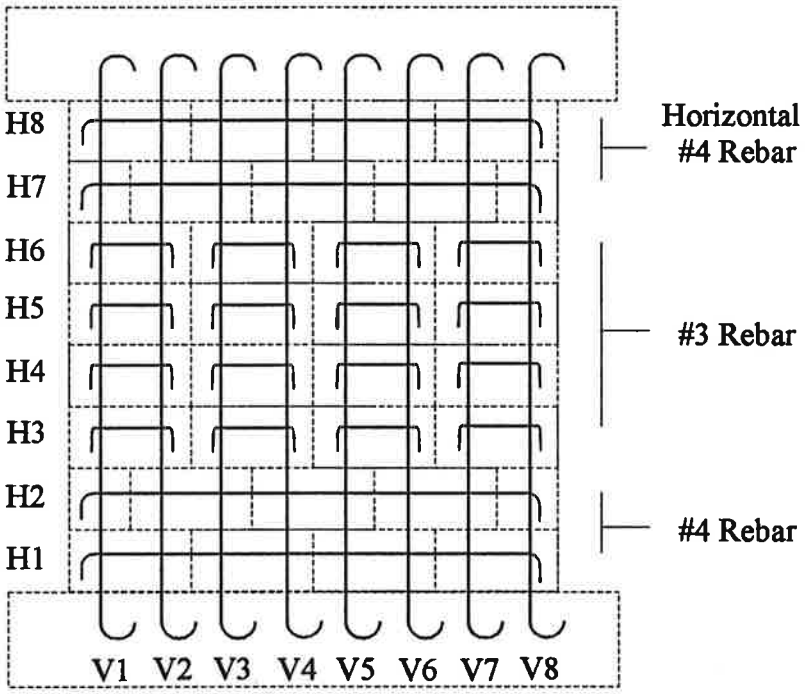

Note: All Vertical Bars Are #4

(b) Slitted Wall

Figure 2.2 Reinforcement Details

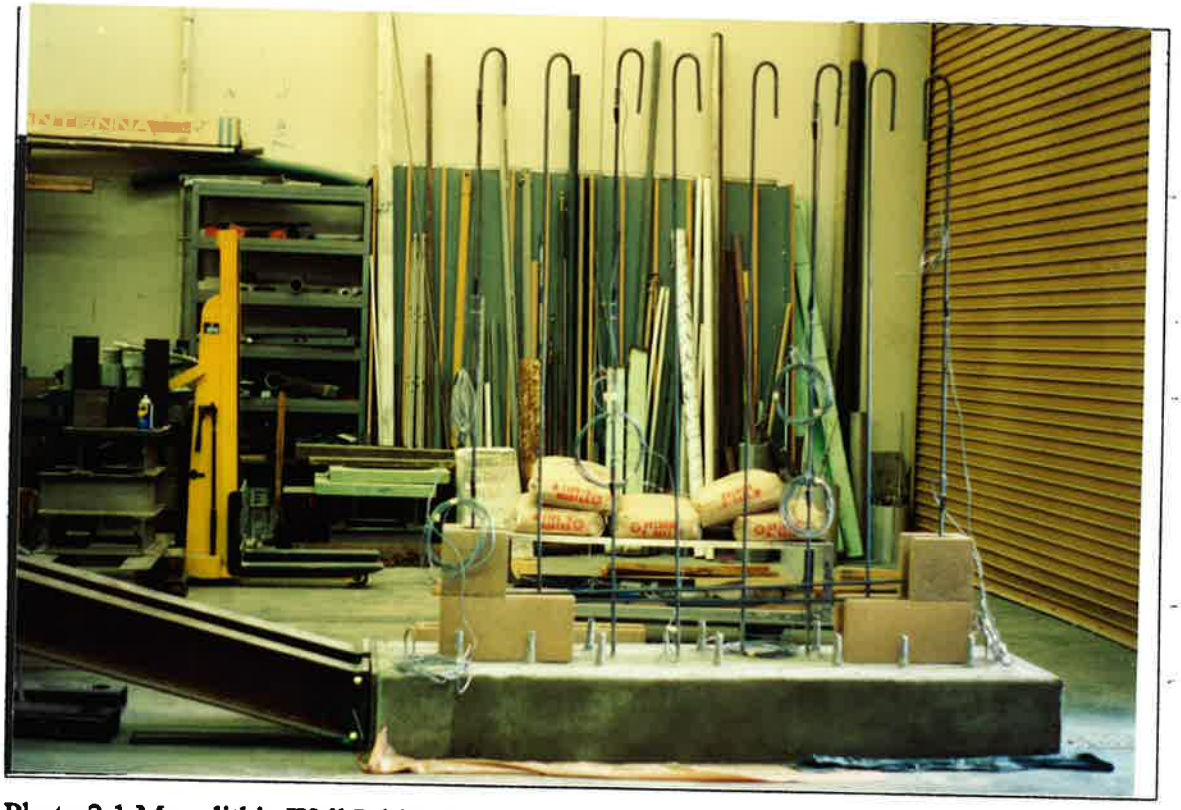

Photo 2.1 Monolithic Wall Initial Construction

Photo 2.2 Monolithic Wall At Completion of Construction

the monolithic wall at the start and at completion of construction. Photos showing the construction of the slitted wall are included in Photos 2.3,2.4,2.5, and 2.6. The polystyrene inserts for forming the slits of the wall can be seen in these photos.

The vertical reinforcement of both walls was provided by #4 bars at 8 in. spacing with a total of eight vertical bars. These vertical bars were anchored top and bottom in the concrete beams with standard 180 degree end hooks. Photo 2.1 shows the vertical bars embedded in the base beam. During construction the blocks were lowered over these bars. The extension of these hooks above the top of the constructed wall can be seen in Photo 2.5. The horizontal reinforcement was provided by #4 bars in the top two and bottom two courses of each wall. In the middle four courses #3 horizontal reinforcing bars were used. Grade 60 bars were used throughout. Figure 2.2 shows the reinforcement details for both walls.

Both specimens were fully grouted. The grout was provided by a local redi-mix company. The minimum specified design strength of the grout was 13.8 MPa (2000 psi). Pea gravel aggregate with a maximum 3/8 inch diameter was used in the grout. Due to the lack of lifting facilities, the grout was manually placed with buckets into the wall cells. The maximum drop of the grout was the height of the wall, which was 162.6 cm (64 inches). The grout was vibrated to eliminate air pockets and to ensure fully grouted walls. The grout level was finished 6.4 mm (1/4 inch) below the top of the wall to provide a shear key between the wall and cap beam.

For assessment of material strengths, four unit high masonry prisms and test cylinders of grout were prepared and subsequently tested. Two masonry prisms were prepared for each wall. Compressive strengths of grout cylinders and prisms are presented in Appendix A.

2.3 Test Setup

Figure 2.3 shows the test setup. The base of each wall was bolted to the existing rails embedded in the laboratory floor slab. Details of the anchorage of the base beam to

Photo 2.3 Initial Phases of Slitted Wall Construction

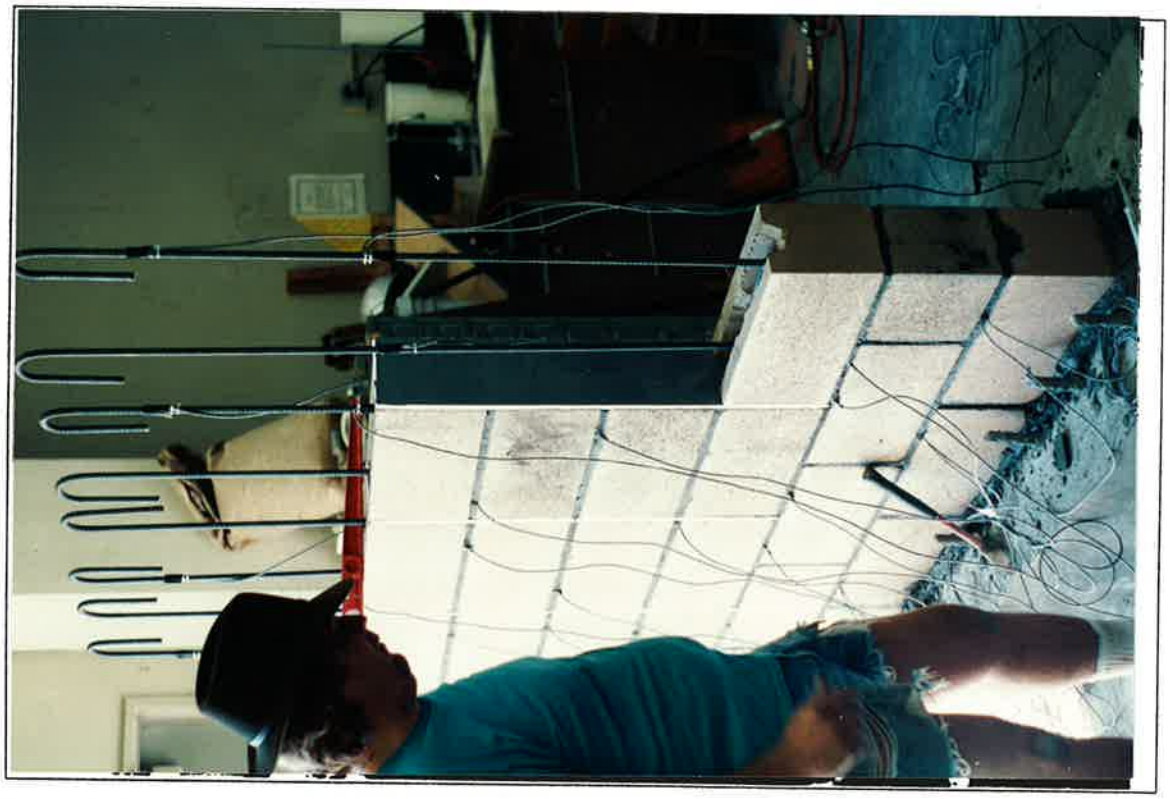

Photo 2.4 Construction of Final Pier In Slitted Portion of Wall

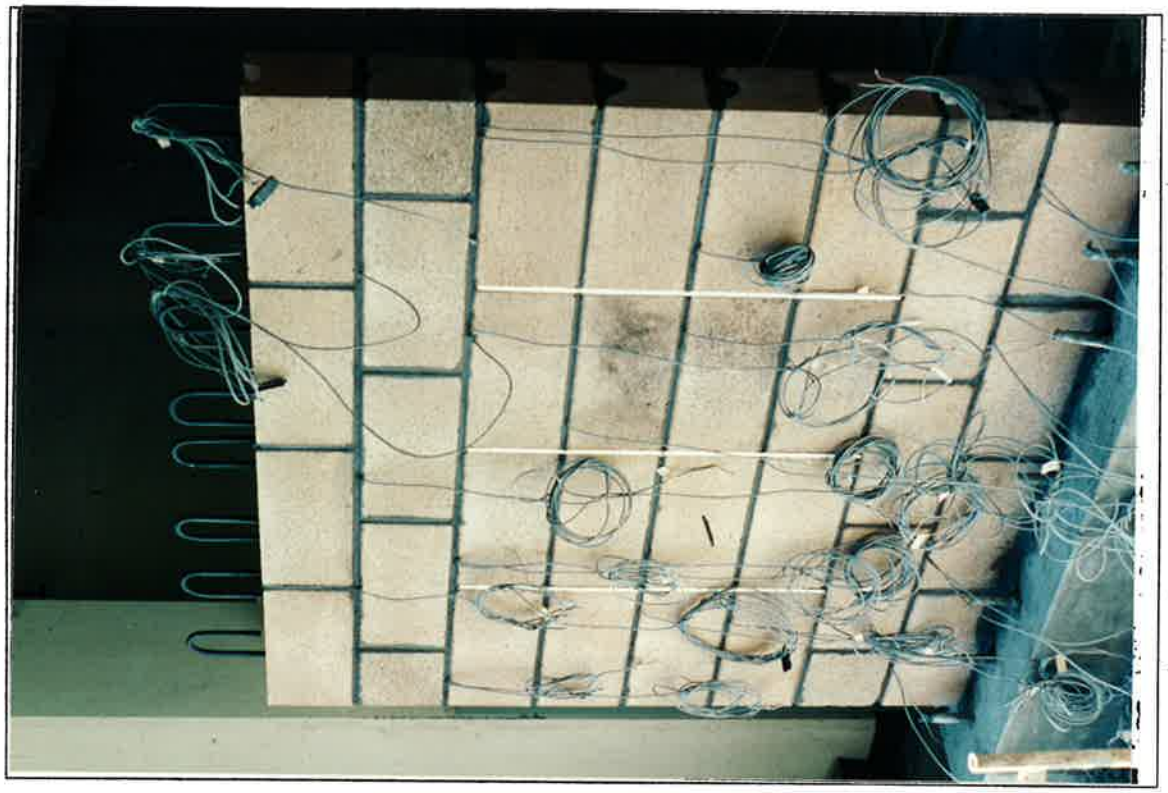

Photo 2.5 Final Stacking Arrangement of Slitted Wall Blocks

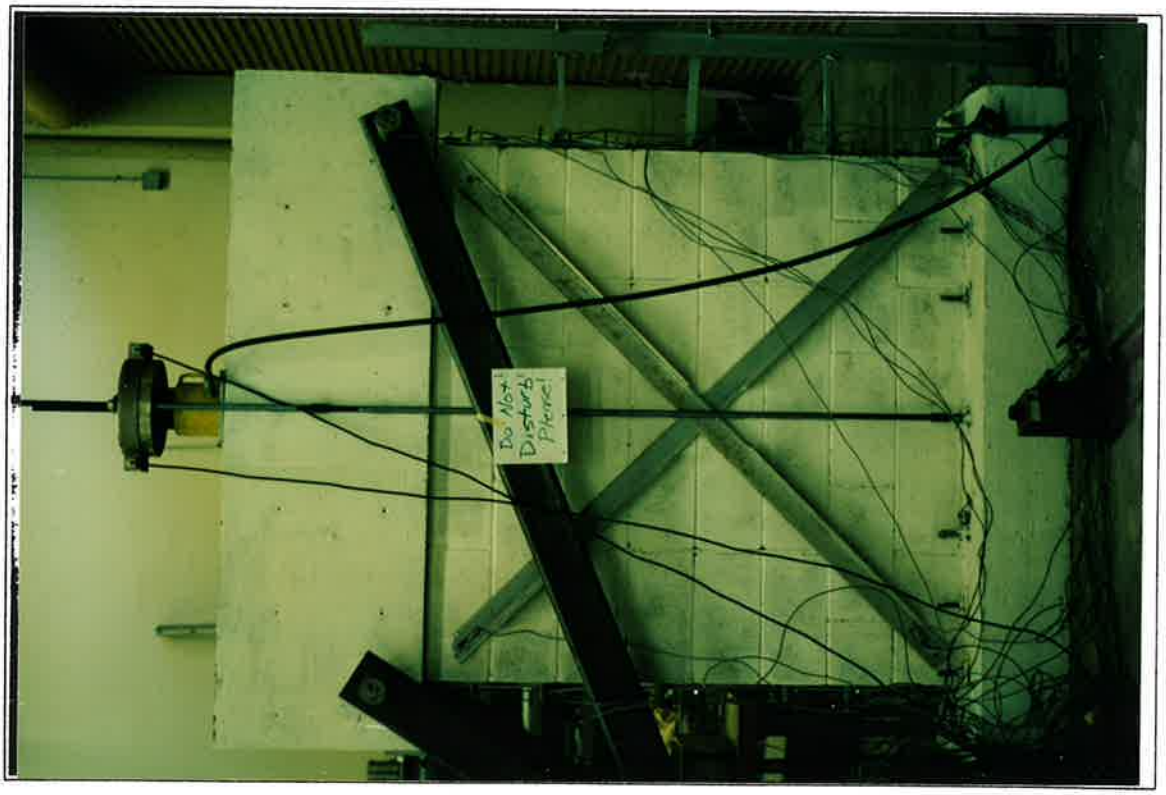

Photo 2.6 Slitted Wall At Completion of Construction Ready For Loading

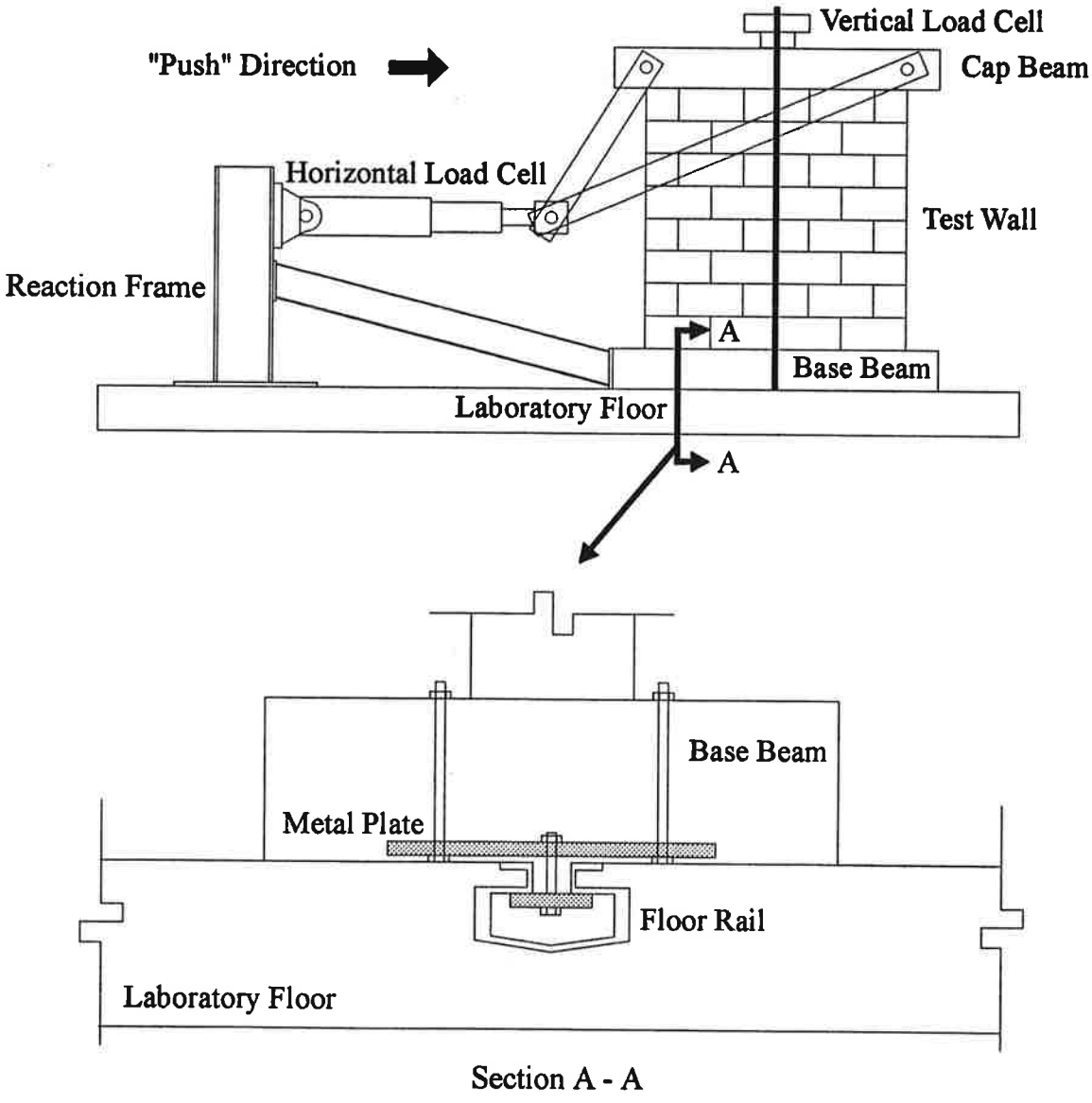

Figure 2.3 Test Setup

the rails is shown in section A-A of Figure 2.3. Plates and bolts were used to anchor the base beam to the floor rail. The dimensions of the base beam were 25.4 cm (10 inches) deep, 55.9 cm (22 inches) wide and 203 cm (80 inches) long. Longitudinal reinforcement was four #5 top and bottom with #4 stirrups at 15.24 cm (6 inch) on center.

A concrete cap beam was formed on the top of each masonry wall. This cap beam performed two tasks. First, it allowed a shear force and a moment couple to be delivered by the hydraulic ram at the top of each test specimen. Second, a vertical point load was distributed by the cap beam into the wall.

For the monolithic wall, the cap beam was 25.4 cm (10 inches) deep, 20.32 cm (8 inches) wide, and 203 cm (80 inches) long. Six #8 longitudinal bars and #4 stirrups were used. The reinforcement was however inadequate, resulting in severe cracking during initial tests of the specimen. For completion of testing, the cap beam was bolted to a steel beam placed on top of the concrete beam. The strengthening of the top concrete beam can be seen in Photo B.6.

For the slitted wall the top cap beam was redesigned to eliminate the problems caused by the inadequate beam capacity. The increase in dimensions of the cap beam for the slitted wall can be seen by contrasting Photo 2.2 and 2.6. This cap beam of the slitted wall specimen was 61 cm (24 inches) deep, 20.3 cm (8 inches) wide and 203 cm (80 inches) long. Again, #8 bars were used longitudinally and #4 stirrups were used. This beam performed much better during testing and allowed completion of the testing for the slitted wall without difficulty.

As mentioned previously the vertical bars of each wall had 180 degree hooks extending above the top of the wall. These hooks were necessary to adequately connect the cap beams to the masonry walls. A connection like this was needed to transfer a bending moment into the top of the wall.

2.4 Load System

A nominal vertical load stress of 689.4 kPa (100 psi) simulating gravity effects was applied to each specimen at the start of the experiment. The vertical load was applied and held constant by a hydraulic jack placed on the top of the wall. This jack reacted against a set of all-thread rods running down either side of the wall and connected at the base slab. A load cell was used to measure the magnitude of the applied vertical load. The setup of vertical load application can be seen in Photo 2.6. Horizontal loads were applied using an independent hydraulic ram at mid-height of the wall. The hydraulic ram, when activated, pushed on tube steel arms which delivered a shear and a moment couple to the top of the wall. A photo of this lateral load system with steel arms, hydraulic ram, and reaction frame can be seen in Photo B.1 of Appendix B. This special loading was done specifically to create a situation of double bending in the wall. Also, this type of loading creates an area with no flexural stress, but shear stress alone at mid height of the wall. Figure 2.3 illustrates the loading configuration.

2.5 Instrumentation

Strains on vertical and horizontal reinforcement were measured using electrical resistance strain gages in both walls. Photo 2.7 illustrates a typical strain gage which was used to measure the strain of the reinforcing steel. Figure 2.4 and 2.5 shows the location of strain gages for both walls. The arrangement of strain gages was selected to enable a comparison between the distribution of strains in the monolithic and slitted walls. Note that the letters V and H shown in Figure 2.4 and 2.5 for strain gages corresponds to gage location on a vertical or horizontal reinforcing bar. Readings of the gages were taken at the peak of each load cycle.

Horizontal displacements were measured at various heights of the wall by using linear potentiometers Horiz. 1,2,3,4 & 5 as shown in Figure 2.6(b). An example of a linear potentiometer used for displacement measurement is shown in Photo 2.8. The linear potentiometer Horiz. 1 measured the in plane lateral displacement at the point of

Photo 2.7 Typical Electrical Resistance Strain Gage

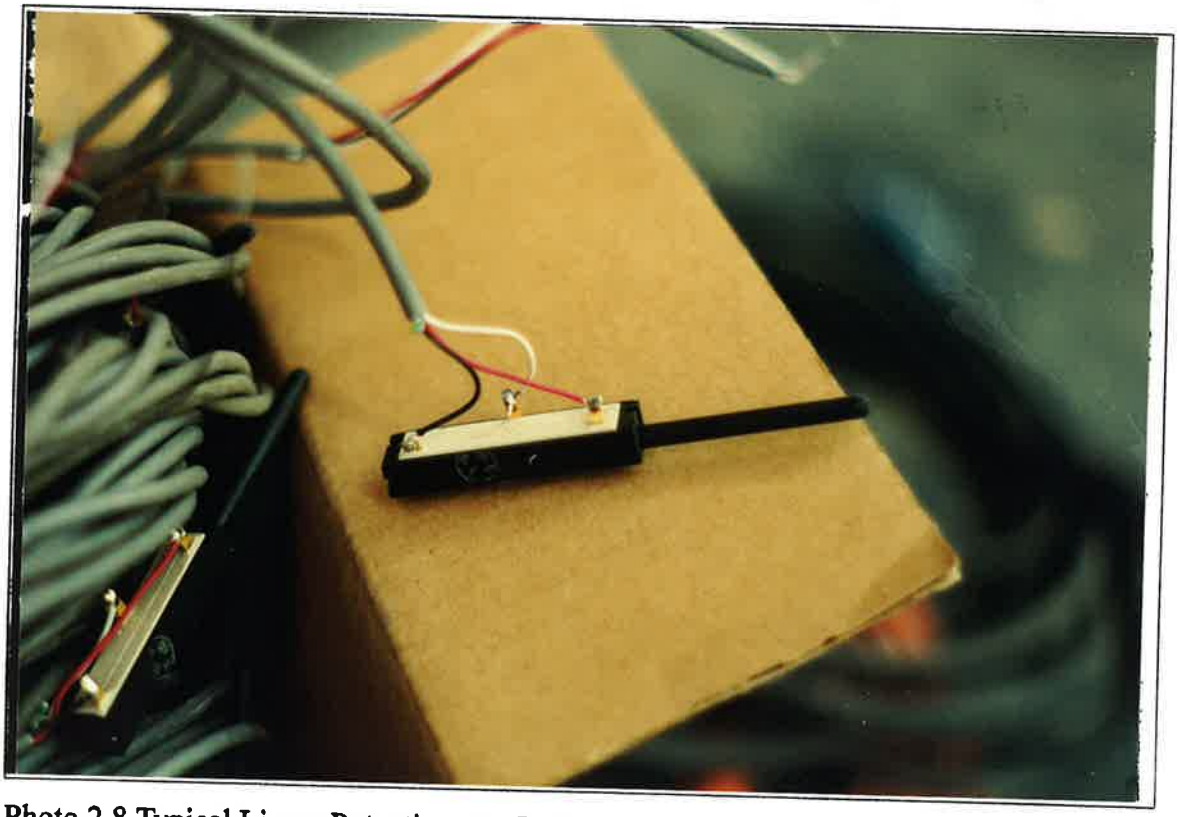

Photo 2.8 Typical Linear Potentiometer Instrument

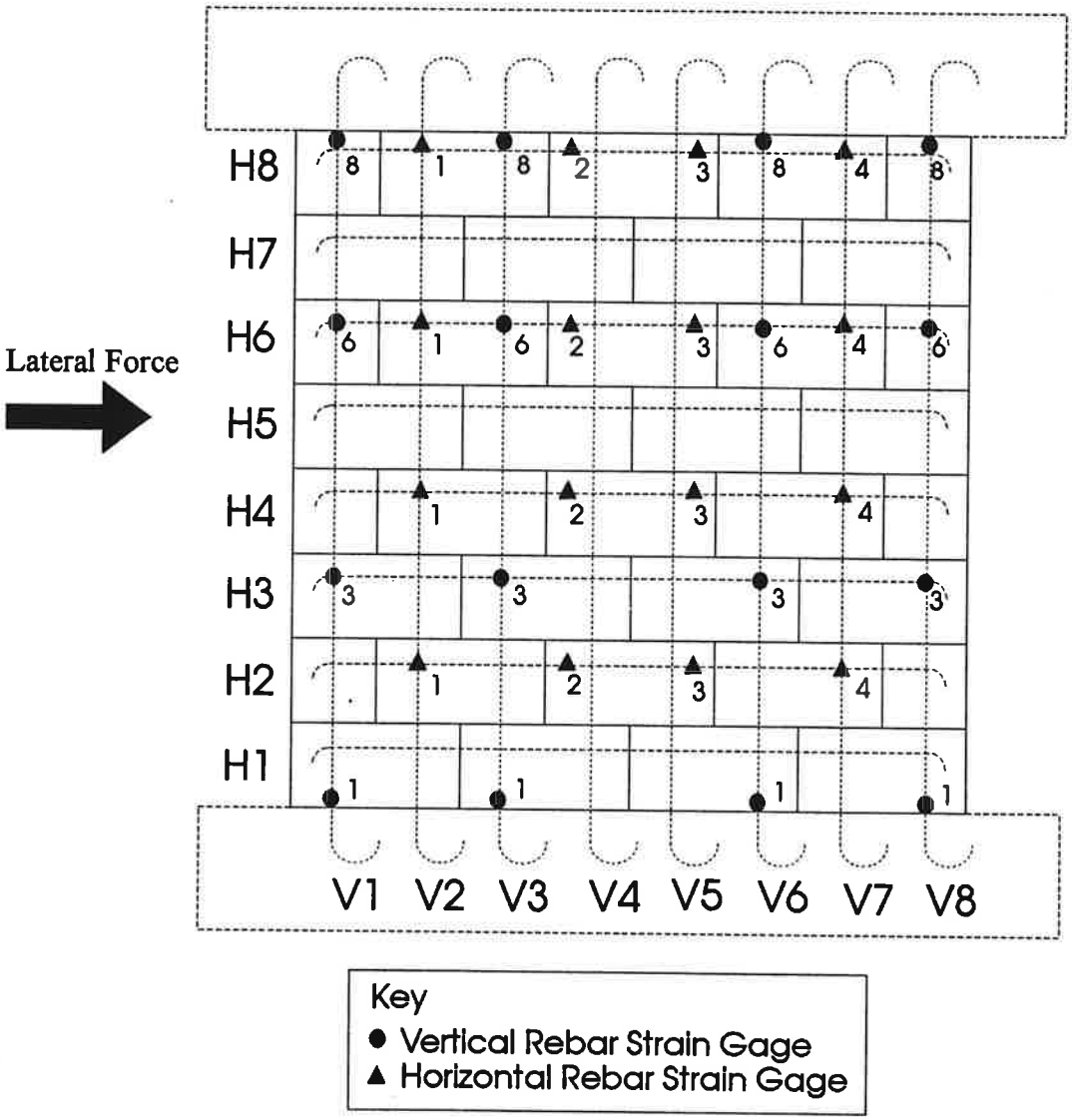

Figure 2.4 Monolithic Wall Reinforcing Bars Strain Gage Positions

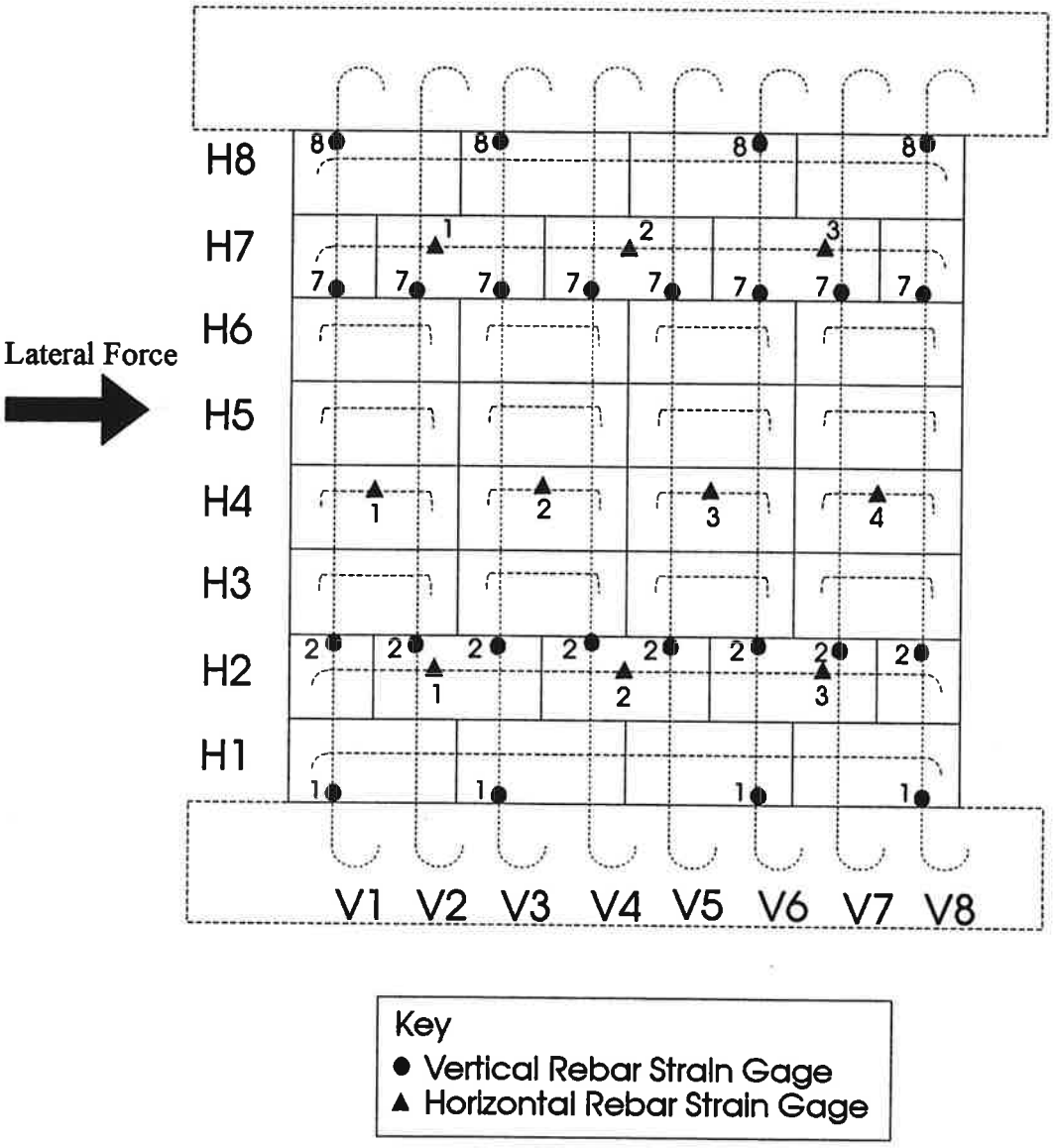

Figure 2.5 Slitted Wall Reinforcing Bars Strain Gage Positions

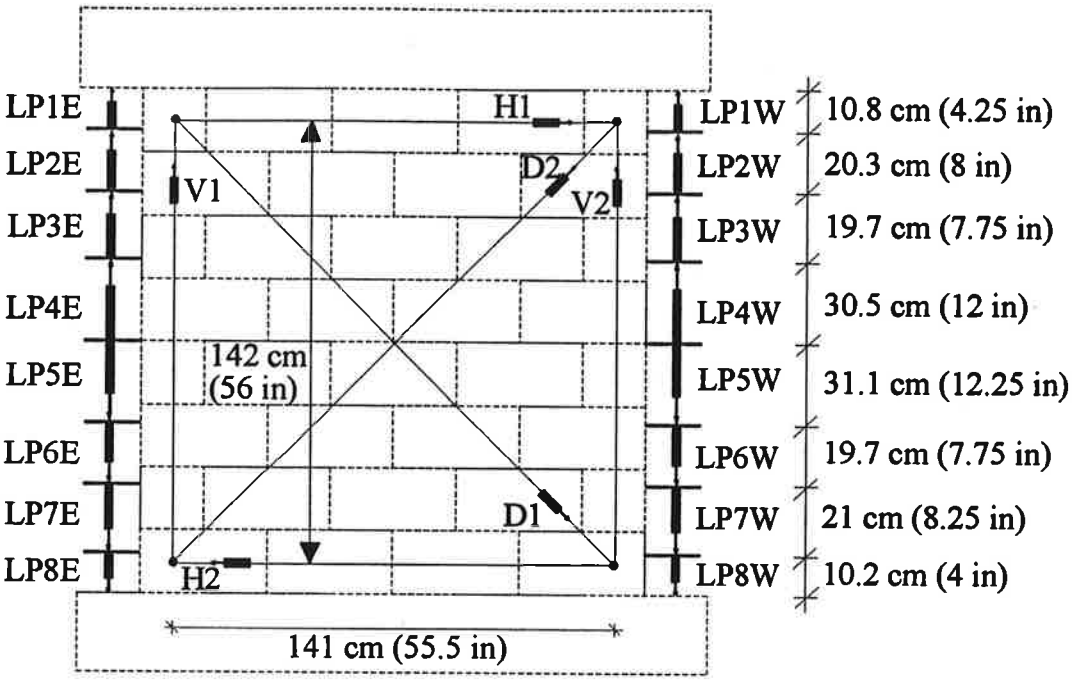

(a) Relative Displacement Measurements

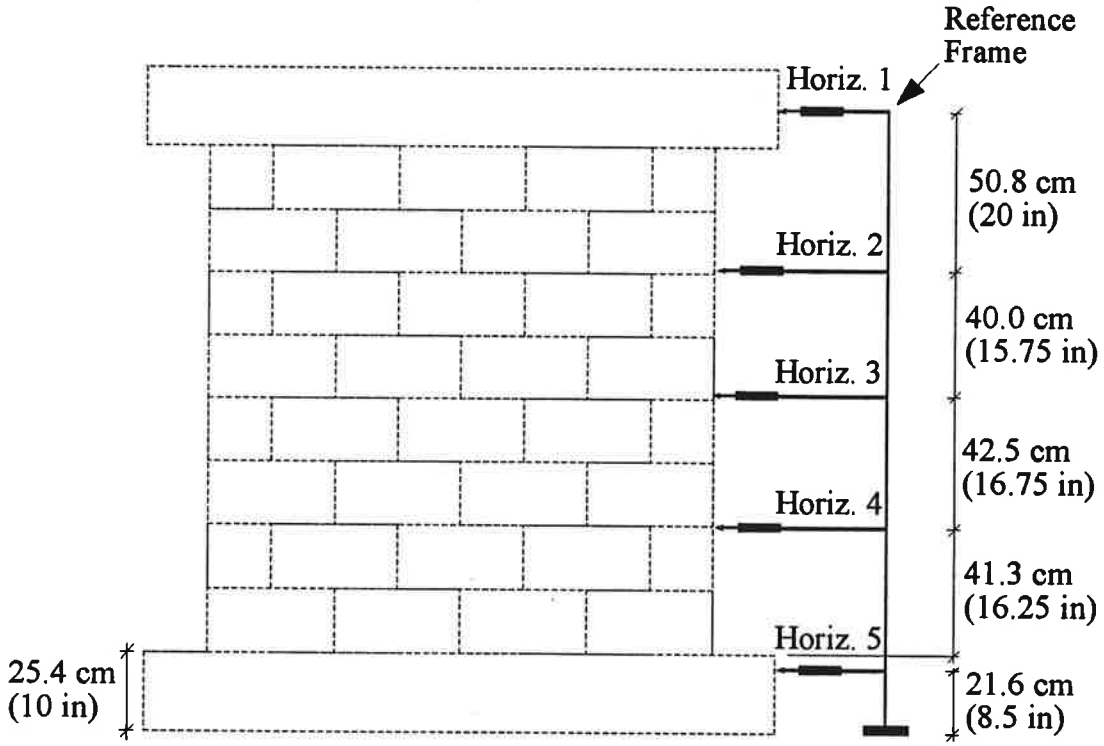

(b) Absolute Lateral Displacement

Figure 2.6 Displacement Measurements

horizontal force application. Three intermediate linear potentiometers, Horiz. 2,3,& 4, measured displacement of the wall at 124(48.8), 84(33), and 41(16.25) cm(in) above the wall base. Horiz. 5 monitored the potential for slip of the specimen base with respect to the laboratory floor.

In addition to lateral displacement measurements, changes in lengths along the vertical (V1 & V2), horizontal (H1 & H2), and diagonal (D1 & D2) (see Figure 2.6(a)) were measured throughout the load tests. These deformations could be used to assess the proportions of flexural and shear deformation to the total lateral deformation of the wall.

The in plane curvatures of the wall were also measured. Linear pots were mounted on the two end faces of the wall as shown in Figure 2.6(a). By measuring relative displacements, curvature could be determined.

2.6 Load History

The load history of both walls consists of an imposed load or displacement of increasing magnitude. Figures 2.7 and 2.8 summarize the load histories for the monolithic wall and the slitted wall respectively. The monolithic wall was first subjected to 3 cycles of ± 25 kips, followed by ± 50 kips, etc. The slitted wall was first subjected to 3 cycles of ± 15 kips, followed by ± 30 kips, etc. Since the predicted ultimate load capacity of the slitted wall was less than the monolithic wall, smaller load increments were used. Lateral load was applied until the lateral strength had degraded to below 50% of the peak force.

2.7 Mapping of Wall Cracks

During the testing damage progression as signified by surface cracking in the masonry was monitored by tracing the cracks which resulted at various load or displacement amplitudes. At each peak load, cracks were located on the walls and labeled by color for push or pull. Load magnitude, and load cycle in the given series were denoted on the traced cracks also as they occurred during the testing. A description of crack formation and crack propagation is provided in Chapter 3.

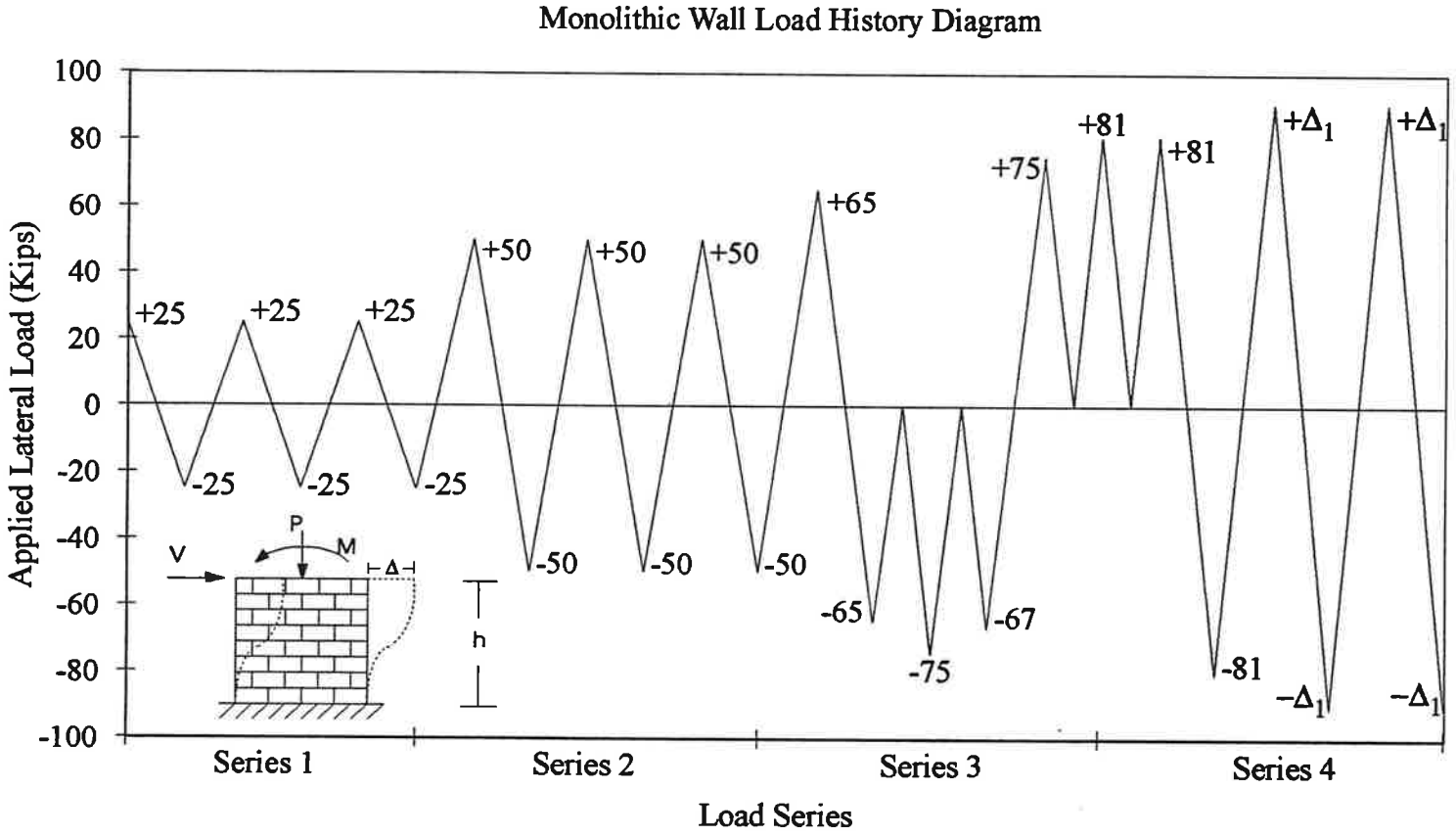

Figure 2.7 Monolithic Wall Load Test History

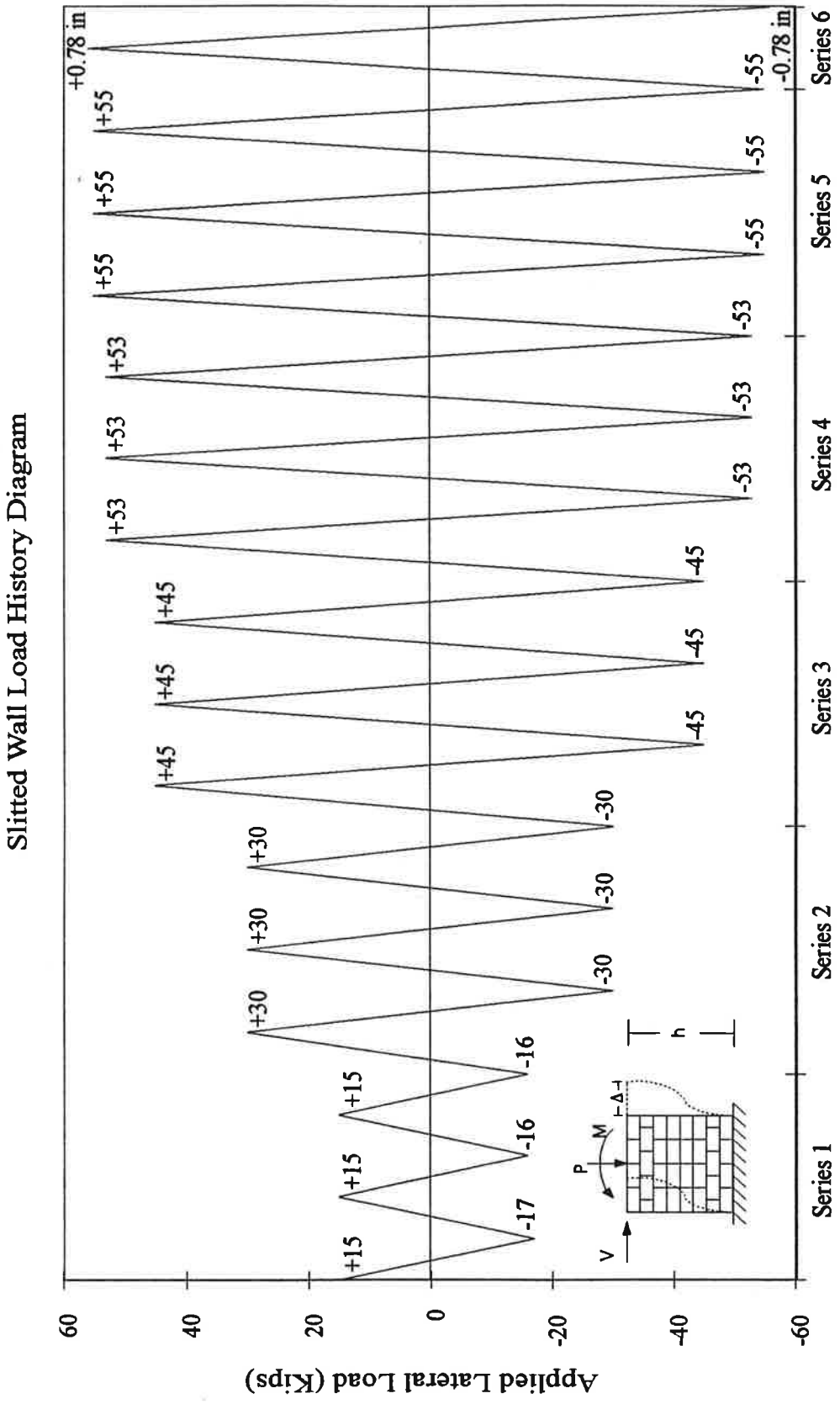

Figure 2.8 Slitted Wall Load Test History

Chapter 3

Results

3.1 General

The results of the cyclic load testing for the monolithic and slitted walls are presented in this chapter. Hysteresis loops of lateral force versus lateral drift angle, reinforcing steel strain distributions, ductility, curvature, crack patterns, displacements, and strength will be discussed for each wall. Quantitative information will also be presented graphically in the accompanying figures.

3.2 Lateral Force Versus Drift Angle Plots

Although the lateral displacement at the point of lateral force application may be used for the definition of drift angle for the wall, the lateral displacements were affected by cracking of the top concrete beam and base rotation. Cracking of the top concrete beam for the monolithic wall was particularly severe. Since it was difficult to provide correction to the measured displacements to account for the cracking and base rotation, drift angle was determined using a set of diagonals mounted on the wall panels. The drift angle was determined by using the average displacement of the pair of diagonals D1 and D2 as shown in Figure 3.1.

The horizontal displacement at the top end of each diagonal can be related to the change in length of the diagonal. The horizontal displacement of a diagonal can be found by using the following expression:

$$\Delta = \frac{\Delta L}{\cos(\phi - \alpha)} \tag{3.1}$$

The change in length of the diagonal is,

$$\Delta L = L - L_i \tag{3.2}$$

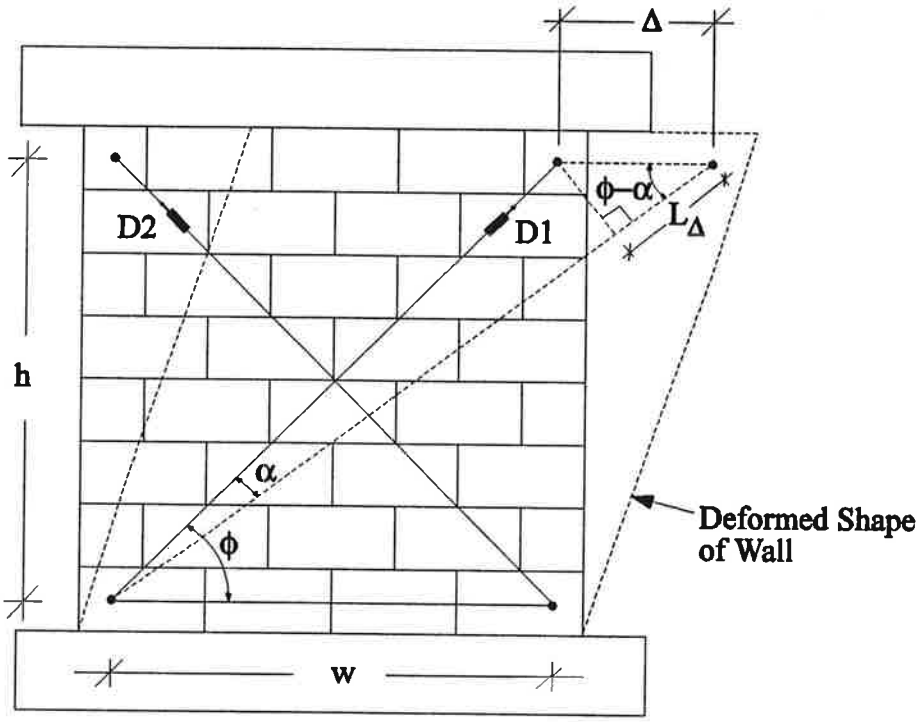

Figure 3.1 Determination of Wall Drift Angle
From Diagonal Measurement

where,

L = deformed length of the diagonal

L_i = initial length of the diagonal

and for small deformations,

$$\cos(\phi - \alpha) \approx \cos(\phi) \tag{3.3}$$

The angle ϕ of the diagonal with respect to the horizontal is given by:

$$\phi = \tan^{-1}\left[\frac{h}{w}\right] \tag{3.4}$$

where,

w = initial horizontal distance between the ends of a given diagonal

h = initial vertical distance between the ends of a given diagonal

and drift angle can be found by the following expression,

$$\theta = drift\ angle = \frac{\Delta}{h} \tag{3.5}$$

The continuous data collected by computer was used to provide lateral force versus drift angle information. By utilizing this information hysteresis loops for the monolithic wall and slitted wall were created, and are as shown in Figures 3.2 and 3.3 respectively.

3.2.1 Monolithic Wall

The lateral response of the monolithic wall specimen (Figure 3.2) was characterized by a near-elastic response during the three initial cycles to V = 111 kN (25 kips). The very minor hysteresis loops noted at this stage of loading was due to the formation of flexural cracks at the top of the wall. A reduction in lateral stiffness was noted upon load increment to V = 222 kN (50 kips) and the reduction in stiffness was primarily due to the extension of the flexural cracks into inclined flexure-shear cracks.

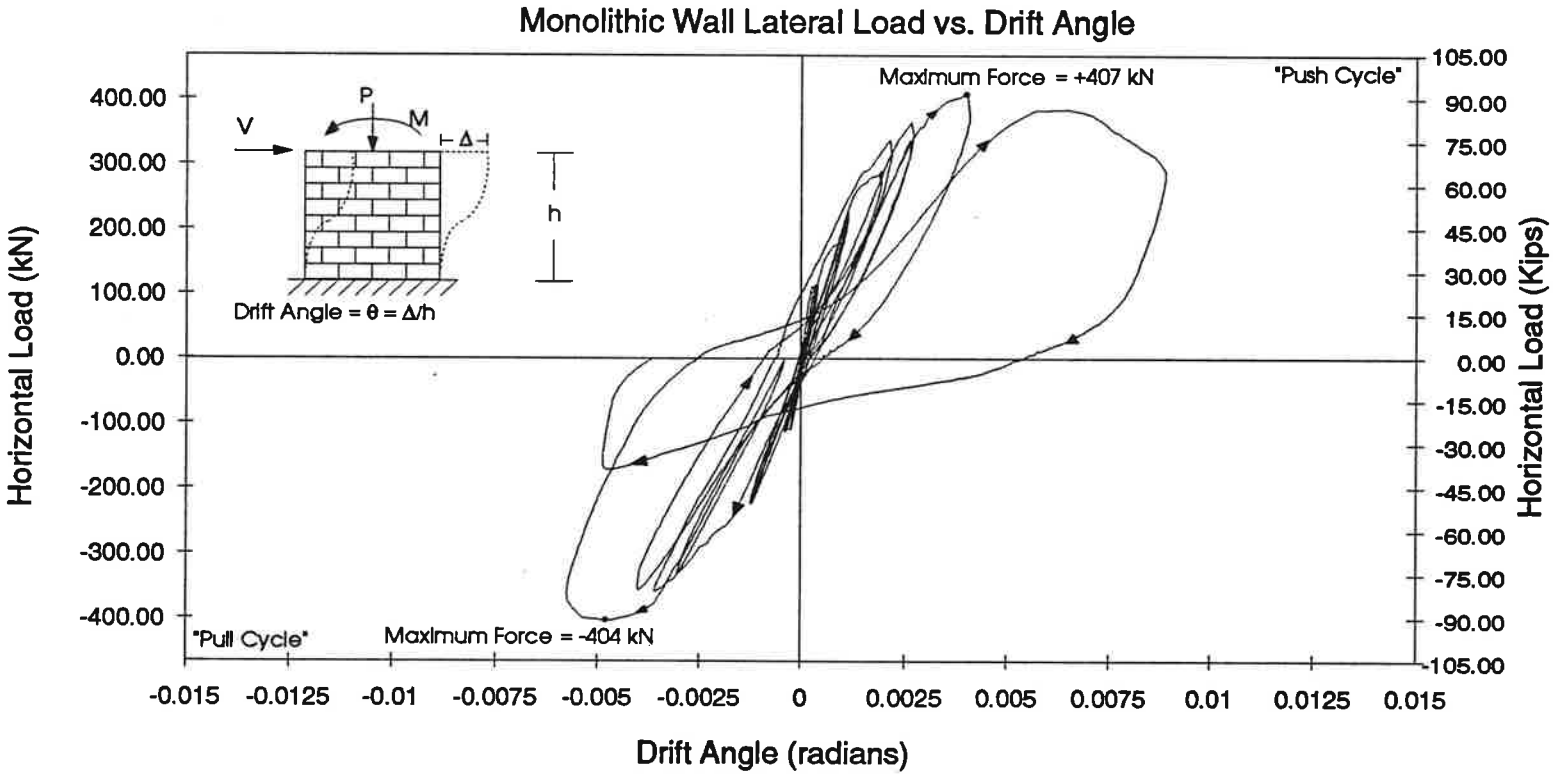

Figure 3.2 Monolithic Wall Hysteresis Loops

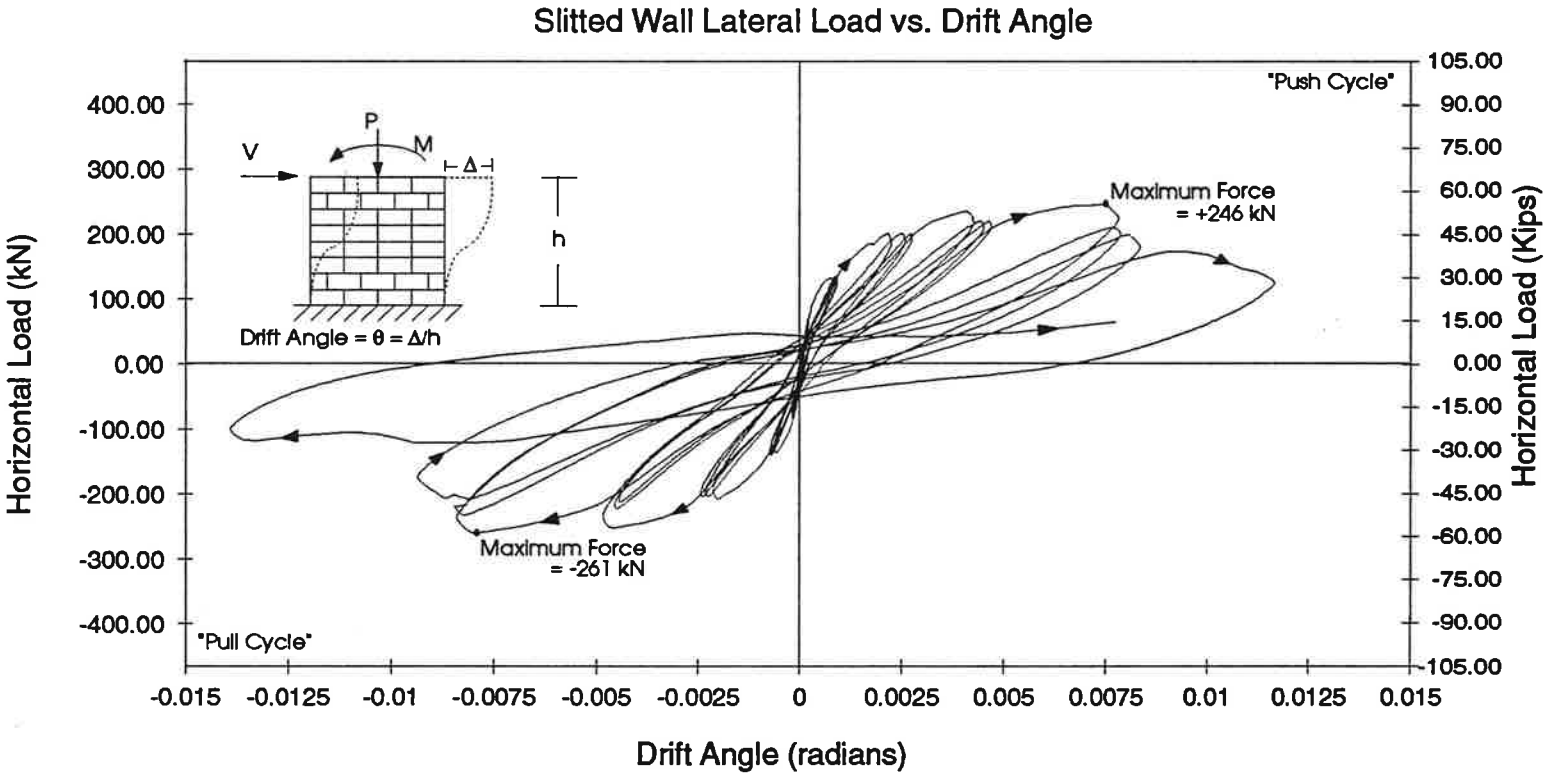

Figure 3.3 Slitted Wall Hysteresis Loops

Despite the reduced stiffness, the response of the wall at V = 222 kN (50 kips) was stable with a fairly repeatable strength in both directions. Further decrease of lateral stiffness occurred upon a lateral force increase to V = 289 kN (65 kips) as new web-shear cracks formed in the center region of the wall. The subsequent two cycles consisted of unequal loading in the two directions with two half cycles to V = 334 and 298 kN (75 and 67 kips) in the push direction, followed by two half cycles to V = 334 and 360 kN (75 and 80.9 kips) in the pull direction.

Although the load cycles were asymmetric, the response of the wall was relatively stable in the two directions with minor degradation of strength between cycles. In the cycle that followed, however, complete reversals in the push and pull direction were imposed. A maximum lateral force of V = 407 kN (91.5 kips) was measured in the push direction, while a maximum lateral force of V = 404 kN (90.8 kips) was measured in the pull direction. Note that Figure 3.2 shows a rapid drop in the lateral strength of the wall after reaching the maximum force in the pull direction. In the final cycle, the largest force measured in the push direction was V = 383 kN (86.3 kips), or corresponding to 94% of the maximum lateral force measured in the previous cycle. Upon a load reversal, the largest force measured was V = 171 kN (38.5 kips) which is substantially smaller than the maximum lateral force measured in the pull direction of the previous cycle.

For the monolithic wall the horizontal steel reinforcement consisted of four #4 bars and four #3 bars with experimental yield strengths of 514 MPa (74.5 ksi) and 414 MPa (60 ksi) respectively. A 45 degree diagonal crack and a contribution of all horizontal reinforcement was assumed. Using the above information and disregarding the shear contribution of the masonry due to severe cracking when plastic hinging occurs, the nominal shear strength of the wall provided by the steel reinforcement alone, according to the 1991 UBC, is V = 383 kN (86 kips). In contrast, the actual strength of the wall was 407 kN (91.5 kips), or about 6.4% higher than the UBC prediction.

3.2.2 Slitted Wall

The response of the slitted wall specimen in Figure 3.3 showed an elastic behavior for three initial cycles to V = 67 kN (15 kips). However, a noticeable reduction in lateral stiffness was noted during the load increment to V = 133 kN (30 kips), due to the formation of flexural cracks at the ends of the wall and at the ends of the 'mini'-piers. Upon further increase to V = 207 kN (46.5 kips), the lateral stiffness decreased further as flexural cracks extended into inclined flexure-shear cracks. A slight softening if the wall also occurred between cycles due to the continued extension of flexure-shear cracks upon cycling. Upon lateral force increase, the response became slightly asymmetric with a lateral force of V = 236 kN (53 kips) measured at a drift angle of γ = 0.0041 radians in the push direction, and a lateral force of V = 253 kN (56.9 kips) measured at a drift angle of γ = 0.0046 radians in the pull direction.

Although the response was slightly asymmetric, the peak lateral force remained approximately constant in both directions for a drift angle greater than 0.005 radians. A maximum lateral force of V = 246 kN (55.3 kips) was measured at a drift angle of γ = 0.0074 radians in the push direction, whereas a maximum lateral force of V = 261 kN (58.7 kips) was measured at a drift angle of γ = 0.0080 radians in the pull direction. A progressively more severe degradation of lateral strength occurred upon cycling to the same displacement after attaining the maximum fore. In the push direction, the lateral strength of the wall in the second and third cycle were 85 and 81% of the maximum force measured in the first cycle, while in the pull direction, the lateral strength of the wall in the second and third cycle were 89 and 80% of the maximum force measured in the first cycle.

In the final cycle, the lateral strength of the wall degraded to V = 173 and 121 kN (38.8 and 27.2 kips) or corresponding to 70 and 46% of the maximum force in the push and pull direction, respectively. The theoretical lateral force, calculated from the summation of the lateral force in each 'mini'-pier assuming that flexural strength was developed at the end of the 'mini'-pier and assuming that the total axial force was equally

divided in the 'mini'-piers, was V = 247 kN (55.5 kips). The theoretical lateral strength of the wall agreed well with the measured lateral force of V = 261 kN (58.7 kips).

3.2.3 Comparison Between the Monolithic and Slitted Walls

The inclusion of vertical separation joints in the slitted wall resulted in a significant reduction in the lateral stiffness of the wall. The lateral stiffness of the monolithic wall, calculated using a secant from the origin to the first push cycle to V = 111 kN (25 kips), was $k_{mono} = 4.43 \times 10^5$ kN/radian (9.96×10^4 kips/radian) whereas the lateral stiffness of the slitted wall based on a lateral force of V = 66.7 kN (15 kips) was $k_{slit} = 3.31 \times 10^5$ kN/radian (7.45×10^4 kips/radian). The slitted wall showed a 25% reduction in lateral stiffness when compared to that of the monolithic wall. The inclusion of vertical separation joints also resulted in a significant reduction in the lateral strength of the slitted wall. In the push direction, the maximum lateral force was V = 407 kN (91.5 kips) for the monolithic wall and 246 kN (55.3 kips) for the slitted wall, and in the pull direction, the maximum lateral force was V = 404 kN (90.8 kips) for the monolithic wall and 261 kN (58.7 kips) for the slitted wall. The slitted wall showed a 40% and 35 % reduction in the lateral strength in the push and pull directions, respectively, when compared to that of the monolithic wall. Using the average strength of the wall in the two directions and the lateral stiffness of the wall, the equivalent elasto-plastic yield drift angles of the monolithic and slitted wall are $(\gamma_y)_{pier} = 0.00092$ and 0.00077 radians, respectively.

A comparison of the two walls also showed an increase in the ultimate drift angle, γ_u, of the slitted wall, which is taken as the drift angle at which the post-peak lateral strength degraded to 80% of the peak lateral force V_{max}. For the monolithic wall in the pull direction, however, 90% of the peak lateral force was used to define the ultimate drift angle since a rapid drop in lateral force occurred after reaching the peak. For the monolithic wall, the ultimate drift angles were $\gamma_u = 0.0082$ and 0.0058 radians in the push and pull directions, respectively, whereas for the slitted wall, the ultimate drift angles were $\gamma_u = 0.0091$ and 0.0087 radians in the push and pull directions, respectively. Using the

average of the two drift angles, i.e. 0.0070 for the monolithic wall and 0.0089 for the slitted wall, the slitted wall specimen showed a 27% increase in ultimate drift angle compared to that of the monolithic wall. The increase in ultimate drift angle is however smaller than that of the slitted concrete infill panels tested in Japan [5].

3.3 Reinforcement Strain Distributions

Three types of data will be presented below from measurement of strains on reinforcement. They are:

1. Vertical rebar strain distributions
2. Individual vertical rebar strains
3. Horizontal rebar strains

For each type listed above, the information has been plotted for both walls. In each case, the information will be discussed for the monolithic wall, the slitted wall and finally the slitted wall compared with the monolithic wall. All strains for a given type listed above are plotted on the same scale.

3.4 Horizontal Distribution of Flexural Steel Strains

For each wall, vertical rebar strain distributions are plotted at four horizontal sections through the wall. These sections are taken at the first, third, sixth and eighth courses from the base of wall. The strain distributions are plotted for the peak loads of the first cycle in each load history increment. Strain distributions in the "push" direction are denoted by a solid line and "pull" direction strain distributions are denoted as a dashed line.

For the monolithic wall the largest strains in the vertical steel are expected at the sections at the top and bottom of the wall because the highest moments occur at these cross-sections. Of these cross-sections, the outermost bars will be subjected to the largest strains. For the slitted wall the largest strains in the vertical steel are expected at the tops and bottoms of the 'mini'-piers since the highest bending stresses will occur at these

locations. As will be seen in Figures 3.4 to 3.11 presented below, this qualitative description of the strains is confirmed by the experimental results.

3.4.1 Monolithic Wall

Figures 3.4, 3.5, 3.6 and 3.7 depict the vertical rebar strain distribution for sections one, three, six and eight respectively. As expected, the largest strains are seen at section one at the base of the wall (Figure 3.4) and at section eight at the top of the wall (Figure 3.7). The third and sixth sections exhibit much smaller strain levels since the sections are near mid-height of the wall where the bending moment is theoretically zero. The largest strains are over 8000 microstrains in vertical bar V8 and V1 in Figure 3.4 and 3.7 respectively. Yield strain of the reinforcement was 2570 microstrains.

First-yield of extreme reinforcement for the monolithic wall occurs at a lateral force of 222 kN in the pull cycle. This corresponds to a yield moment of 180 kN-m and occurred at section one. The experimental neutral axis depth at first-yield was approximately 36.4 cm. The experimental neutral axis depth was determined at first-yield by linear interpolation between the reinforcement with the maximum steel compression strain and the reinforcement with the smallest steel tensile strain. The theoretical neutral axis at first-yield occurs at 48.6 cm. Thus the experimental neutral axis is 75% of the theoretical value. First-yielding of reinforcement in the push direction occurs at 289 kN at section eight and the corresponding moment is 234 kN-m.

3.4.2 Slitted Wall

Figures 3.8, 3.9, 3.10 and 3.11 depict similar vertical rebar strain distributions at sections one, two, seven, and eight respectively. The largest strains occur at sections two and seven and is expected since the wall is more flexible at the bottom and top of the slitted portion of the wall. The highest strains are between 17000 and 18000 microstrains. These highest strains occur in the pier second from the left. The strains at the bottom and top of the wall are less than 8000 microstrains.

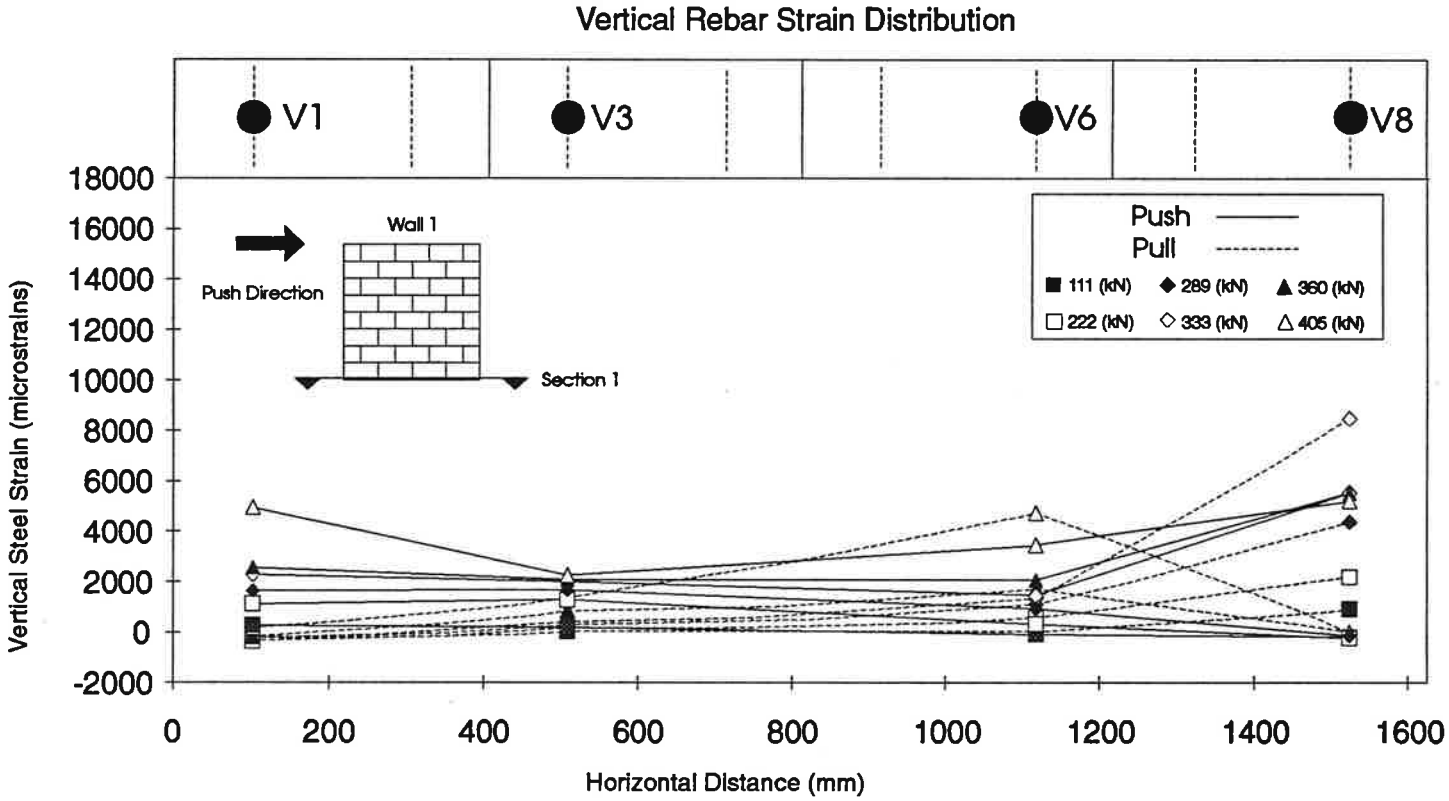

Figure 3.4 Monolithic Wall (Section 1) Vertical Rebar Strain Distribution

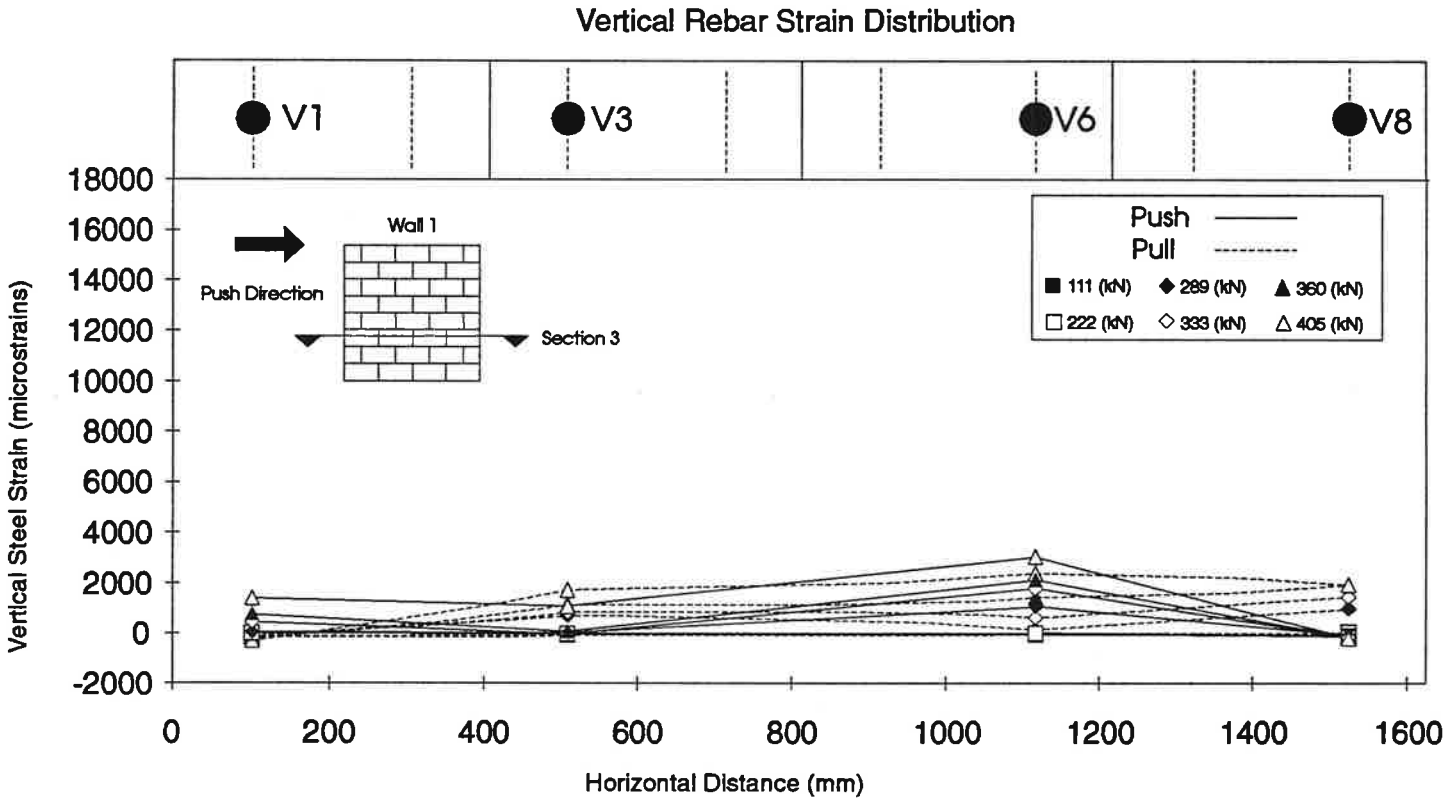

Figure 3.5 Monolithic Wall (Section 3) Vertical Rebar Strain Distribution

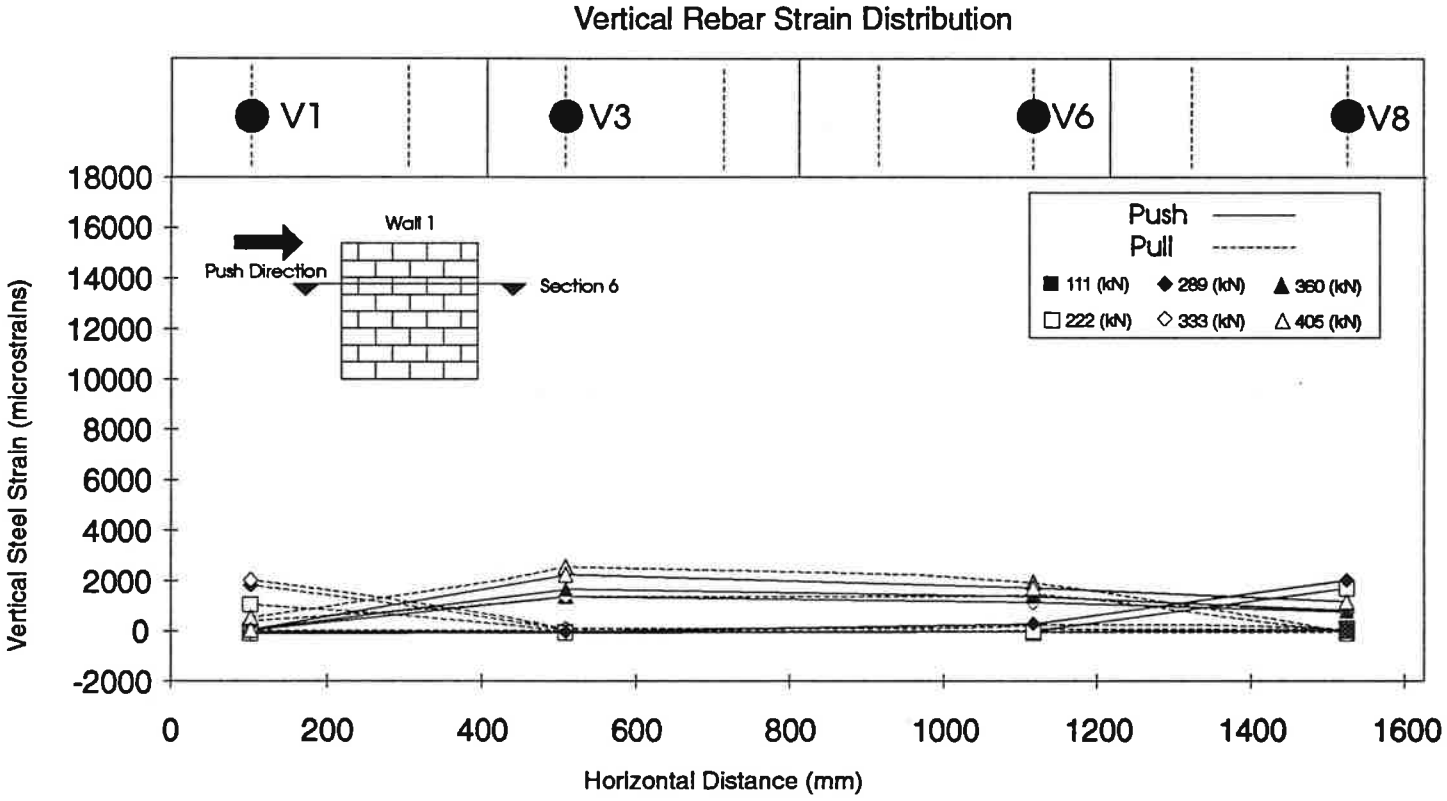

Figure 3.6 Monolithic Wall (Section 6) Vertical Rebar Strain Distribution

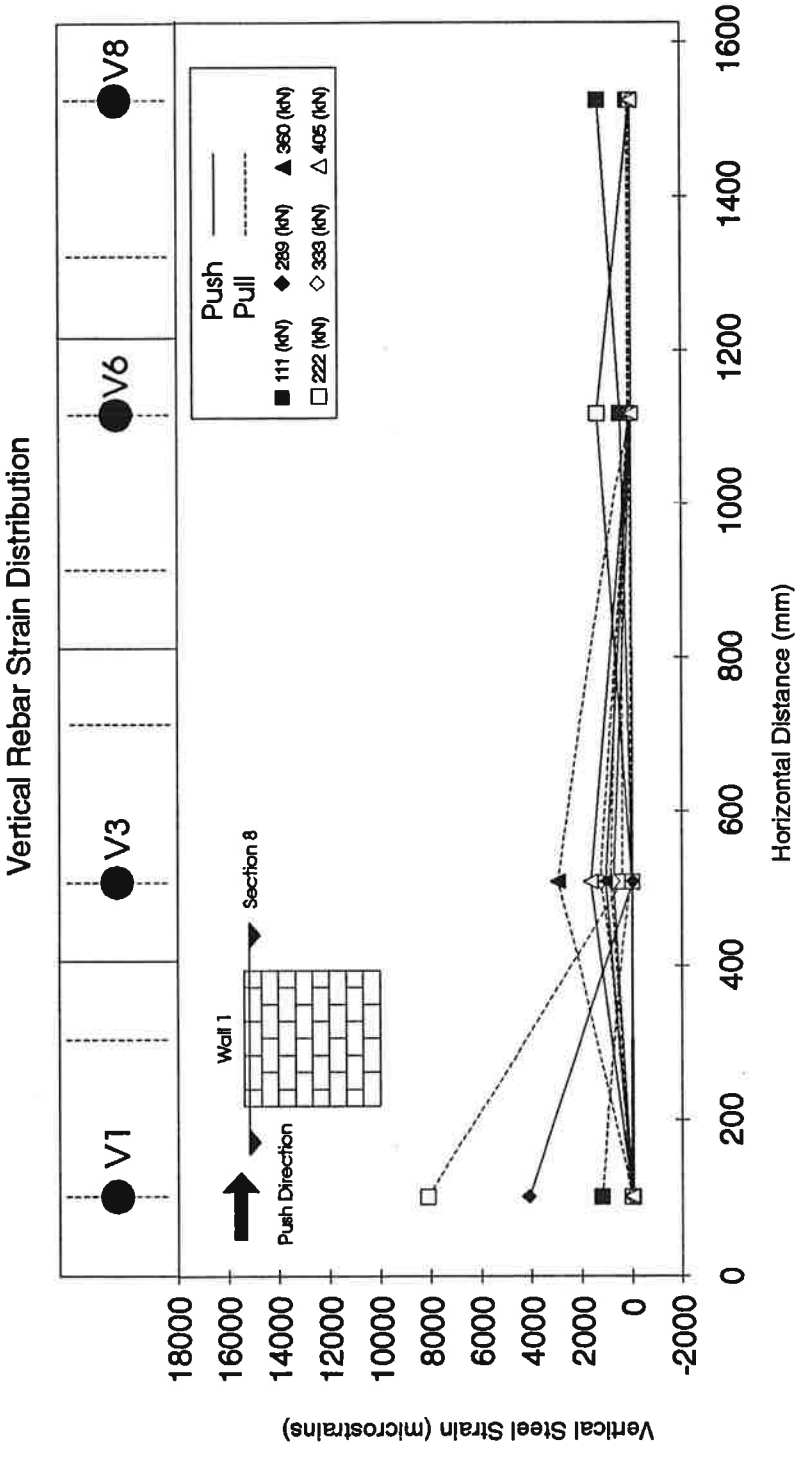

Figure 3.7 Monolithic Wall (Section 8) Vertical Rebar Strain Distribution

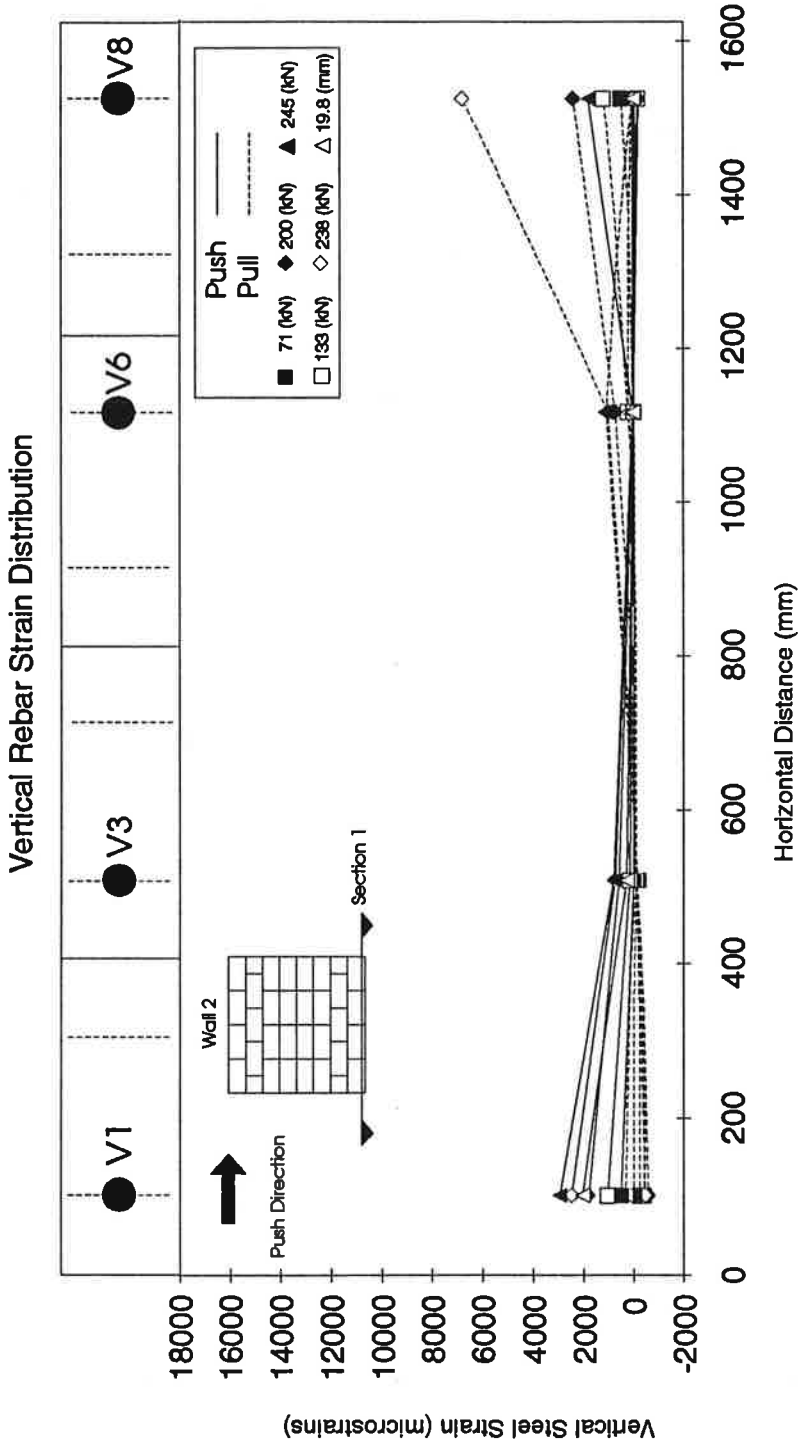

Figure 3.8 Slitted Wall (Section 1) Vertical Rebar Strain Distribution

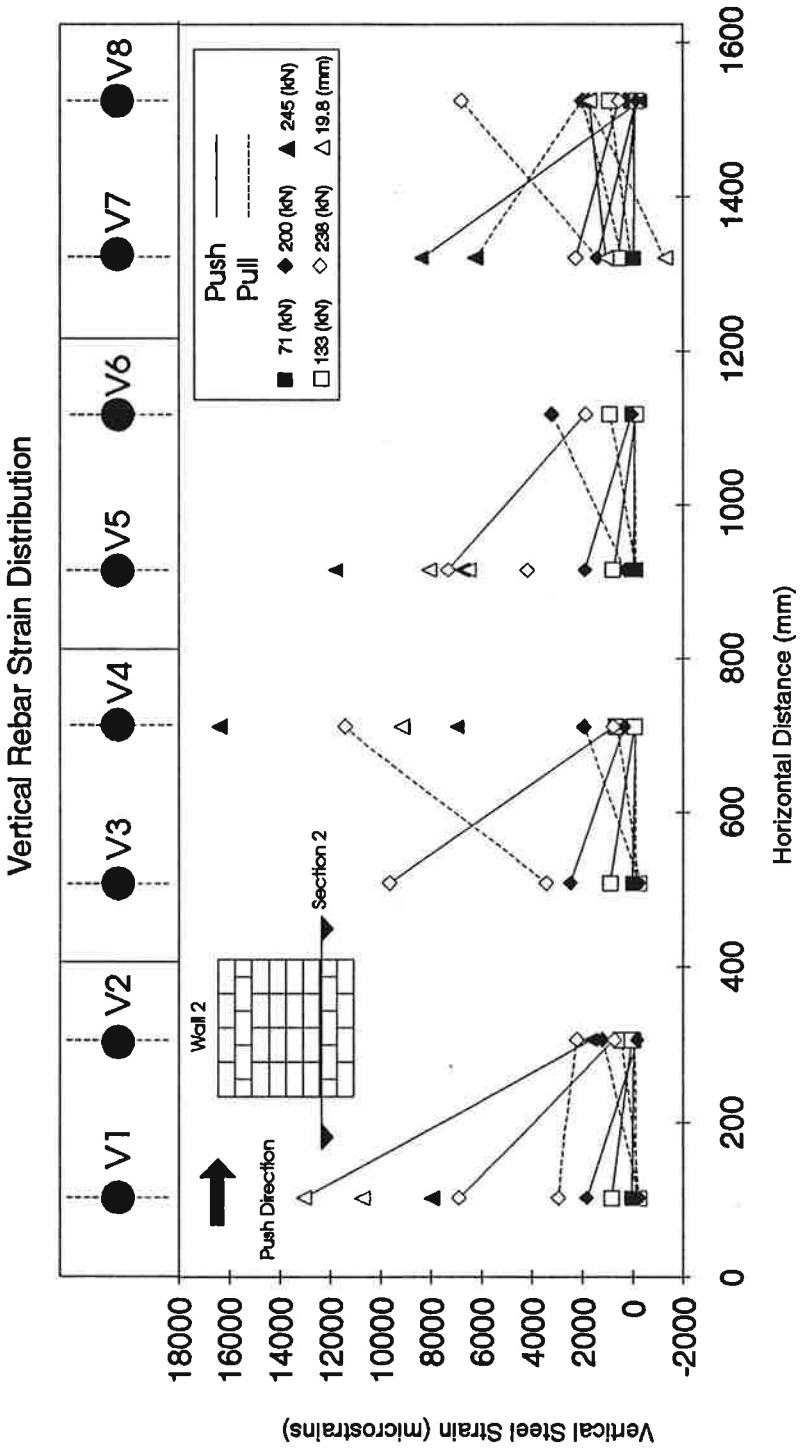

Figure 3.9 Slitted Wall (Section 2) Vertical Rebar Strain Distribution

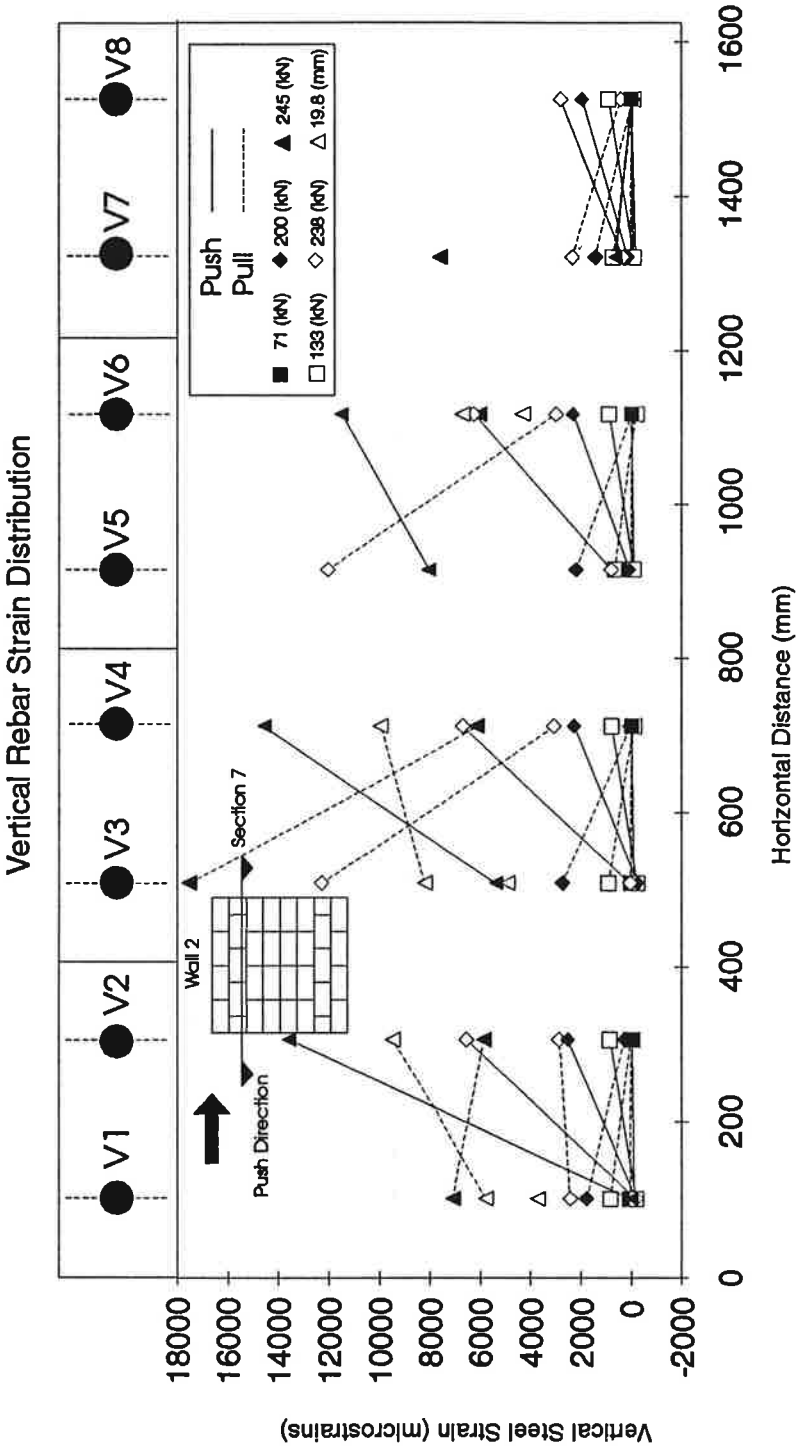

Figure 3.10 Slitted Wall (Section 7) Vertical Rebar Strain Distribution

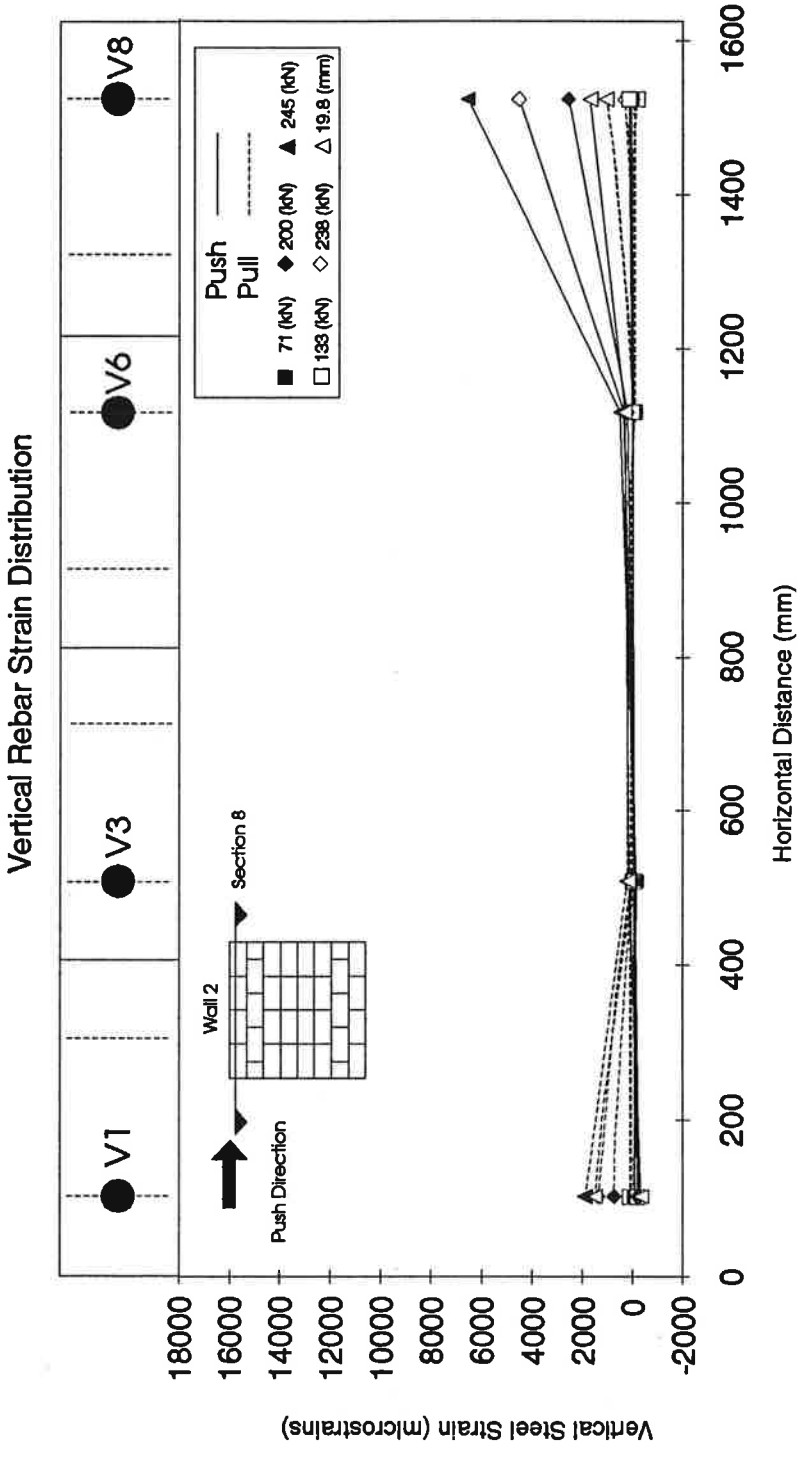

Figure 3.11 Slitted Wall (Section 8) Vertical Rebar Strain Distribution

Experimental first-yield for the slitted wall occurs at about 200 kN in the push direction. This yielding takes place at the pier containing bars V1 and V2 (Figure 3.10). In the pull direction experimental first-yield also occurs at about 200 kN and occurs in the pier containing bars V5 and V6 (Figure 3.9). After this initial yielding, most of the subsequent yielding occurs at sections two and seven when the higher loads are applied.

For the piers, the corresponding moment at the experimental first-yield of the vertical rebar is 20.3 kN-m. This value is about 88% of the theoretical yield moment of 23.2 kN-m. The experimental neutral axis at first-yield is approximately 11.5 cm from the left of pier one. The theoretical neutral axis is at 11.3 cm, which is within 2% of the experimental value.

3.4.3 Slitted Wall Compared to Monolithic Wall

The slitted wall, as expected, is much more flexible, than the monolithic wall, particularly in the middle portion of the wall. As a result, the majority of the high vertical rebar strains occur in the middle four piers. Whereas in the monolithic wall, the highest strains occurred at the top and bottom of the wall. The slitted wall recorded strains over two times greater than the monolithic wall. The loads required to yield the slitted wall were smaller than the loads required to cause first-yield of the monolithic wall.

3.5 Vertical Distribution of Flexural Steel Strains

For the monolithic and the slitted walls, the strains of individual vertical rebar are plotted. Figures 3.12 and 3.13 illustrate the vertical distribution of steel strains at various loads for the monolithic wall, while Figures 3.14 and 3.15 show the slitted wall vertical rebar strains for various loads.

3.5.1 Monolithic Wall

The outer two bars (bar one and bar eight) of the monolithic wall exhibit the highest strains, since these bars are located at the largest distance from the neutral axis. Also, these outer bars have the highest strains at the top and the bottom of the wall. This is expected since the tensile stresses, due to the applied moments, are highest at the top

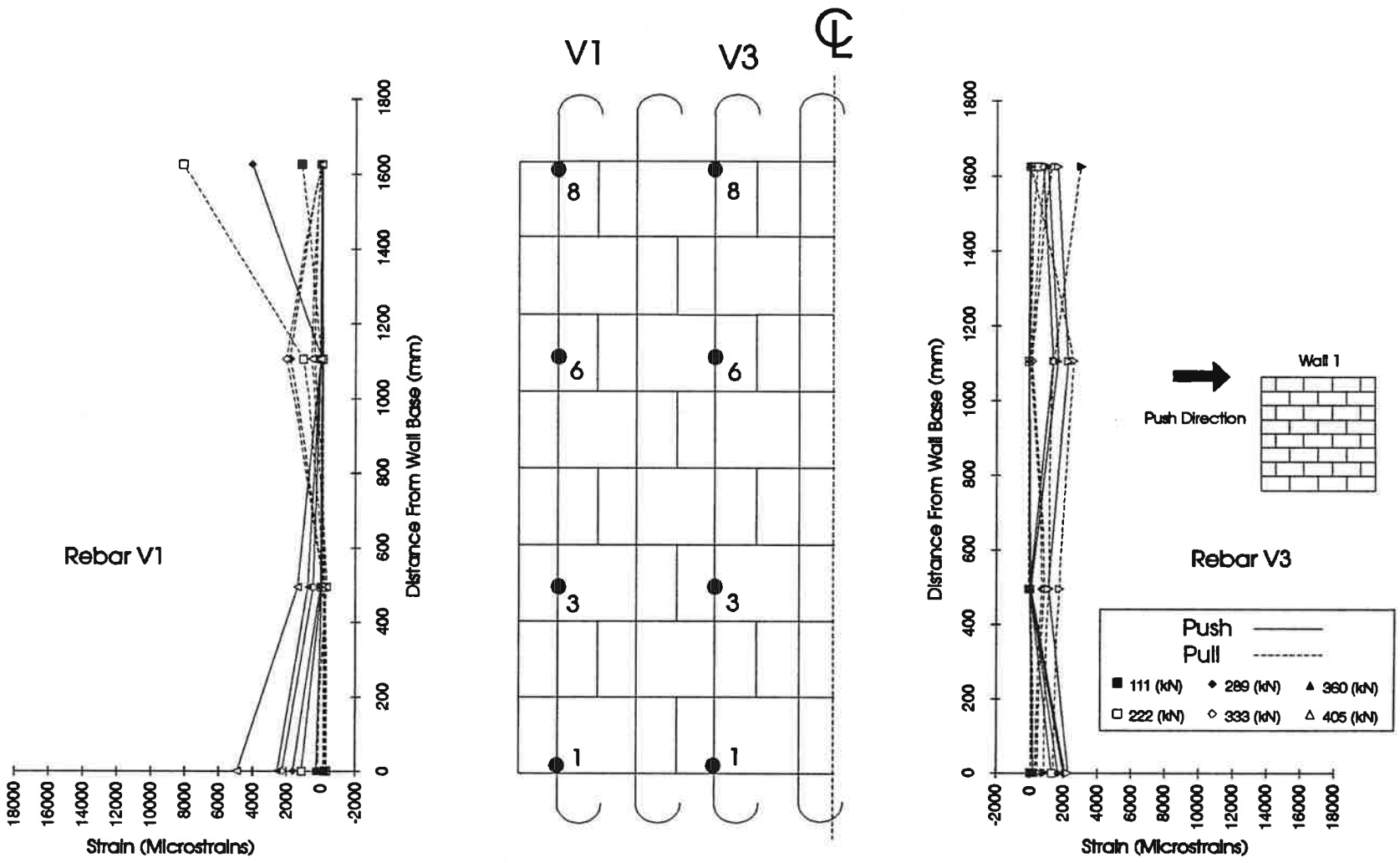

Figure 3.12 Monolithic Wall Strain Distribution of Bars V1 and V3

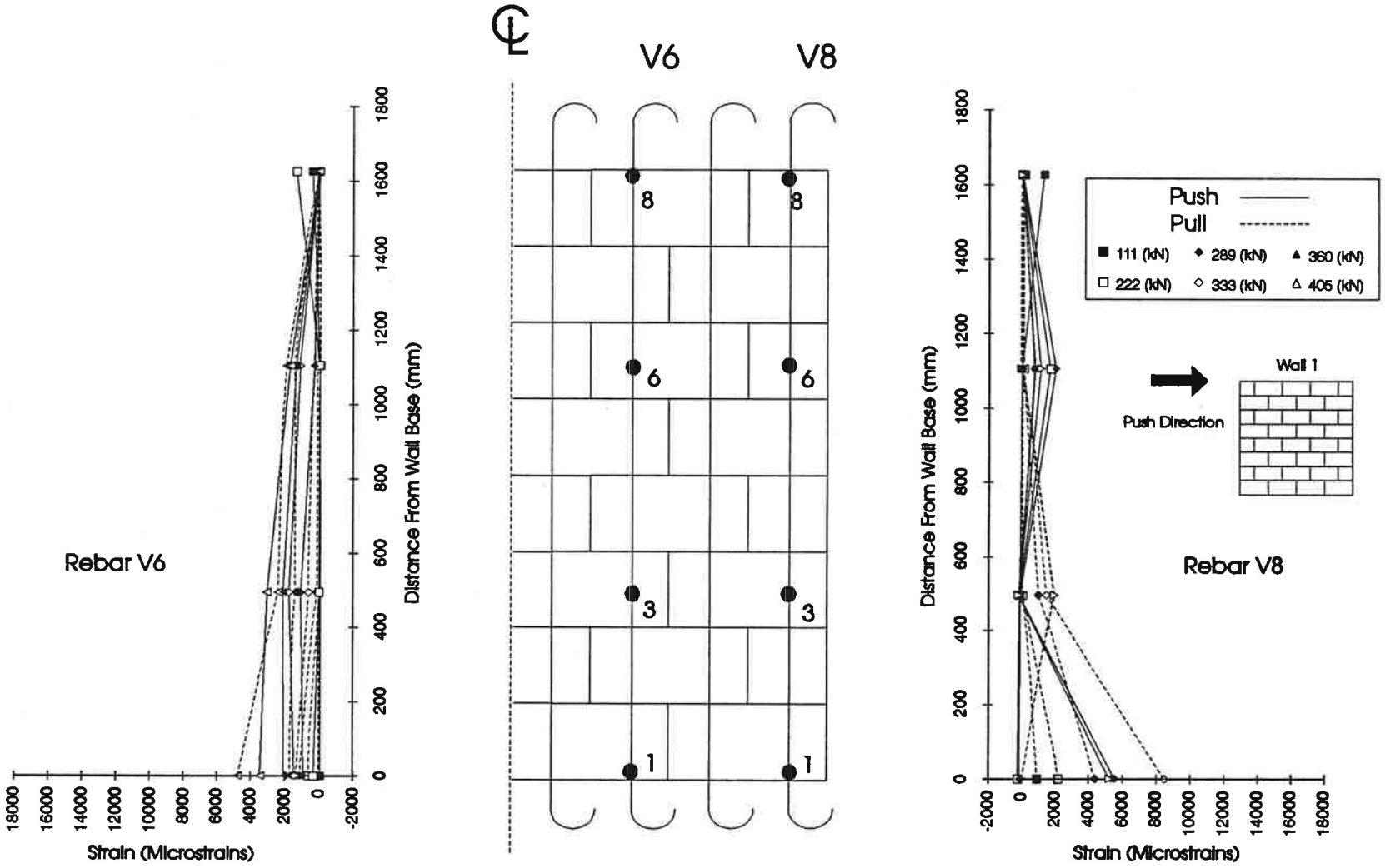

Figure 3.13 Monolithic Wall Strain Distribution of Bars V6 and V8

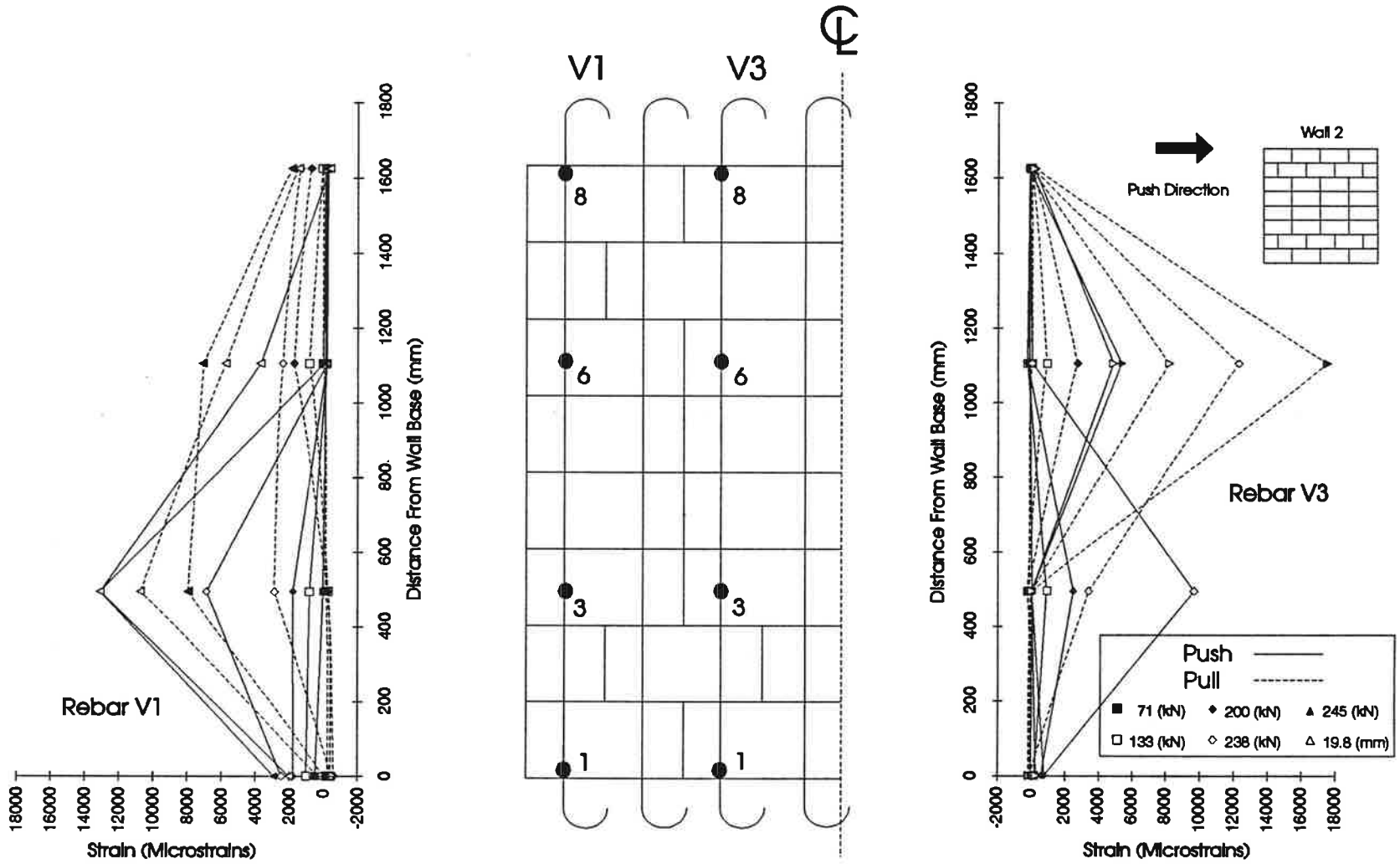

Figure 3.14 Slitted Wall Strain Distribution of Bars V1 and V3

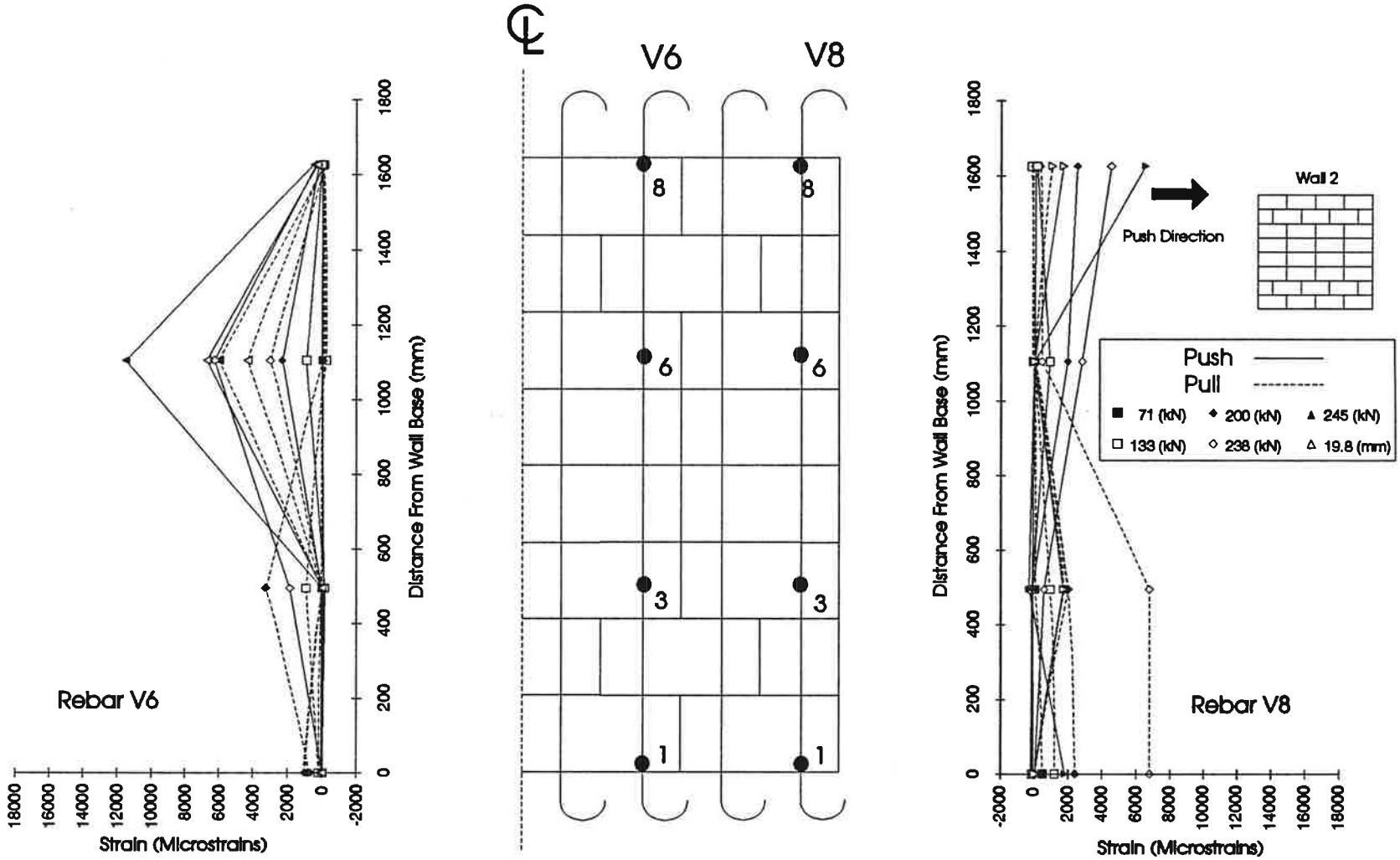

Figure 3.15 Slitted Wall Strain Distribution of Bars V6 and V8

and bottom of the wall. The middle bars, three and six, have fairly uniform strains unlike the outer bars which have relatively high strains at their ends.

3.5.2 Slitted Wall

In the slitted wall, the effect of the slits is immediately visible. On the vertical bars the strains concentrate at the top and bottom of the slitted portion of the wall. The strain plots in Figures 3.14 and 3.15 show peak strains at the top or bottom of the slits. The outer gages at the top and bottom of the overall wall, have relatively small strains. All four bars plotted participate similarly in resisting the applied loads.

3.5.3 Comparison of the Slitted and Monolithic Walls

The maximum strains for the slitted wall are two times larger than the monolithic wall. The slitted wall has its highest strains at the top and bottom of the slitted portions unlike the monolithic wall which has its highest strains at the top and bottom of the overall wall. The strains in the vertical bars of the slitted wall are fairly evenly distributed through the wall. This illustrates that each individual vertical reinforcing bar of the slitted wall contributes in a fairly uniform fashion in resisting lateral loads in flexure, whereas the outermost vertical bars of the monolithic wall contribute the most in resisting lateral loads by flexure.

3.6 Horizontal Distribution of Shear Reinforcement Strains

Figures 3.16, 3.17, 3.18 and 3.19 show horizontal steel strains for the monolithic wall at sections two, four, six and eight respectively, and Figures 3.20, 3.21 and 3.22 show horizontal steel strains for the slitted wall at sections two, four and seven respectively. For the horizontal bars, the figures illustrate the strain along the length of the bar at various loads in the push and pull directions.

3.6.1 Monolithic Wall

The middle sections four and six show the highest strains. The largest horizontal rebar strain for the monolithic wall was at section four in Figure 3.17. The largest strain exceeded 8000 microstrains, which is greater than three times the yield strain, and

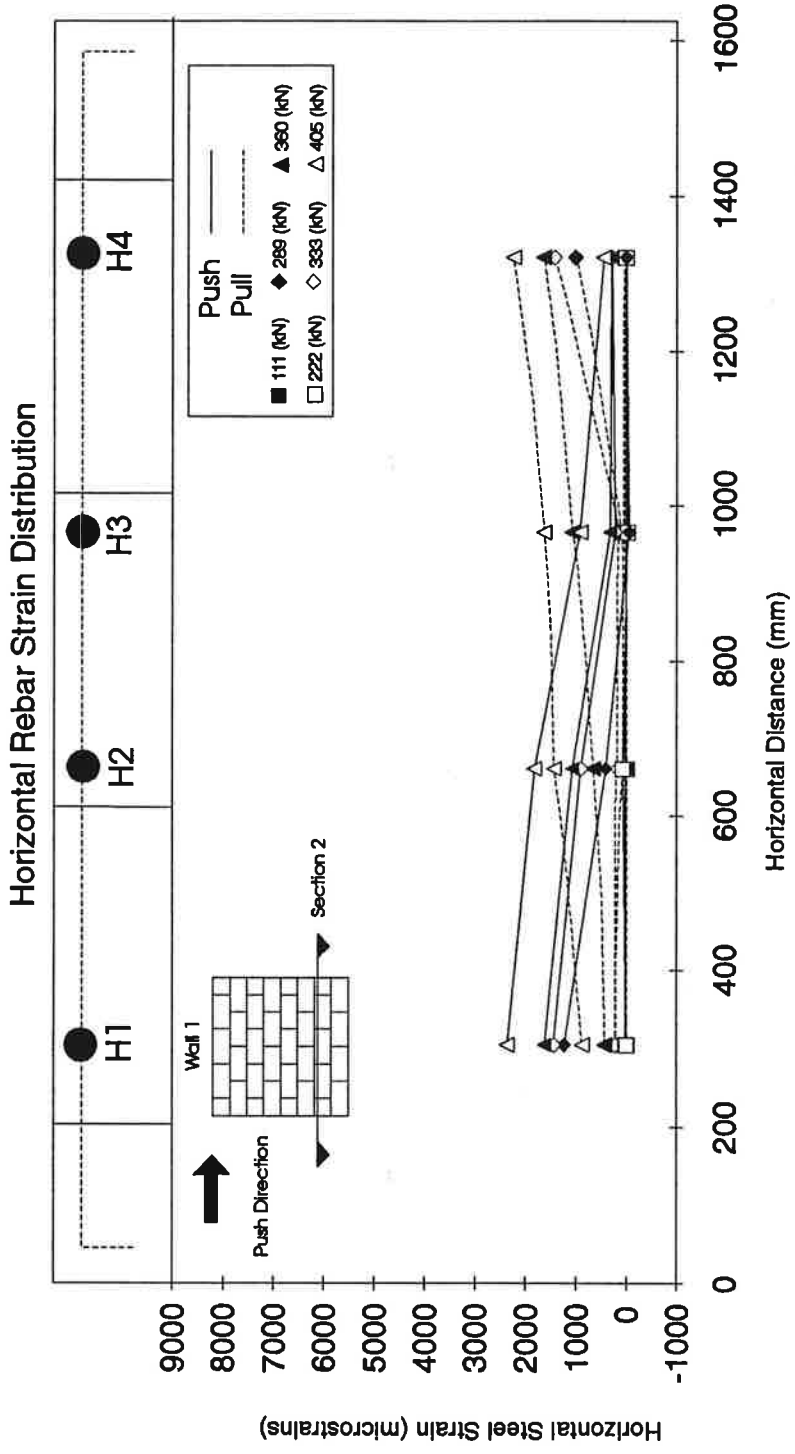

Figure 3.16 Monolithic Wall (Section 2) Horizontal Bar Strain Distribution

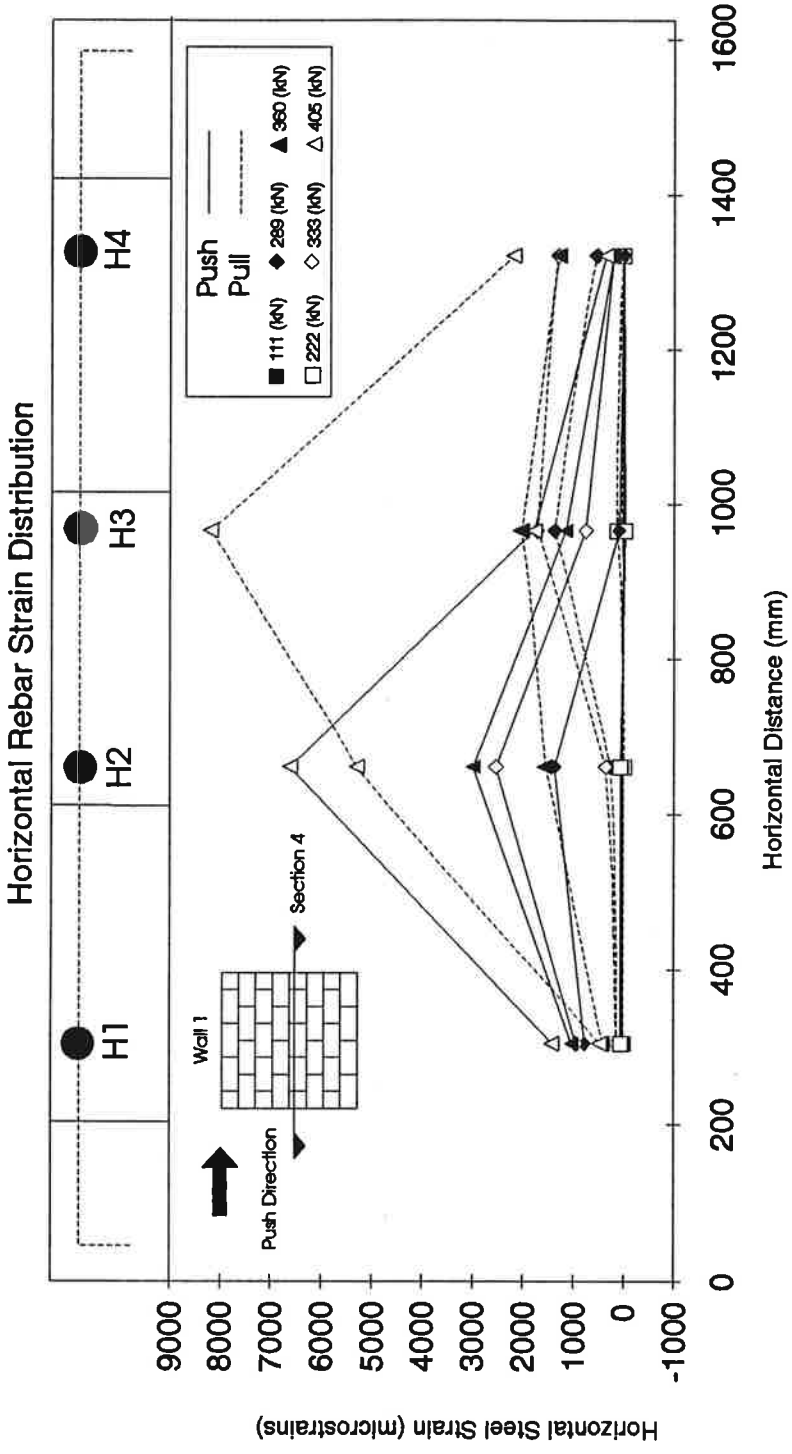

Figure 3.17 Monolithic Wall (Section 4) Horizontal Bar Strain Distribution

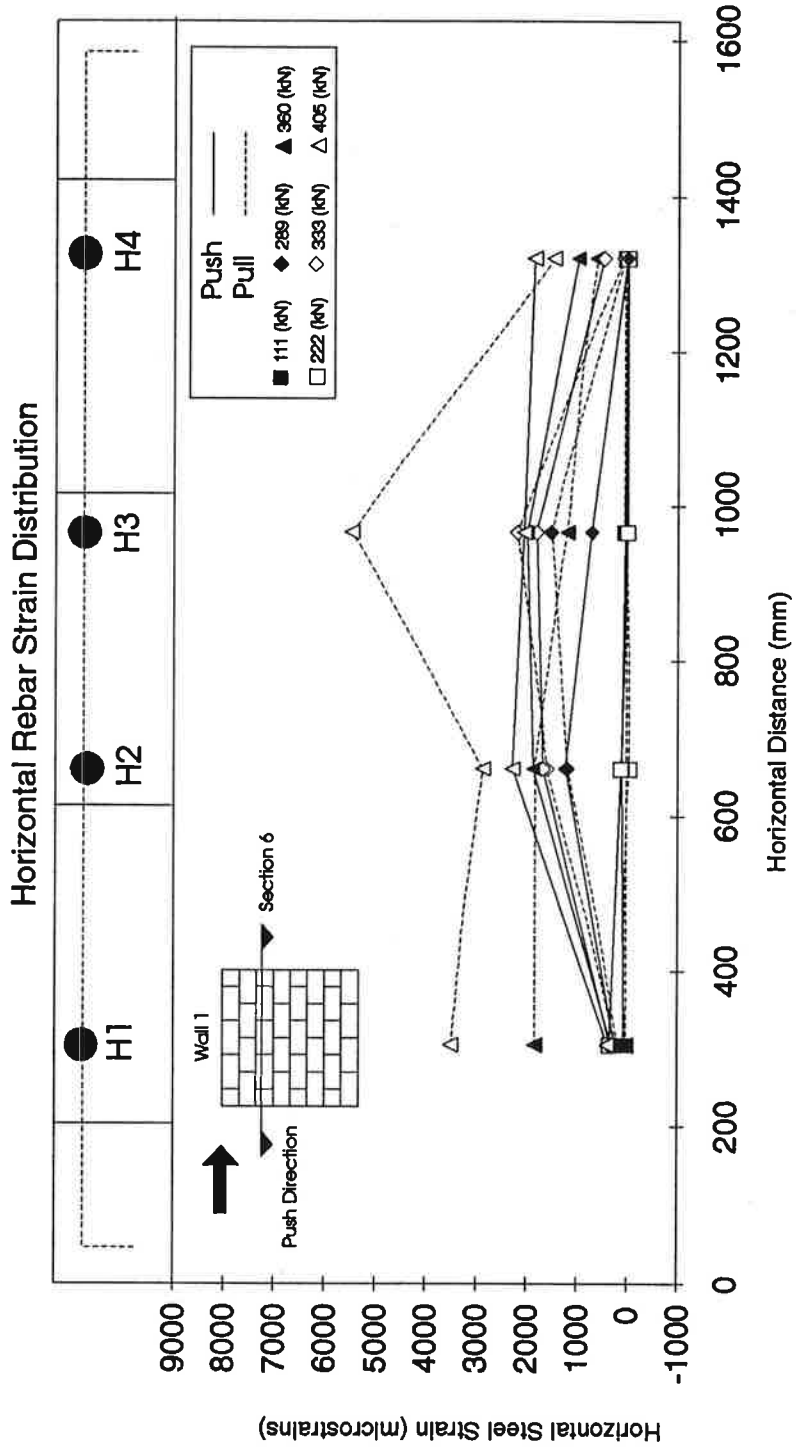

Figure 3.18 Monolithic Wall (Section 6) Horizontal Bar Strain Distribution

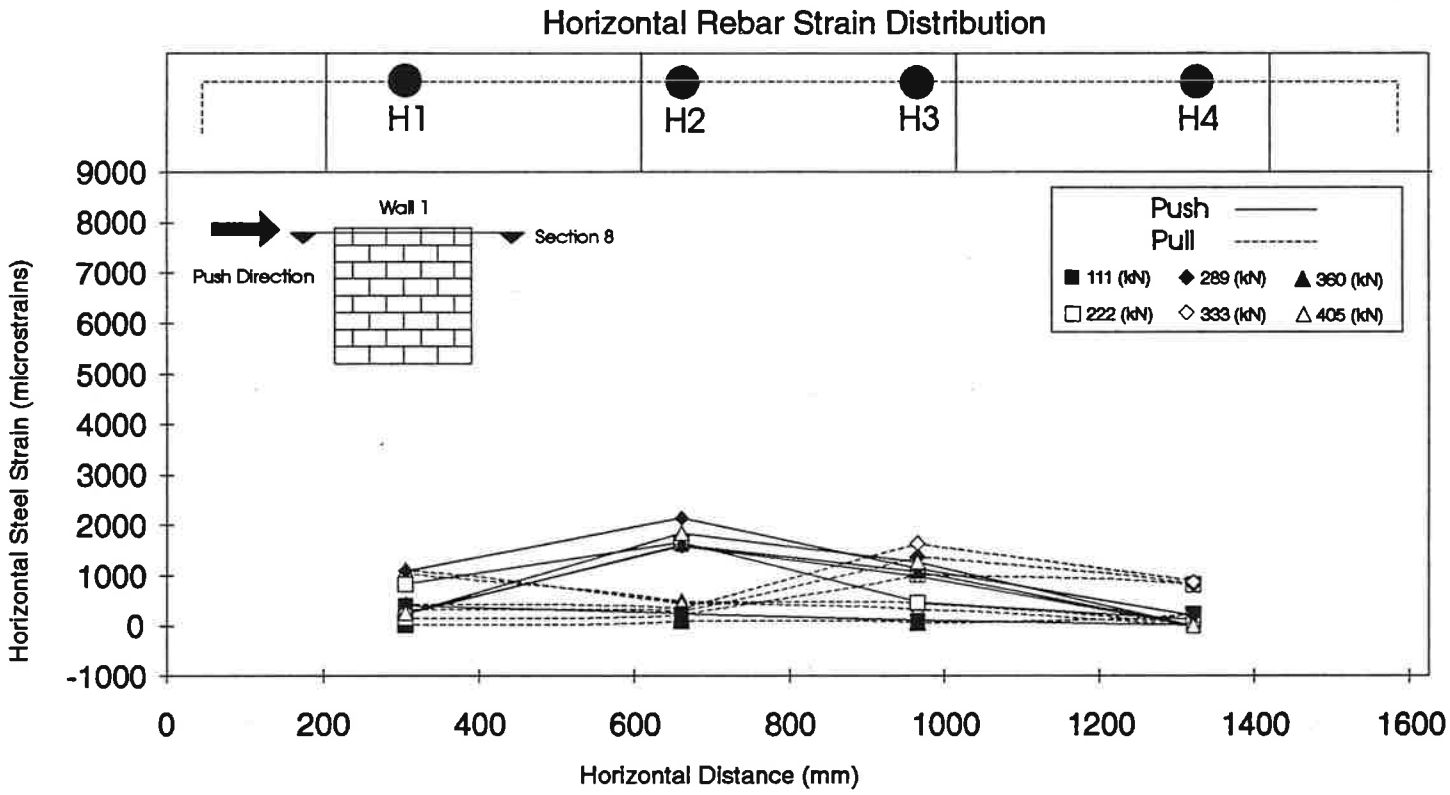

Figure 3.19 Monolithic Wall (Section 8) Horizontal Bar Strain Distribution

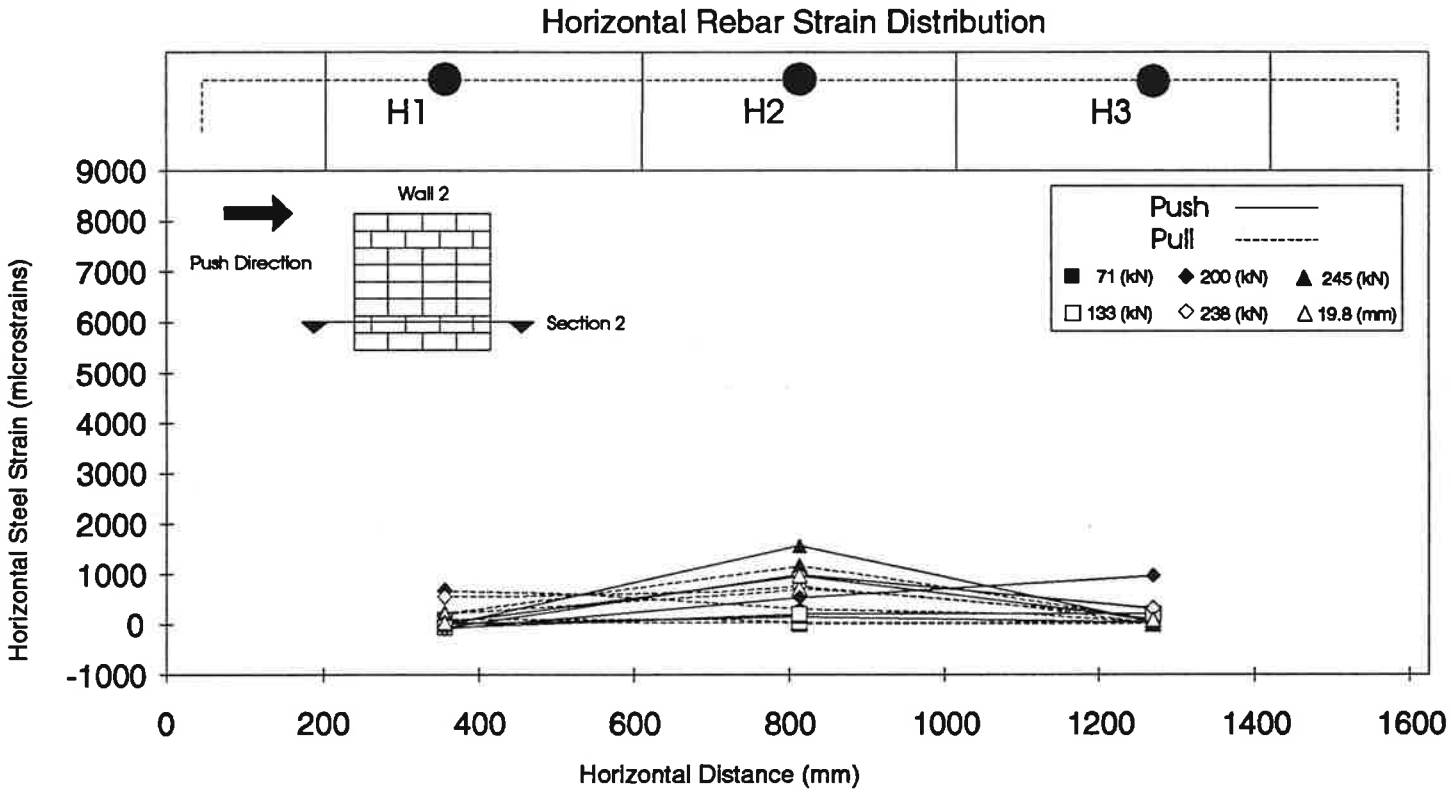

Figure 3.20 Slitted Wall (Section 2) Horizontal Bar Strain Distribution

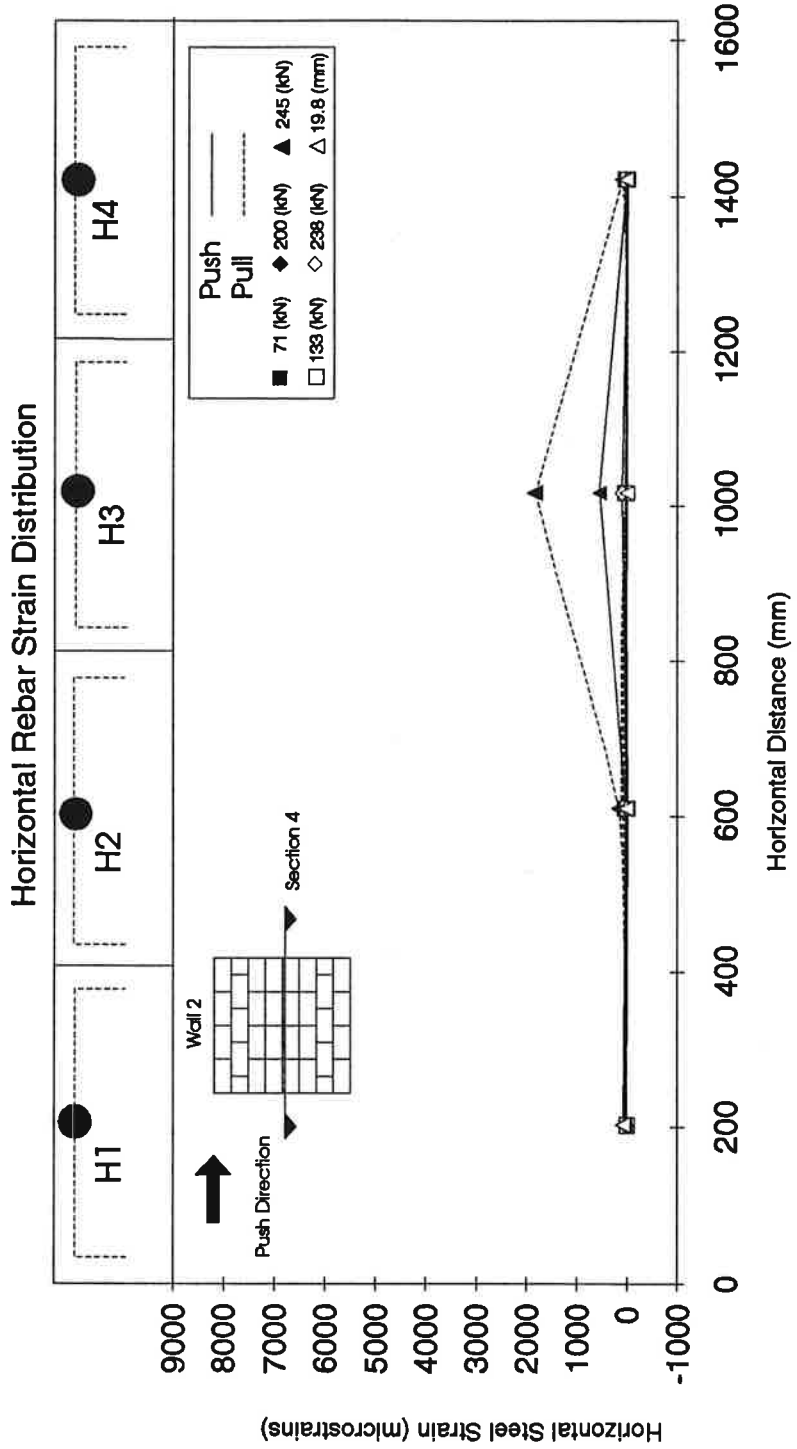

Figure 3.21 Slitted Wall (Section 4) Horizontal Bars Strain Distribution

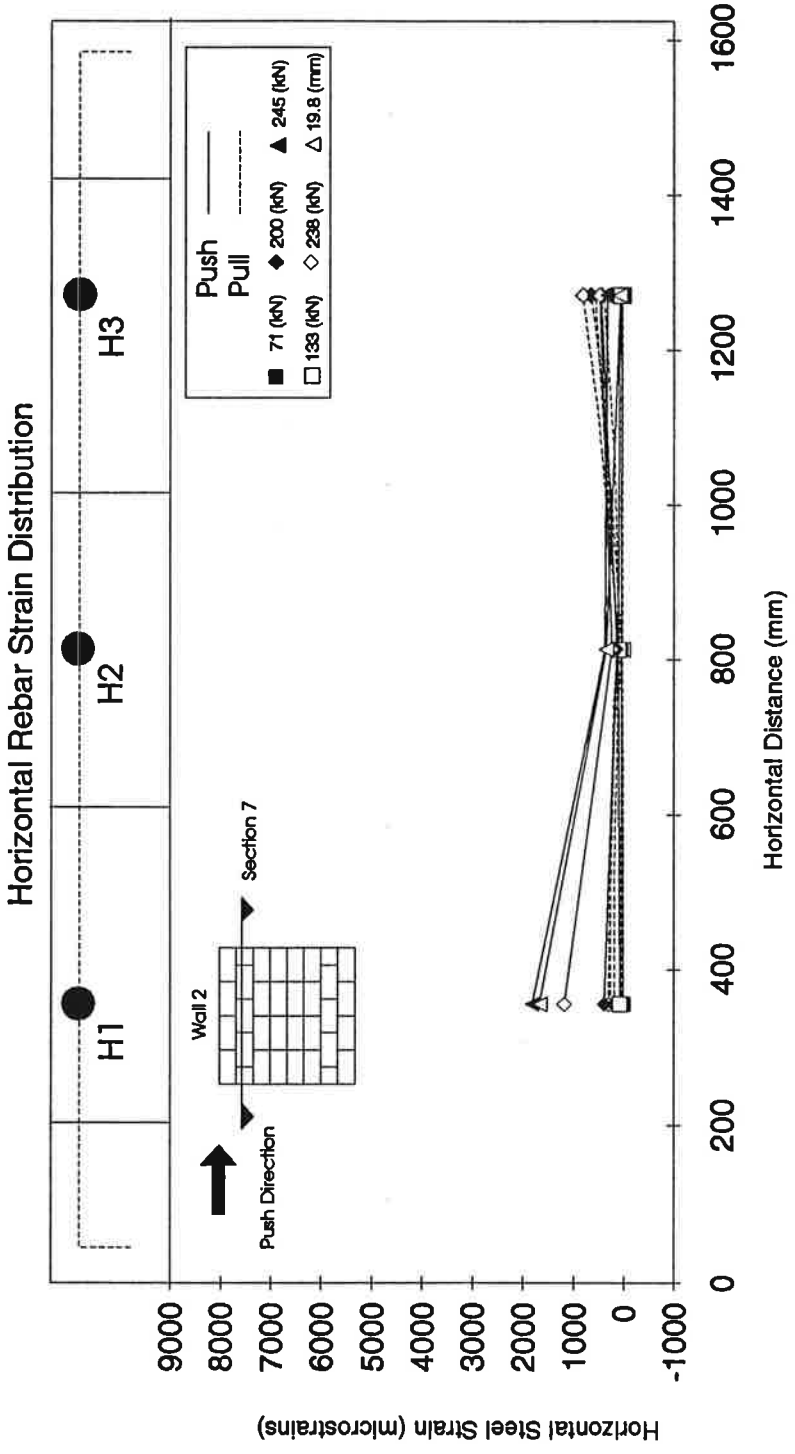

Figure 3.22 Slitted Wall (Section 7) Horizontal Bar Strain Distribution

occurred at the largest applied load of -405 kN. Sections two and eight of Figures 3.16 and 3.19 show smaller strains of less than 3000 microstrains. For the top and bottom bars in Figures 3.16 and 3.19 strains were fairly uniform across the section. However, for horizontal bars in Figures 3.17 and 3.18, the strains are largest in the middle portion of the wall.

3.6.2 Slitted Wall

For the slitted wall, only three horizontal sections were plotted, and these sections are two, four and seven. For section two shown in Figure 3.20, the strains are fairly uniform across the section and these strains are less than the yield strain. Figure 3.21 shows section four which is across the slitted portion of the wall. As can be seen, the strains in the individual bars of each pier are very small. Although pier three shows a more noticeable strain relative to the other three piers, the strain of pier three is less than yield strain. The highest section shown in Figure 3.22 again indicates small strain levels. None of the strains at this section are above yield. Perhaps the most noteworthy result is the almost nonexistent strains of section four through the slitted portion of the wall. This seems to indicated that the shear strains in the wall are evenly distributed to each of the four piers.

3.6.3 Slitted Wall Compared To Monolithic Wall

The most notable difference between the two walls is the magnitude of strain in the horizontal reinforcing steel. By including the slits in the slitted wall, the shear stress is more evenly distributed across the wall. This fact is evident as none of the horizontal rebar of the slitted wall indicated yielding of steel, whereas every horizontal rebar in the monolithic wall showed yielding of the reinforcement. The strain magnitude in the horizontal reinforcement of the monolithic wall was as large as four times the yield strain. Where the slitted wall showed the smallest rebar strains in the slitted cross-section, the monolithic wall showed the highest strains near the similar middle unslitted portion of the

wall. Slits in the shear panel redistribute the flow of diagonal shear stress more evenly across the wall.

3.7 Deflections

The lateral displacement of the wall is estimated by summation of flexural and shear deformations. The equation for shear deflection is

$$\Delta_s = \frac{1.2Vh}{AG} \tag{3.6}$$

and the equation for flexural deflection before cracking is

$$\Delta_f = \frac{Vh^3}{12EI} \tag{3.7}$$

Combining equations (3.7) and (3.8) yields the cracking deflection [1],

$$\Delta_{cr} = \frac{V_{cr}h^3}{12EI} + \frac{1.2V_{cr}h}{AG} \tag{3.8}$$

where,

Δ_f = deflection of wall in double flexure

Δ_s = shear deflection of wall

Δ_{cr} = cracking deflection

V = lateral force applied at the top of the wall

V_{cr} = lateral force at which flexural cracking occurs

h = clear height of wall

E = modulous of elasticity for masonry

I = moment of inertia of the masonry shear panel

A = cross-sectional area of the masonry shear panel

G = shear modulous for masonry

The basic theory above was used to calculate theoretical deflections up to the cracking deflection. For deflections beyond the cracking, the moment-area method for deflection calculation as presented in reference [1] was used to determine the theoretical yield and ultimate deflections. These theoretical values of Δ_{cr}, Δy, and Δ_u were used to calculate theoretical drift angles which are compared to the experimental values in the conclusion of Chapter 4.

3.8 Ductility

In structural design, ductility can be defined as the ability of a structure to maintain resistance to repeated application of cyclic loads in the inelastic range. A large ductility capacity implies that the structure can sustain large deformations while absorbing energy by hysteretic behavior. In ductile structures the lateral strength is maintained while undergoing large inelastic deformations.[7] The ultimate displacement ductility capacity of a specimen can be defined as:

$$\mu = \frac{\Delta_u}{\Delta_y} \tag{3.9}$$

where,

Δ_u = ultimate displacement

Δy = elasto-plastic yield displacement

Equation (3.9) provides a measure of a structural element's ability to deflect inelastically beyond first yield. By dividing the displacement by the height of the specimen, equation (3.9) is equivalent to the ratio of ultimate drift angle to the yield drift angle. A comparison of ductility between the monolithic and slitted walls is made in Chapter 4.

3.9 Curvature

The curvature of the wall was determined by taking measurements of vertical displacement along both edges of each wall. Figure 2.6(a) shows the location of the linear potentiometers used for curvature measurement. The results for the monolithic wall are

plotted in Figures 3.23 and 3.24, and the results for the slitted wall are plotted in Figures 3.25 and 3.26. Two plots are used for each wall to show curvature for push cycles and pull cycles separately.

3.9.1 Monolithic wall

The curvature distribution along the height of the monolithic wall is represented in Figures 3.23 and 3.24, which show the push and pull cycles respectively. In the push direction, the curvature is axis-symmetric and exhibits curvature as expected associated with reversed bending. Curvatures as large as 0.0005 rads/mm are visible by looking at the plots and occur at 200 mm from the bottom and the top of the wall. This is expected since the top and bottom of the wall are the areas of highest bending moment. The 200 mm distance is approximately the height of one course of blocks. Similar magnitudes of curvature were recorded at the top and bottom section of the wall.

In the pull direction, the wall behaves similarly to the push direction. Maximum curvatures are in the same range and inelastic curvature occurs in the same areas as expected. Reversed curvature is again achieved. Figure 3.24 shows curvature in the pull direction with an unexpected value at ultimate load at the top of the wall. Spalling of masonry dislodged the instrumentation near the top of the wall and affected the curvature measurement causing the unexpected value.

3.9.2 Slitted Wall

In contrast to the curvature distribution in the monolithic wall, the curvature of the slitted wall shows a more uniform distribution. Small curvatures were recorded at the center of the wall. However, a noticeable transition in curvature occurs where the slits of the wall stop at both the upper and lower ends of the vertical slits. This is largely due to the change of stiffness at these regions of the wall.

The plot of the curvature distribution in the slitted wall in the pull direction is similar to the push direction. However, a slightly higher curvature was noted at the base of the wall in the push cycle (Figure 3.25). In general, the wall showed very small

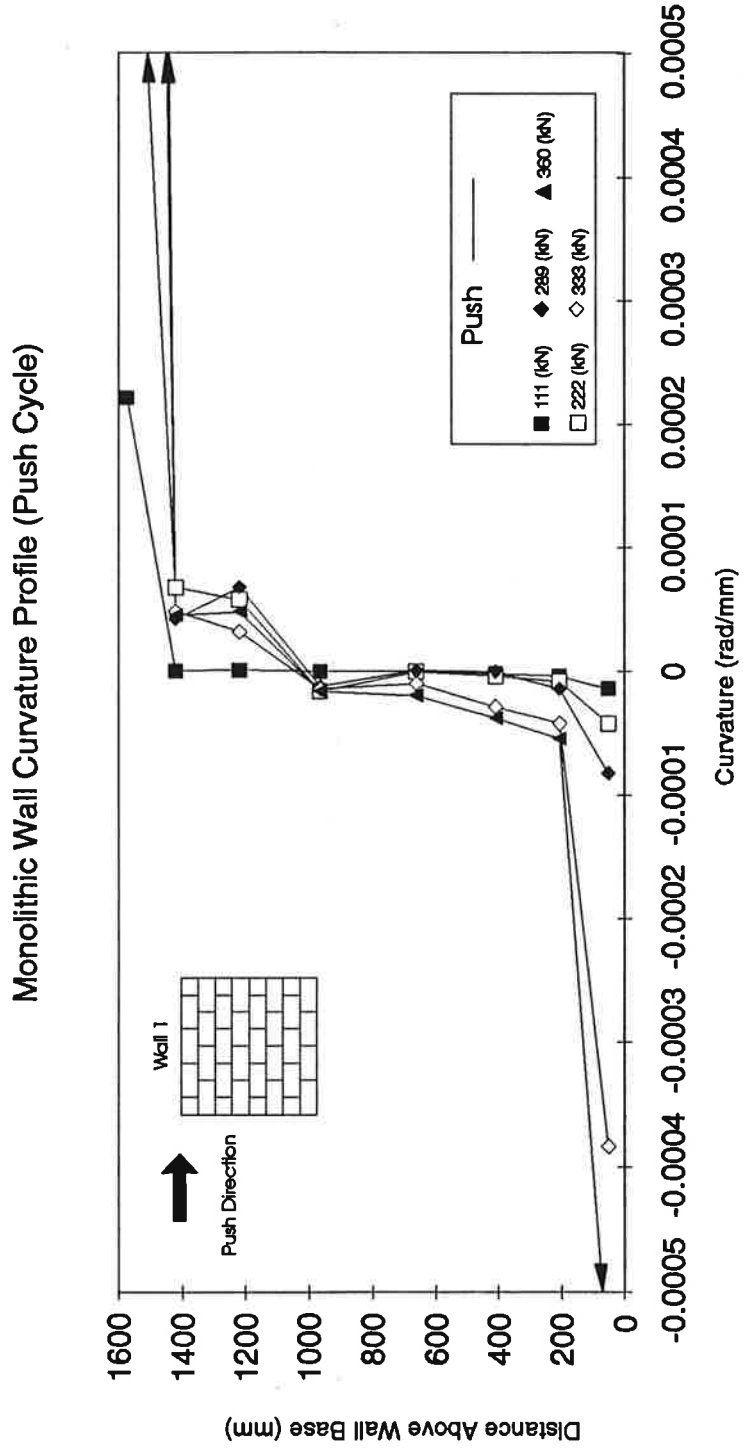

Figure 3.23 Monolithic Wall Push Cycle Curvature Profile

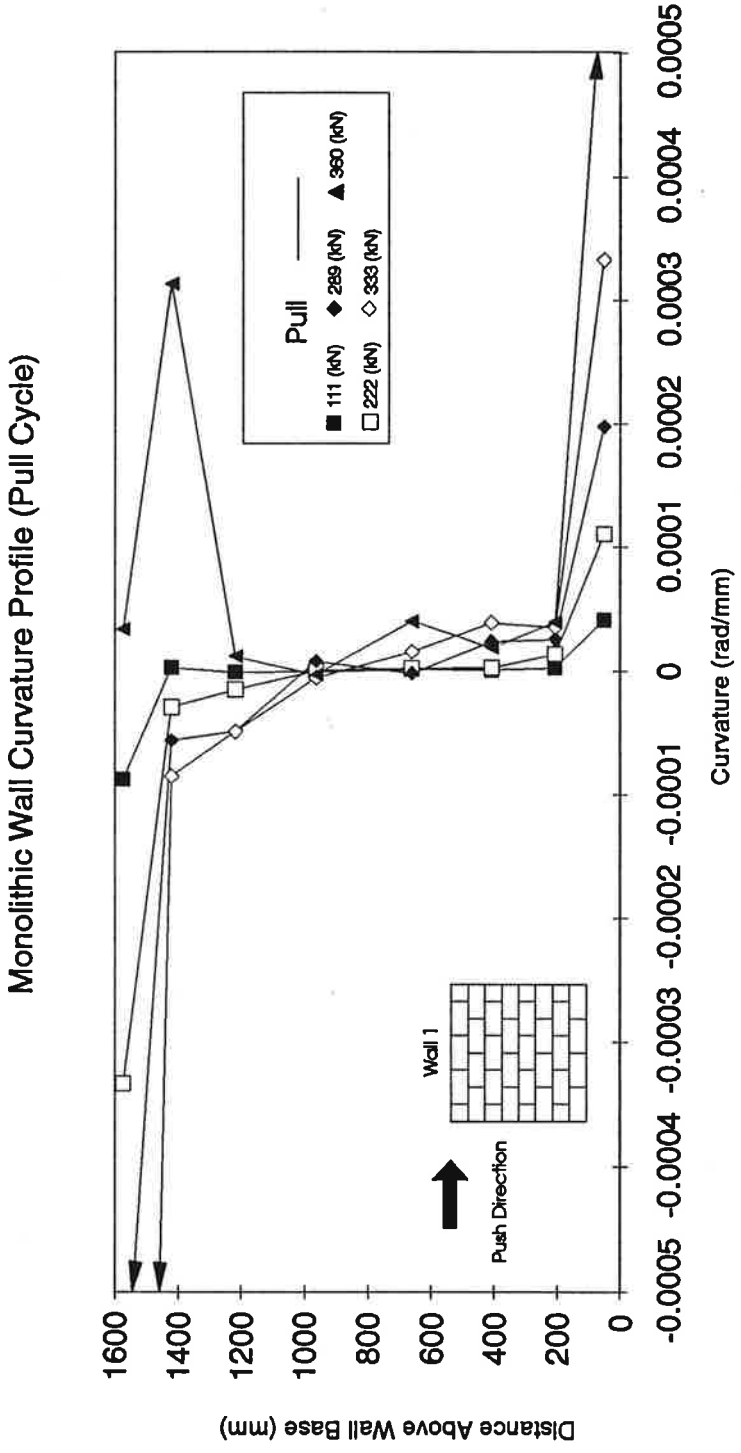

Figure 3.24 Monolithic Wall Pull Cycle Curvature Profile

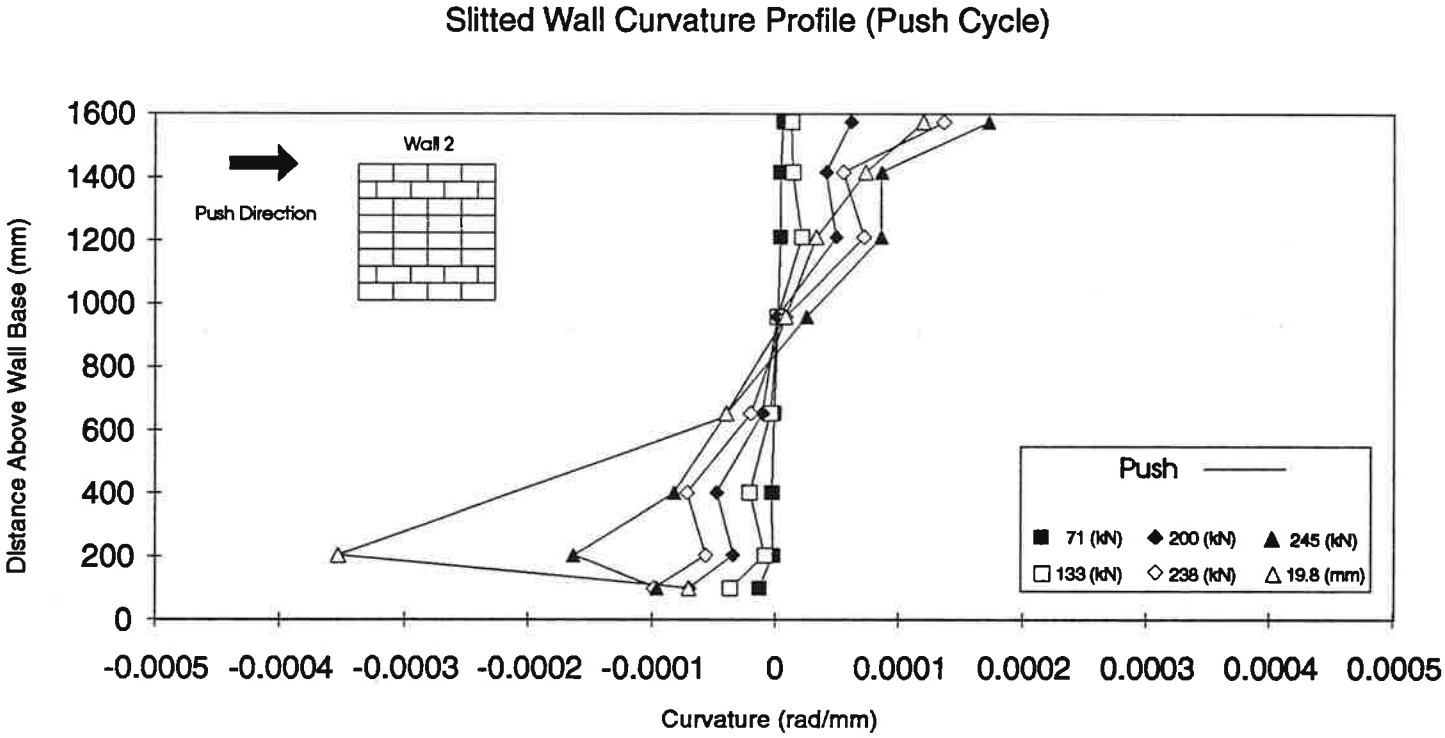

Figure 3.25 Slitted Wall Push Cycle Curvature Profile

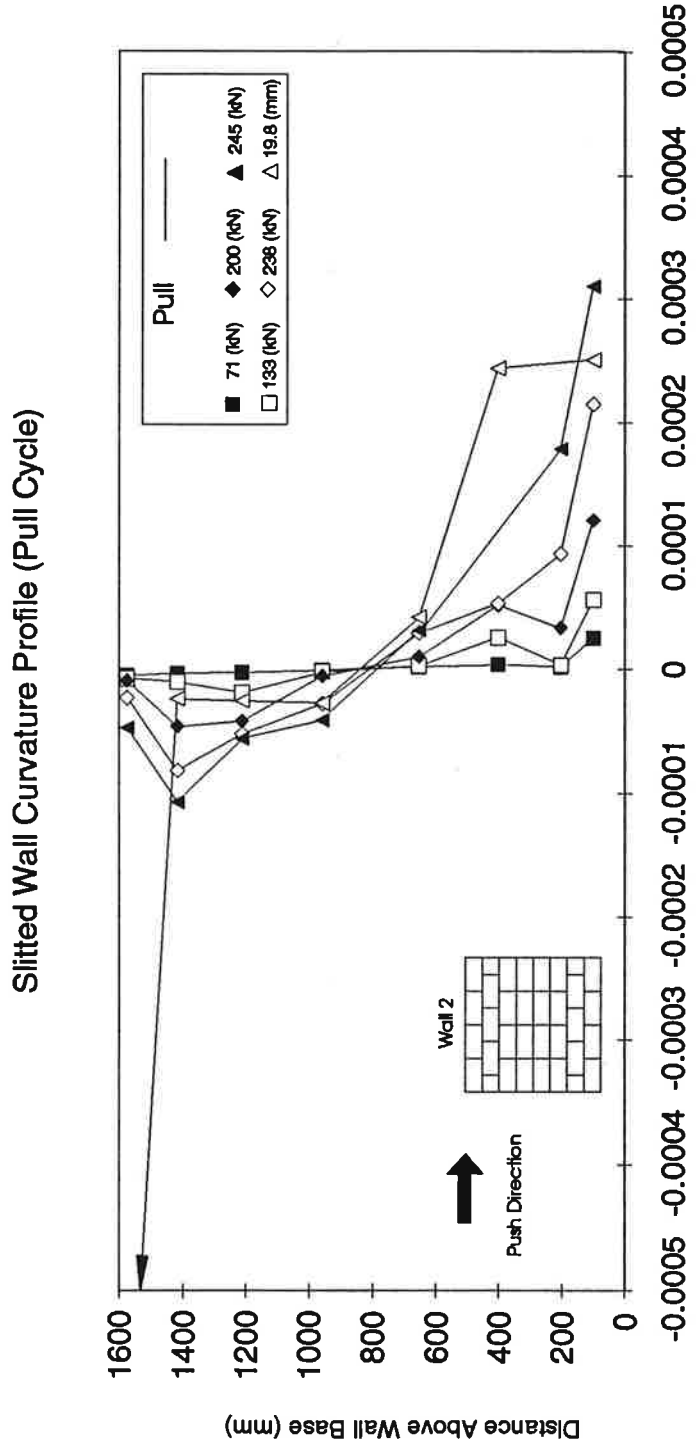

Figure 3.26 Slitted Wall Pull Cycle Curvature Profile

curvature in the middle, and increased curvature towards the top and bottom of the wall. Noticeable changes in curvature again occur at the top and bottom of the vertical slits.

3.9.3 Slitted Wall Compared To Monolithic Wall

In general, the largest curvatures were recorded at the top and bottom of the walls. The most notable difference between the two walls lies in the shape of the curvature distributions. Curvatures for the slitted wall increase gradually from the middle of the wall to the top and bottom of the wall. The monolithic wall however shows very low curvature in the middle of the wall with a gradual increase towards the two ends, but increases abruptly at approximately 200 mm from the top and bottom of the wall. For the slitted wall the curvature is more uniformly distributed along the height.

3.10 Crack Patterns

At the peak loads of each load cycle, cracks were highlighted on the test specimens with a red or blue felt tip pen. The load level was also written next to the crack. Blue corresponds to cracks occurring during push load cycles and red corresponds to pull load cycles. This technique enabled the history of crack development to be documented as damage progressed throughout the testing. Both flexural and shear cracks were observed during the tests. Shear cracks followed mortar joints as well as propagating through masonry blocks. Flexural cracks tended to follow mortar joints.

3.10.1 Monolithic Wall

Minor flexural cracking was noted in the monolithic wall specimen during the initial stages of loading. At a lateral force of V = 111 kN (25 kips), two flexural cracks extending for about the length of one masonry block were noted in the top two bed joints. No flexural crack was observed in the bottom region. The difference in crack pattern was due to the application of the concentrated axial force on top of the specimen. A non-uniform axial stress distribution resulted in the upper region with higher compression directly under the axial force while a more uniform distribution of axial stress existed in the bottom region. The lesser axial compression in the outer fibers caused more flexural

cracking in the upper region. At a higher lateral force of V = 222 kN (50 kips), the flexural cracks were seen to extend as inclined cracks into the face shell of the masonry blocks in the top two courses. Two inclined web-shear cracks first appeared in the center region of the wall at a lateral force of V = 289 kN (65 kips), one extending from the second course to the fifth course while the other extended from the fifth course to the seventh course. At the maximum lateral force of V = 407 kN (91.5 kips), major extension of diagonal cracking occurred and these cracks extended all the way to the bottom course of the wall, as can be seen in Photos B.7 and B.8. The diagonal cracks were, however, wider in the upper region than the bottom region of the wall due to the application of lateral force at the top of the specimen. A large difference in force existed between the two points of the top concrete beam where the lateral force was transferred from the pin-ended steel struts. This differential force resulted in a net horizontal tensile force in the upper region of the wall in the push direction. Final failure of the wall involved widening of the diagonal cracks in the upper region of the wall and sliding of the upper two courses along the horizontal bed joints.

The Photos B.1 to B.8 in Appendix B show in chronological order the progression of cracking for the monolithic test wall. These photos are taken at the loads indicated, and show the push and pull cracks marked in blue and red respectively.

3.10.2 Slitted Wall

For the slitted wall specimen, no cracks were noted during the three initial cycles to V = 67 kN (15 kips). Flexural cracks first appeared at a lateral force of V = 133 kN (30 kips) in the top and bottom two courses and at the ends of the 'mini'-piers formed by the vertical slits. These flexural cracks extended horizontally along the bed joint for about half a masonry block. At a higher lateral force of V = 207 kN (46.5 kips), the flexural cracks at the ends of the outer two 'mini'-piers extended as inclined flexure-shear cracks and propagated away from the slitted region into the continuos region of the wall. For the inner 'mini'-piers, similar flexure-shear cracks developed but these cracks propagated into

the 'mini'-piers. The propagation of the flexure-shear cracks into the center region of the inner 'mini'-piers and not in the outer 'mini'-piers suggested that the inner 'mini'-piers were resisting a larger proportion of the total shear force. With increased loading to the maximum lateral force of V = 261 kN (58.7 kips), the differential shear deformation of the 'mini'-piers caused a compression in the polystyrene sheets, and led to an eventual contact of the 'mini'-piers. The post-peak crack pattern was dominated by the propagation of major diagonal cracks in the inner two 'mini'-piers into the continuous region of the wall. The final crack pattern of the slitted wall can be seen in Photos B.15 and B.16. Note the closure of the vertical separation joints and spalling of the face-shell masonry at the top of the inner 'mini'-piers in Photo B.16.

Photos B.9 to B.16 in Appendix B show in chronological order the progression of cracking for the slitted test wall. Again the push and pull cracks are marked in blue and red.

Both the slitted wall and the monolithic wall had predominant shear cracks; however, both did have flexural cracks. In general shear cracks for both walls propagated across masonry blocks, while flexural cracks tended to follow mortar joints. Spalling also occurred for both walls near the end of testing. Spalling tended to focus in regions of high flexural compressive stress.

The monolithic wall had shear cracks typically at 45 degrees, whereas the slitted wall shear cracks were typically a steeper angle than 45 degrees. More cracking seemed to concentrate in the center of the wall for the slitted wall than was the case for the monolithic wall. The diagonal tension stress cracks present on the monolithic wall were forced to redistribute themselves on the slitted wall. This observation is perhaps the most visible result caused by the addition of slits.

Chapter 4

Discussion and Conclusions

4.1 General Summary of Research

Much research is devoted to increasing the ductility of structural elements. Ductile structural elements can enhance the survivability of an entire building structure if designed properly. The intent of this research was to test a new idea for increasing the ductility of masonry shear panels. Since walls are often used as lateral resisting elements of structures there is direct practical application of this research.

In order to test the new idea, two walls were tested. The first wall was constructed in a typical running bond pattern and grouted monolithically. The second wall was constructed in a running bond pattern for the bottom two and top two courses of block. The middle four courses were placed in a stacked bond pattern. This allowed three slits, four blocks high, in the middle of the wall. Figure 2.1 illustrates the arrangement of masonry blocks for each wall described above.

Both walls had continuous vertical reinforcing in every cell. The monolithic wall also had continuous horizontal reinforcing at every course. While the slitted wall only had continuous horizontal reinforcing at the top and bottom two courses. The middle four courses had horizontal reinforcing, but the reinforcing was discontinuous at the slits. These slits were filled with sheets of polystyrene. Essentially the slitted wall had four piers in its center. Reinforcing steel arrangements can be seen for the two walls in Figure 2.2.

Each wall was subjected to reversed cyclic in plane lateral loads. The loads were applied to induce double bending of the walls. A constant axial load was also applied during testing to simulate typical gravity loads. Data was recorded by using strain gages on the reinforcing steel and linear potentiometers on the exterior of the wall. This allowed strain profiles at different load levels to be plotted graphically. Also wall curvature and hysteresis loops were developed by using external instrumentation data. The graphs and results of the instrumentation measurements are presented in Chapter 3.

The remainder of this chapter will briefly summarize results and present conclusions for each wall and the research as a whole.

4.2 Comparison Between Monolithic Wall and Slitted Wall

The focus of this study was to test and compare two walls that were constructed differently. One wall was constructed monolithically and the other was constructed with slits. This single difference causes many of the resulting differences in characteristics between the two walls. During testing the slitted wall had different crack patterns, stiffness, strength, curvature, and ductility than the monolithic wall. The slitted wall was of lower strength, but more flexible and had more ductility. Strain profiles for the slitted wall were also much different than in the monolithic wall.

4.3 Load Versus Drift Angle Curves

By examining the quantitative information of Figure 4.1 additional comparisons can be made between the two walls. As stated previously the slitted wall is more flexible, and thus requires less lateral force for a given drift angle, than the monolithic wall. The slitted wall experimental load versus drift angle follows the theoretical prediction in strength fairly well. The theoretical prediction was based on flexural strength, and since the experimental curve follows the theoretical curve of the slitted wall a flexural mode of failure is indicated. One should also note that the ultimate experimental drift angle for the slitted wall is much larger than the theoretical prediction. Also it can be seen from Figure 4.1 that the slitted wall sustained a higher drift angle at its ultimate load than the monolithic wall. The monolithic wall experimental load versus drift angle does not follow the theoretical curve very well. Also the experimental ultimate load did not reach the theoretical ultimate flexural-based lateral force. This indicates that the monolithic wall failed in a shear mode rather than a flexural failure mode. Hence, the ultimate shear strength of the monolithic wall is less than the ultimate flexural-based lateral force.

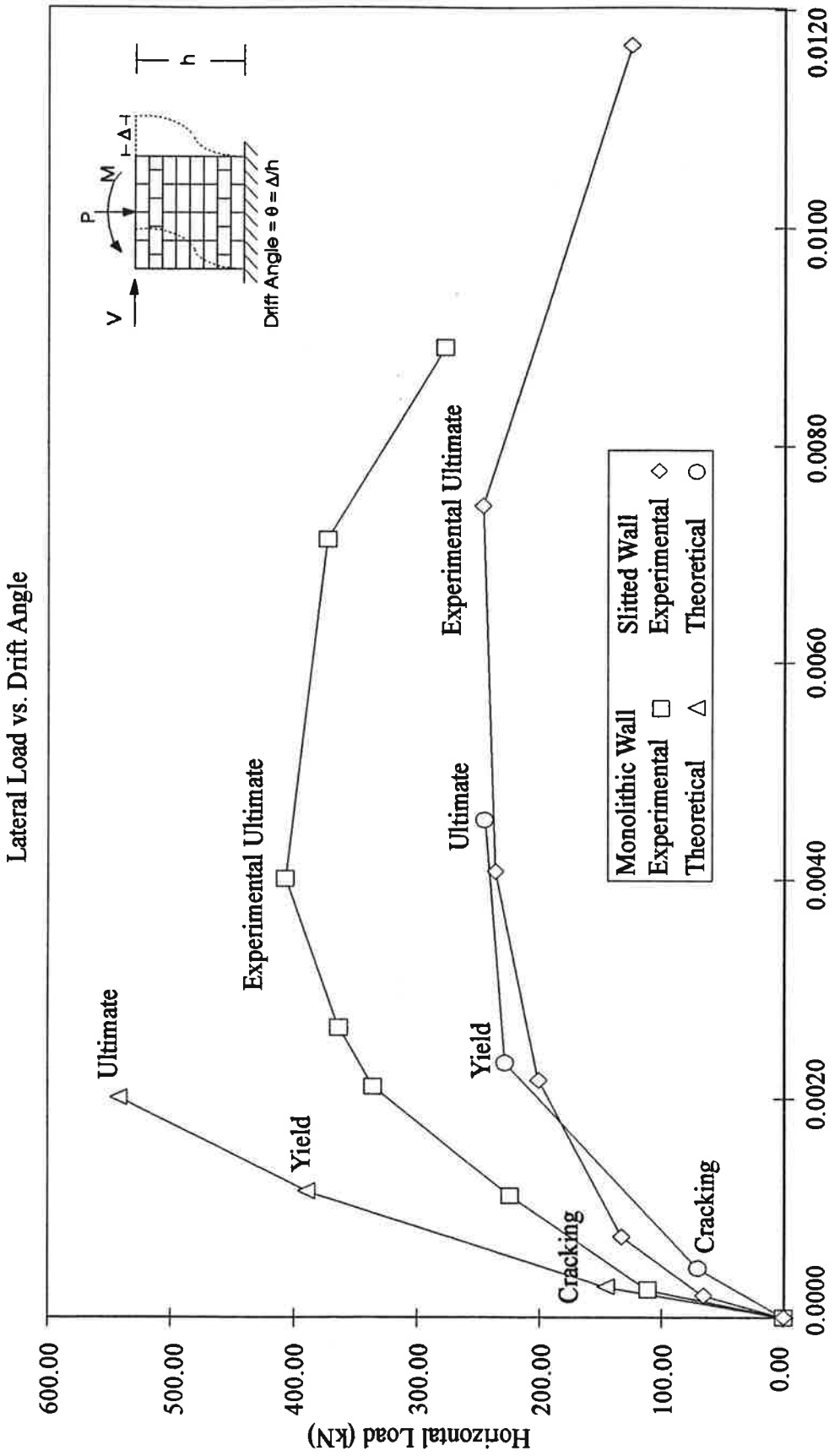

Figure 4.1 Experimental Versus Theoretical Drift Angle for Monolithic and Slitted Walls

4.4 Drift Angle

The drift angle limit states are labeled on the load deformation envelope in Figure 4.1. The theoretical and experimental drift angles at cracking, first yield, and ultimate limit states for the two walls are listed in Table 4.2. The stiffness at theoretical first yield for the monolithic wall is almost 6.5 times greater than the slitted wall at theoretical first yield. At experimental first yield the monolithic wall is twice as stiff as the experimental first yield of the slitted wall. These comparisons were reached by using the flexural based yield shear forces of Table 4.1 and yield drift angles presented in Table 4.2. Theoretical and experimental cracking drift angles for the monolithic wall were in good agreement. For the slitted wall, the theoretical and experimental cracking drift angles did not agree very well. In fact the slitted wall was stiffer than the theoretical predication indicated. The yield drift angles for the slitted wall agree fairly well experimentally and theoretically. For the monolithic wall the theoretical and experimental yield drift angles did not agree very well. This is due to the fact that the monolithic wall was not following a flexural failure mode, but rather a shear mode of failure dominated by significant diagonal cracking during first yield. Therefore, the monolithic wall degraded in stiffness faster then was predicted in theory. The ultimate drift angles for the two walls did not agree with the theoretical predictions. The reduction in stiffness due to the degradation of the walls, which occurred during testing, may contribute to the discrepancy between the theoretical and experimental ultimate drift angles.

The lateral stiffness of the slitted wall was smaller than the monolithic wall. Comparing the theoretical stiffness up to yield, the monolithic wall was stiffer than the slitted wall. Experimentally, the monolithic wall was stiffer as well. The reduction in stiffness, of the slitted wall, can be attributed to the reduction in moment of inertia caused by the added slits. Four flexible piers at the mid-section of the slitted wall are less stiff than a monolithic shear panel.

	Ultimate Shear Strength	Flexural Based Shear		
Theoretical	Vn (*)	Vcr	Vy	Vu
Monolithic	383 kN	146 kN	390 kN	543 kN
Slitted	230 kN	71 kN	228 kN	245 kN
Experimental				
Monolithic	405 kN	111 kN	222 kN	-
Slitted	-	66 kN	200 kN	246 kN

(*) [12] UBC

Table 4.1 Shear Strengths for Monolithic and Slitted Walls

Drift Angle (radians)				
Theoretical	Cracking	Yield	Ultimate	Ductility
Monolithic	0.00028	0.0012	0.0020	1.67
Slitted	0.00045	0.0023	0.0045	1.96
Experimental				
Monolithic	0.00025	0.00211	0.00400	1.9
Slitted	0.00020	0.00216	0.00744	3.44

Table 4.2 Drift Angles and Ductility for Monolithic and Slitted Walls [1]

4.5 Ductility Ratio

Theoretical and experimental estimates of ductility are listed in Table 4.2 The theoretical ductility ratios were obtained by dividing the theoretical ultimate drift angles by the theoretical yield drift angles. The drift angle reached at the experimental ultimate load, for each wall, divided by the experimental yield drift angle is the experimental ductility ratio presented in Table 4.2. The slitted wall is 17% more ductile, theoretically, than the monolithic wall. The estimated experimental ductilities are in a similar range to the theoretical predictions. One objective of this research was to establish that the slitted wall was more ductile than the monolithic wall. These drift angle and ductility results support the conclusion that the slitted wall is in fact a more ductile wall.

The theoretical ultimate displacement ductility factor is calculated to be 1.67 for the monolithic wall and the theoretical displacement ductility factor for the slitted wall is 1.96. Experimentally, ultimate displacement ductility factor of the monolithic wall is 1.9. The experimental ultimate displacement ductility factor for the slitted wall is 3.44. This illustrates that the experimental displacement ductility factor of the slitted wall is 81% greater than the monolithic wall. And theoretically the displacement ductility factor for the slitted wall is 17% greater than the monolithic wall. As a result it can be said that a modest increase in ductility has been achieved by introducing slits into the construction of the masonry shear panel.

4.6 Shear Strength

The experimental and theoretical values of shear strength for the two walls are presented in Table 4.1. The monolithic wall failed in shear and had a higher experimental ultimate shear strength than predicted theoretically by the UBC by about 5.7%. The slitted wall failed in flexure and its ultimate experimental shear capacity compared very well with the theoretical flexural based ultimate shear capacity. The theoretical ultimate shear strength in Table 4.1 was calculated assuming that only the reinforcement provides shear strength when plastic hinging is induced as was the case in these tests. Thus the

monolithic wall ultimate shear strength was based on the strength provided by four #4 bars of 514 MPa (74.5 ksi) yield strength and four #3 bars of 414 MPa (60 ksi) yield strength. The theoretical ultimate shear strength of the slitted wall provided by the four individual 'mini'-piers were calculated similarly realizing that the reinforcement was provided in the 'mini'-piers solely by four #3 bars of 414 MPa (60 ksi) yield.

Where the cracking shear strength occurs, for each wall, was hard to establish by just observing the walls during the tests. It was difficult to see when the very first cracks started for each wall. A better way of experimentally determining the cracking load for each wall can be done by using Figure 4.1. Both of the two walls have a load versus drift angle curve which starts straight initially then bends sharply. This noticeable change in the load versus drift angle curve occurs approximately at the cracking load. Comparing the load at which these abrupt changes occur with the theoretical cracking loads for each wall reveals close agreements. Table 4.1 lists the approximated cracking loads for each wall determined experimentally from Figure 4.1. The theoretical cracking loads are listed as well.

The yield load for each wall was determined experimentally by noting at which load yielding is first indicated on a vertical bar strain gage. The loads at which first yield occurred are in Table 4.1 and can be compared to the theoretical predictions. The slitted wall fit the theoretical prediction fairly well. The monolithic wall, however, did not if one considers the indications of first yield as indicated by the rebar strain gages.

The experimental and theoretical lateral strength of the monolithic and slitted reinforced concrete walls were determined in this research. A distinct reduction in lateral strength occurred due to the included slits in the slitted wall. The reduction in strength of the slitted wall was 55% theoretically when compared to the monolithic wall. Experimentally, the slitted wall showed a 40% and 35 % reduction in the lateral strength in the push and pull direction, respectively, when compared to that of the monolithic wall. The difference in reduction theoretically and experimentally can be explained by the fact

that the theoretical strength was based on flexural failures when in fact the monolithic wall failed in shear at a lower strength then it would have attained had it failed in flexure. Table 4.1 compares the strengths of each wall theoretically and experimentally.

4.7 Conclusions

The intent of this study was to illustrate by experimentation that a slitted wall is more ductile than a normally constructed masonry wall. Part of the goal was to create a wall with more ductility, and this goal appears from the results to have been achieved. The theoretical ductility of the slitted wall increased 17% and the experimental ductility increased 81% when compared to that of the monolithic wall. In addition to more ductility it has also been shown that one can alter the stiffness of a given shear wall by altering its construction. This is as one would expect and the results of the slitted wall were fairly predictable by theory. The slitted wall experimental lateral stiffness was reduced by 25% compared to the stiffness of the monolithic wall. The slitted wall showed a 40% and 35% reduction in the lateral strength in the push and pull direction, respectively, when compared to that of the monolithic wall. The ultimate drift capacity for the slitted wall was 27% larger than that of the monolithic wall; however, the increase in ultimate drift capacity of the slitted masonry wall was less than that of the reinforced concrete infill panels tested in Japan [5]. Although this study was limited, the increased ductility of the slitted wall would allow the design of such a wall to be based on a larger displacement ductility factor than and ordinarily constructed monolithic wall. However, further testing is warranted to ensure that the results are repeatable and that a larger displacement ductility factor can indeed be used.

References

[1] Brandow, Gregg E., Hart, Gary C., Virdee, Ajit, *Design of Masonry Structures.* Concrete Masonry Association of California and Nevada, 1995.

[2] Chen, Shy-Wen J. et al, Cyclic Loading Tests of Masonry Single Piers (Volume 2 - Height to Width Ratio of 1), *Report No. UCB/EERC - 78/28*, Earthquake Engineering Research Center, Berkeley, 1978.

[3] Hart, Gary, "Seismic Design of Ductile Masonry Walls", *The Masonry Society Journal*, Vol. 9, No. 2, February 1991, pp 24-35.

[4] Hidalgo, Pedro A., et al, Cyclic Loading Tests of Masonry Single Piers (Volume1 - Height to Width Ratio of 2), *Report No. UCB/EERC - 78/27*, Earthquake Engineering Research Center, Berkeley, 1978.

[5] Muto, Kiyoshi, "Earthquake-Resistant Design of High-Rise Buildings in Japan", *Japan Society of Civil Engineers*, Vol. 12, 1973, pp 13-25.

[6] Okada, Tsuneo, *Earthquake Resistance of Reinforced Concrete Structures.* University of Tokyo Press, Tokyo, 1993.

[7] Paulay, T. and Priestley, M.J.N., *Seismic Design of Reinforced Concrete and Masonry Buildings.* John Wiley and Sons, New York, 1992.

[8] Priestley, M.J.N., "Cyclic Loading Tests of Slender Concrete Masonry Shear Walls", *Bulletin of the New Zealand National Society for Earthquake Engineering*, Vol. 15, No. 1, March 1982, pp 3-21.

[9] Priestley, M.J.N., "Ductility of Confined Concrete Masonry Shear Walls", *Bulletin of the New Zealand National Society for Earthquake Engineering*, Vol. 15, No. 1, March 1982, pp 22-26.

[10] Shing, P.B., Noland, J.L., Klamerus, E., and Spaeh, H., "Inelastic Behavior of Concrete Masonry Shear Walls", *Journal of the Structural Division, ASCE*, Vol. 15, No. 9, September 1989, pp 2204-2225.

[11] Shing, P.B., Schuller, M., Hoskere, V.S., and Carter, E., "Flexural and Shear Response of Reinforced Masonry Walls", *ACI Structural Journal*, Vol. 87, No. 6, November-December 1990, pp 646-656.

[12] *Uniform Building Code*, International Conference of Building Officials, 1991.

Appendix A

Material Properties

A.1 General

Tests were performed upon the materials used for the construction of the shear walls of this research. The materials tested were as follows:

1. Reinforcing Steel
2. Grout Strength
3. Masonry Block Strength (Ungrouted Masonry Block)
4. Masonry Prism Strength

A.2 Reinforcing Steel

Two lengths of reinforcing steel were tested to establish the yield strength for the bars used in the construction of the test walls. One #3 bar and one #4 bar was used. Both bars were placed under axial tension until failure. Figures A.1 and A.2 show the stress strain curves for the #3 and #4 bar respectively. Table A.1 summarizes the yield and ultimate strengths established by testing the #3 and #4 bars.

Bar Size	Yield Stress	Ultimate Stress
#3 Bar	Fy = 414 MPa (60 ksi)	Fu = 699 MPa (101 ksi)
#4 Bar	Fy = 514 MPa (74.5 ksi)	Fu = 741 MPa (108 ksi)

Table A.1 Steel Strength

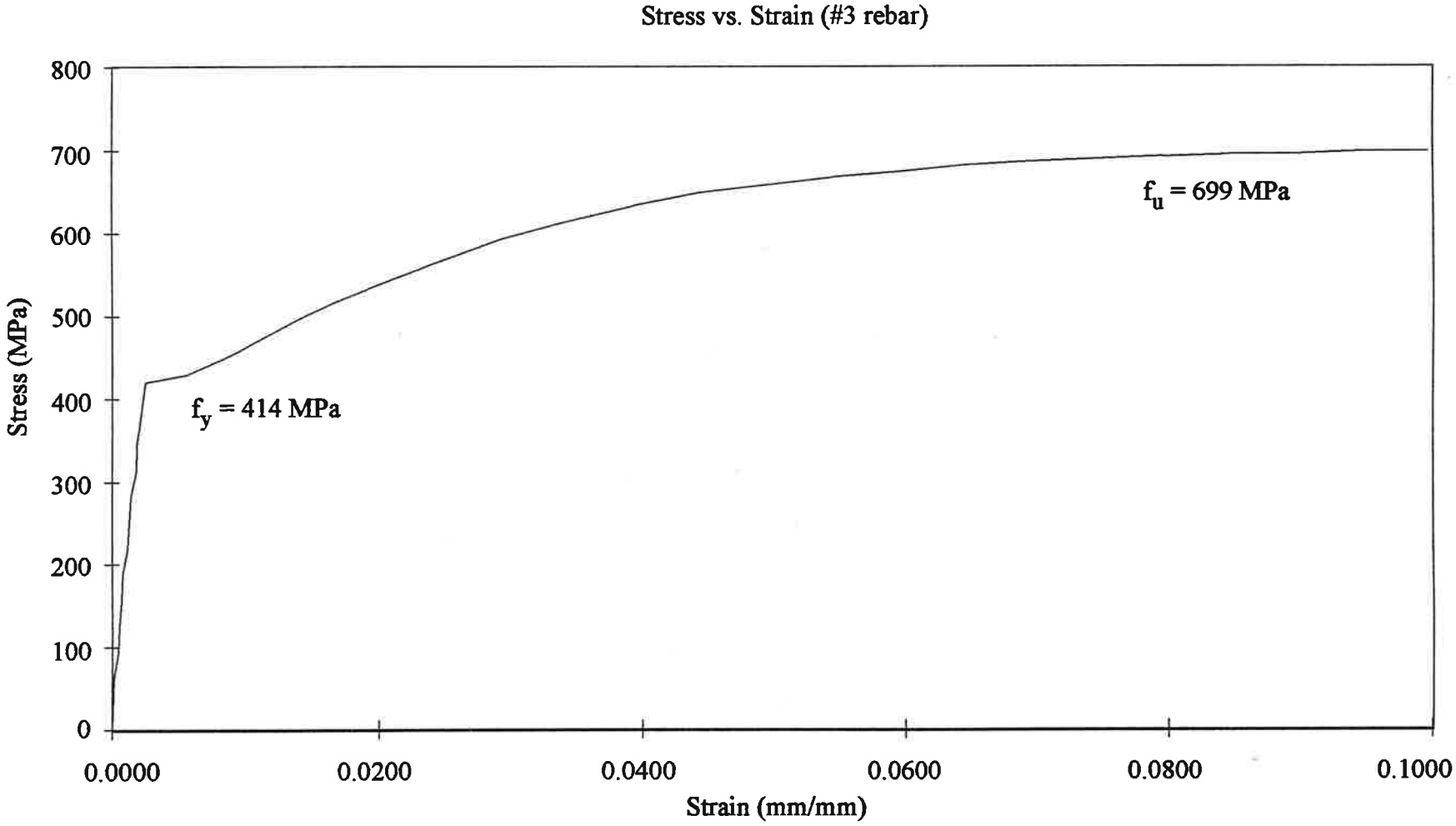

Figure A.1 Stress Strain Curve For #3 Rebar

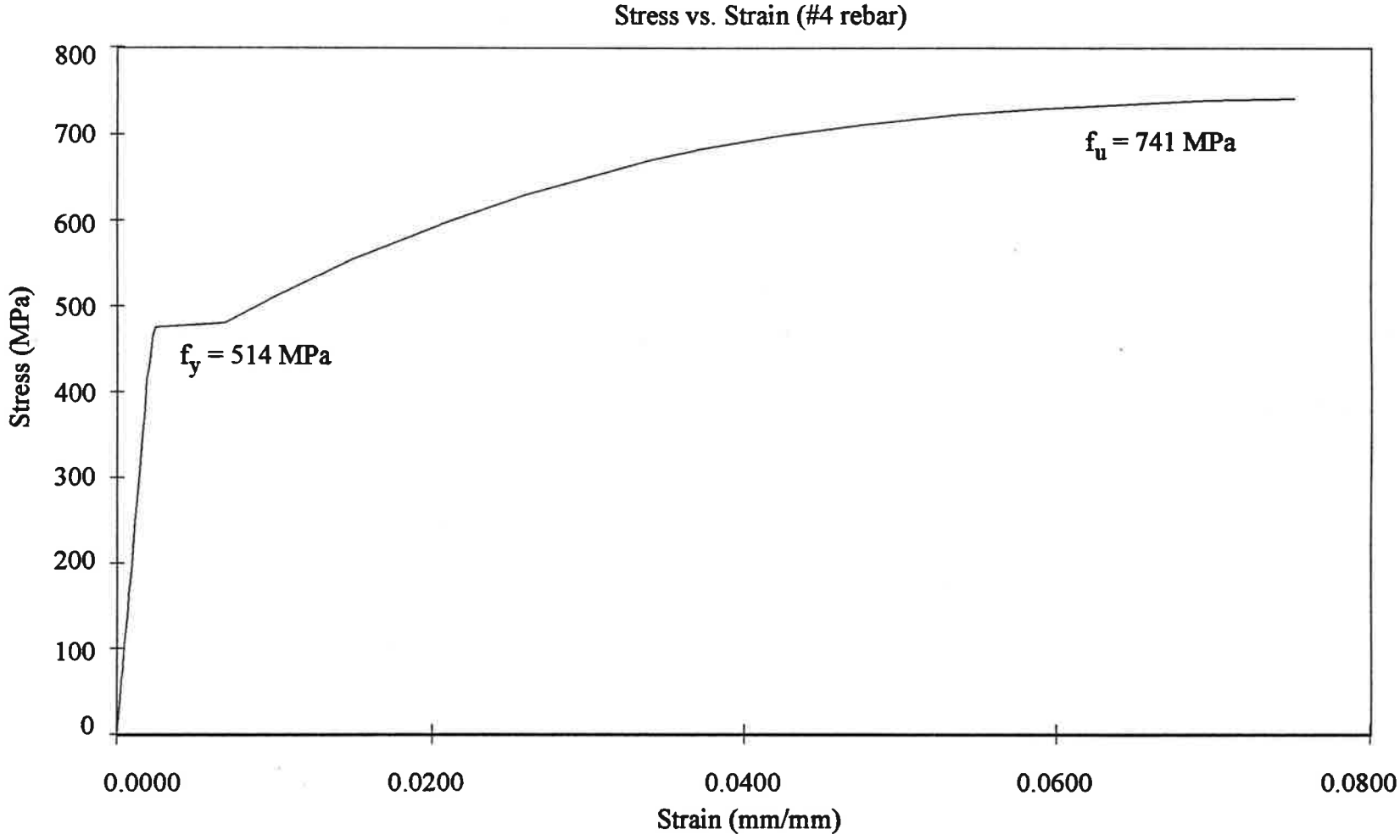

Figure A.2 Stress Strain Curve For #4 Rebar

A.3 Grout

The grout used for construction of the two masonry test walls was delivered by Dixon Redi-Mix, Inc. of Dixon, California. The aggregate for the mix was provided by 3/8 inch pea gravel and river sand. The cement was specified as ASTM C150 Portland Cement Type II. The water cement ratio was 0.70 and slump before placing was 8 inches. The unit weight of the concrete was 137 pcf. Design strength for the grout was 2000 psi.

Table A.2 lists the actual grout cylinder strengths of the monolithic and slitted walls.

Wall	Cylinder Size	Ultimate Compression Stress
Monolithic	8" X 4" Diam.	29707 kPa (4309 psi)
Slitted	6" X 12" Diam.	17649 kPa (2560 psi)

Table A.2 Grout Strength

A.4 Masonry Block Strength (Ungrouted)

Masonry blocks for the walls were tested to determine their ultimate compressive strength. Open end bond beam blocks and half blocks were tested in an orientation which was the same as they were positioned in the as built walls. A typical compression test for an open end bond beam unit can be seen in Photo A.1. The results of these tests based on net areas are tabulated in Table A.3 below.

Block	Ultimate Compression Load	Ultimate Compression Stress
6"x8"x16"	818 kN (184 kips)	25087 kPa (3639 psi)
6"x8"x8"	330 kN (74 kips)	19262 kPa (2794 psi)

Table A.3 Block Strengths

A.5 Masonry Prism Strength

Two masonry prisms were made for each wall. Each prism consisted of four open end bond beam units stack bonded with type S mortar. The bond beam open ends were closed with plywood and the prisms were filled with grout. These four prisms were tested to determine the average ultimate compressive strength of the two masonry walls. Photos A.2 to A.4 show several of the prisms after failure from compression testing. Table A.4 lists the results for the masonry prism strengths.

Wall Prism	Ultimate Compression Load	Ultimate Compression Stress
Monolithic Wall	681 kN (153 kips)	12002 kPa (1741 psi)
Slitted Wall	692 kN (155 kips)	12195 kPa (1769 psi)

Table A.4 Prism Strength

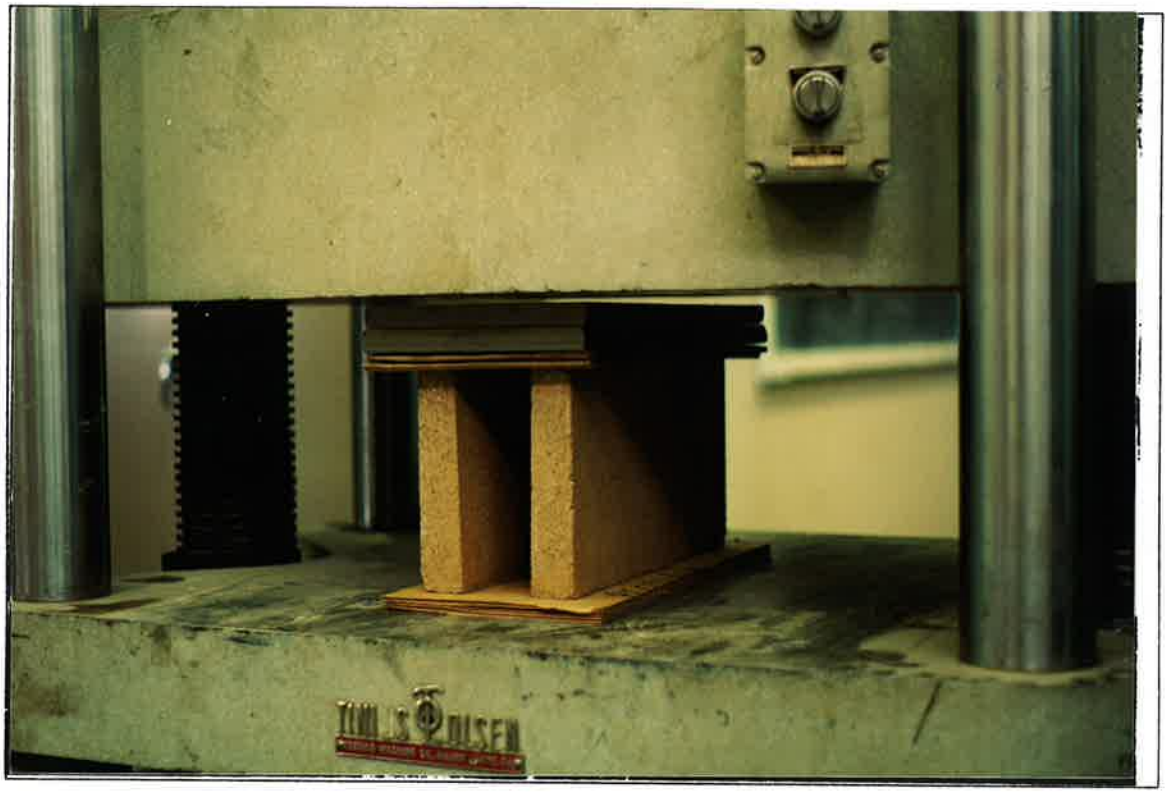

Photo A.1 Compression Test of Typical Open End Bond Beam Unit

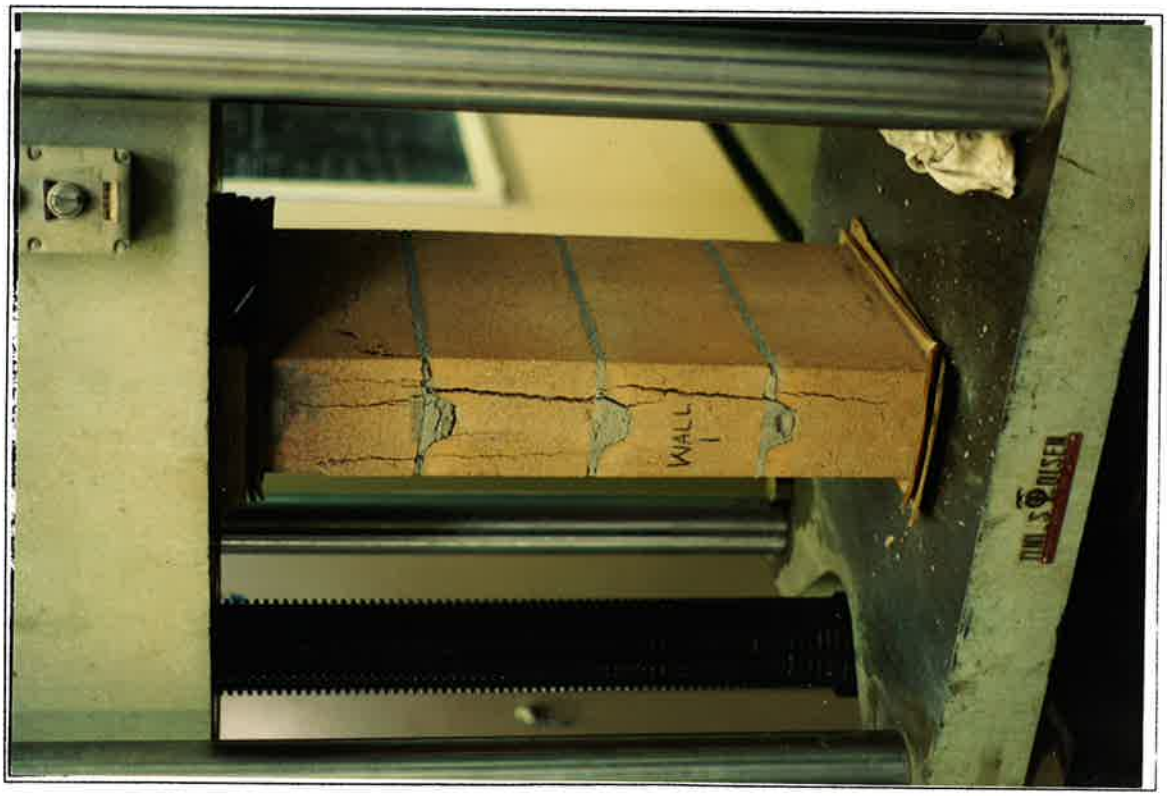

Photo A.2 Masonry Prism Test For Monlithic Wall

Photo A.3 Masonry Prism Test For Slitted Wall

Photo A.4 Masonry Prism At Completion of Compression Test

Appendix B

Chronological Photos of Walls During Testing

B.1 General

In this Appendix, Photos B.1 to B.8 are presented for the monolithic wall and Photos B.9 to B.16 illustrate the slitted wall. These photos are shown in chronological order and show the monolithic wall and slitted wall at different stages of testing. These photos document the difference in the development of cracks for both walls. Typical diagonal cracking is seen for the monolithic wall, while the slitted wall cracking is profoundly altered due to the included slits. Blue lines have been used to trace cracks caused during load cycles which push on the wall. Red lines trace cracks which form during pull cycles. The loads at which the cracks occur are also written next to the crack lines.

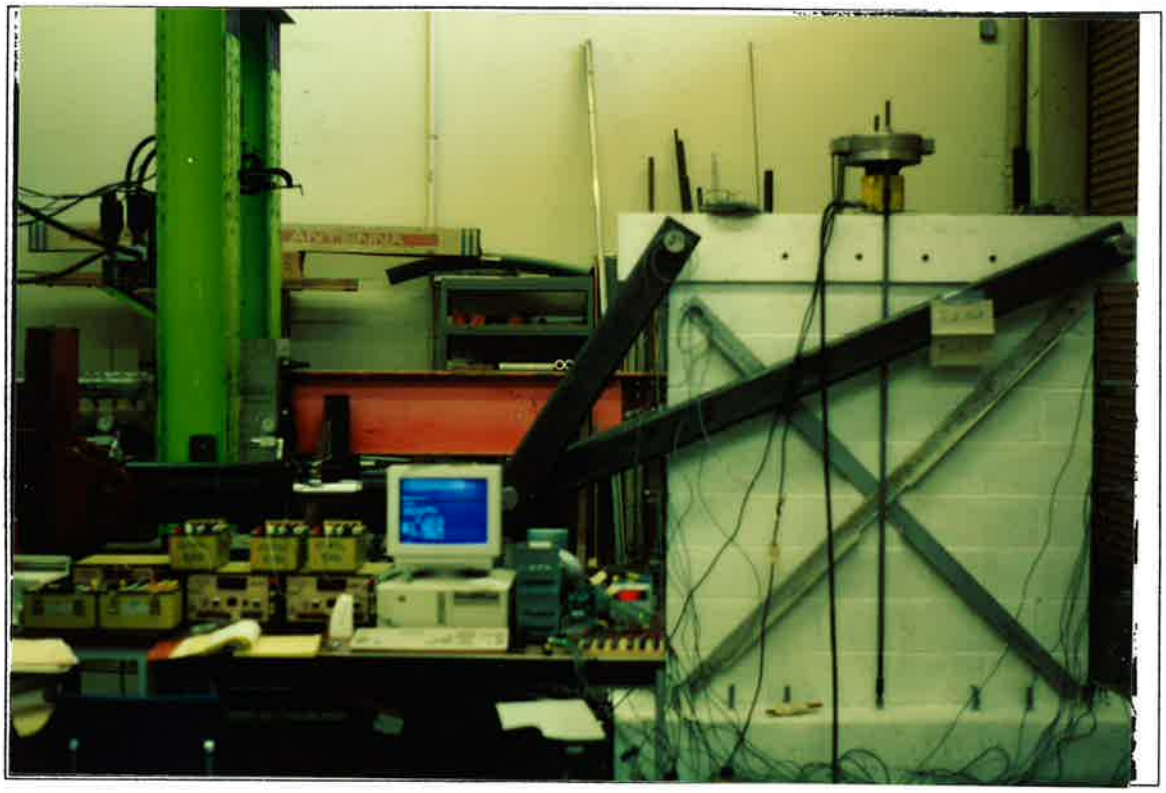

Photo B.1 Monolithic Wall At Start of Testing

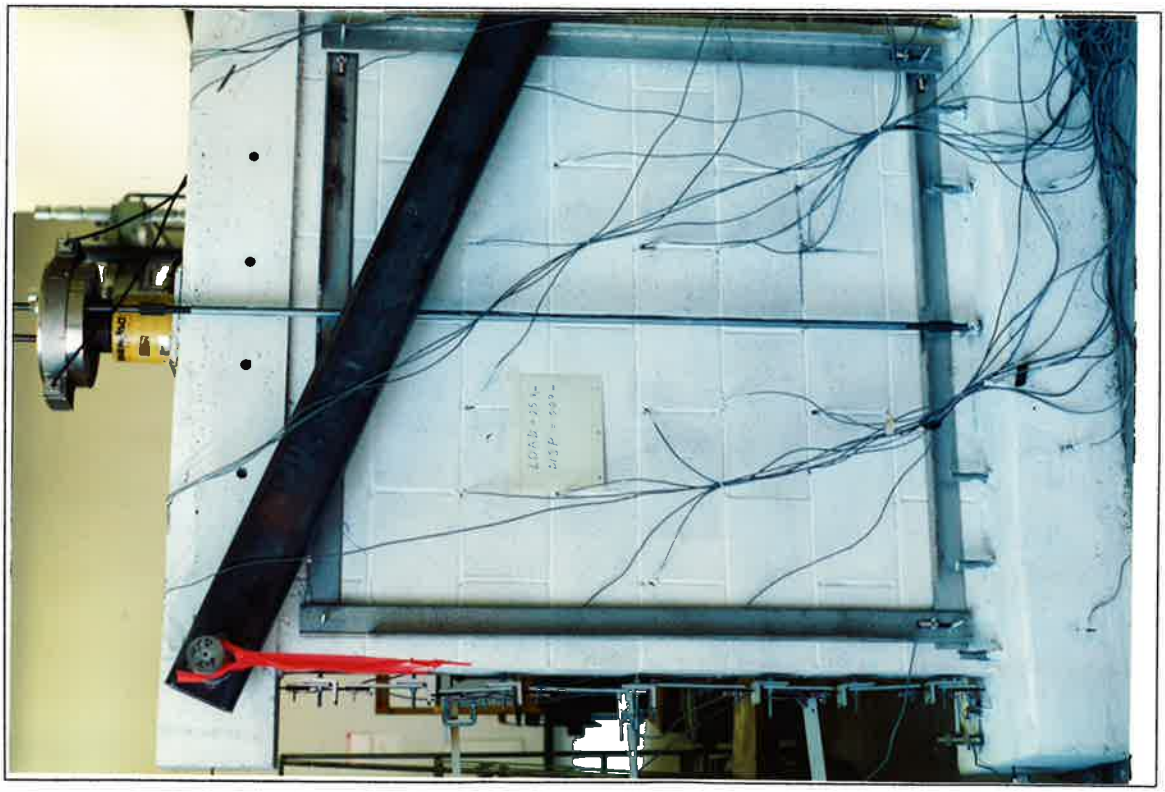

Photo B.2 Monolithic Wall At 111 kN (25 Kips) Lateral Load

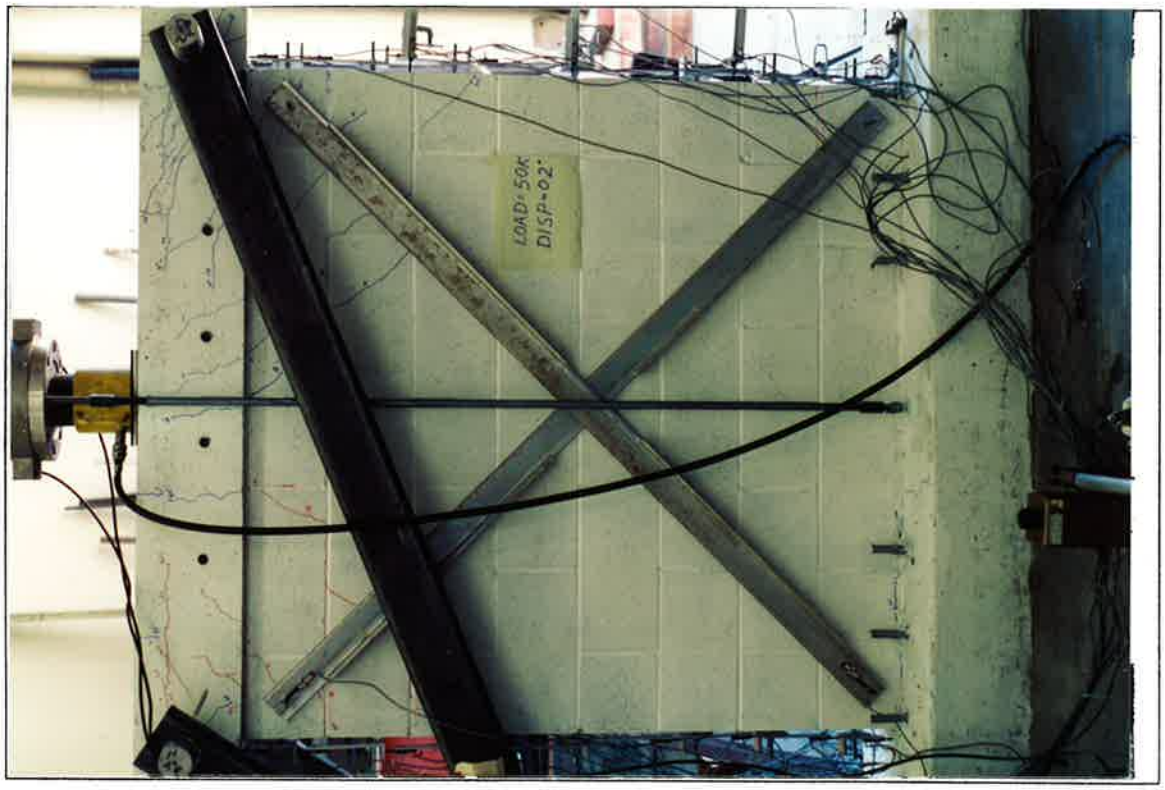

Photo B.3 Monolithic Wall At 222 kN (50 Kips) Lateral Load

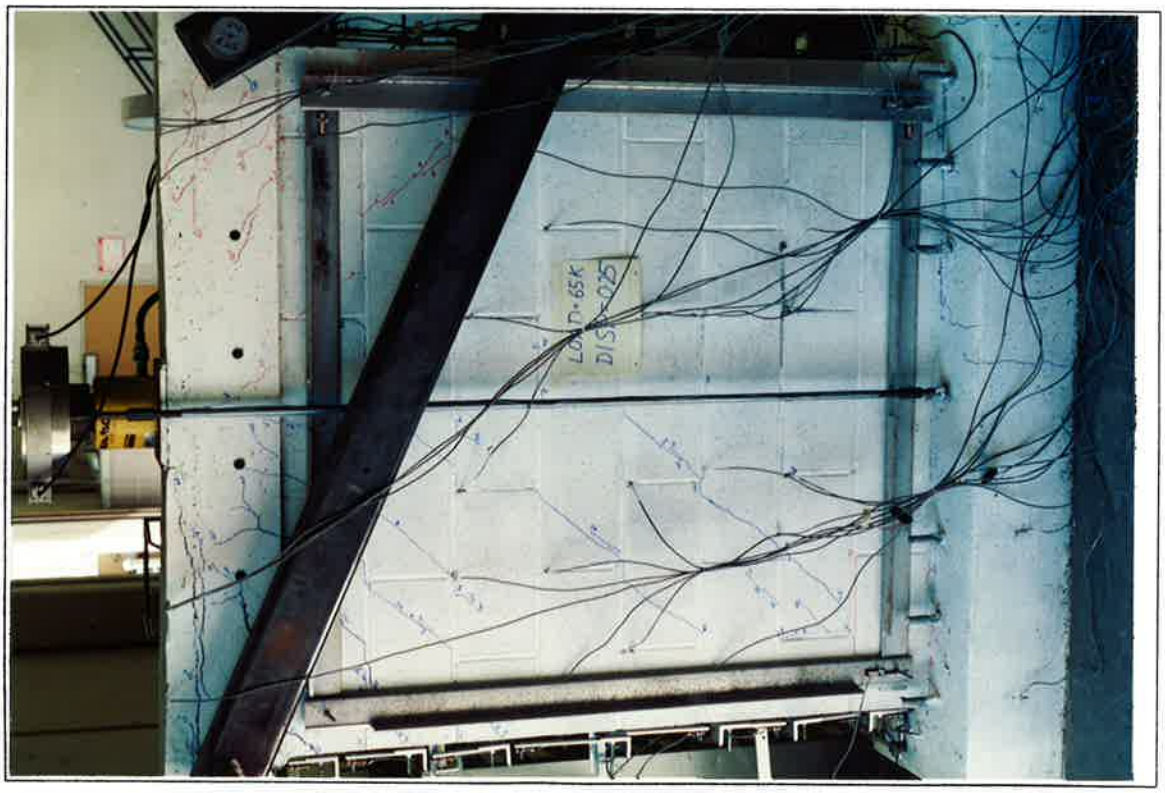

Photo B.4 Monolithic Wall At 289 kN (65 Kips) Lateral Load (South Face)

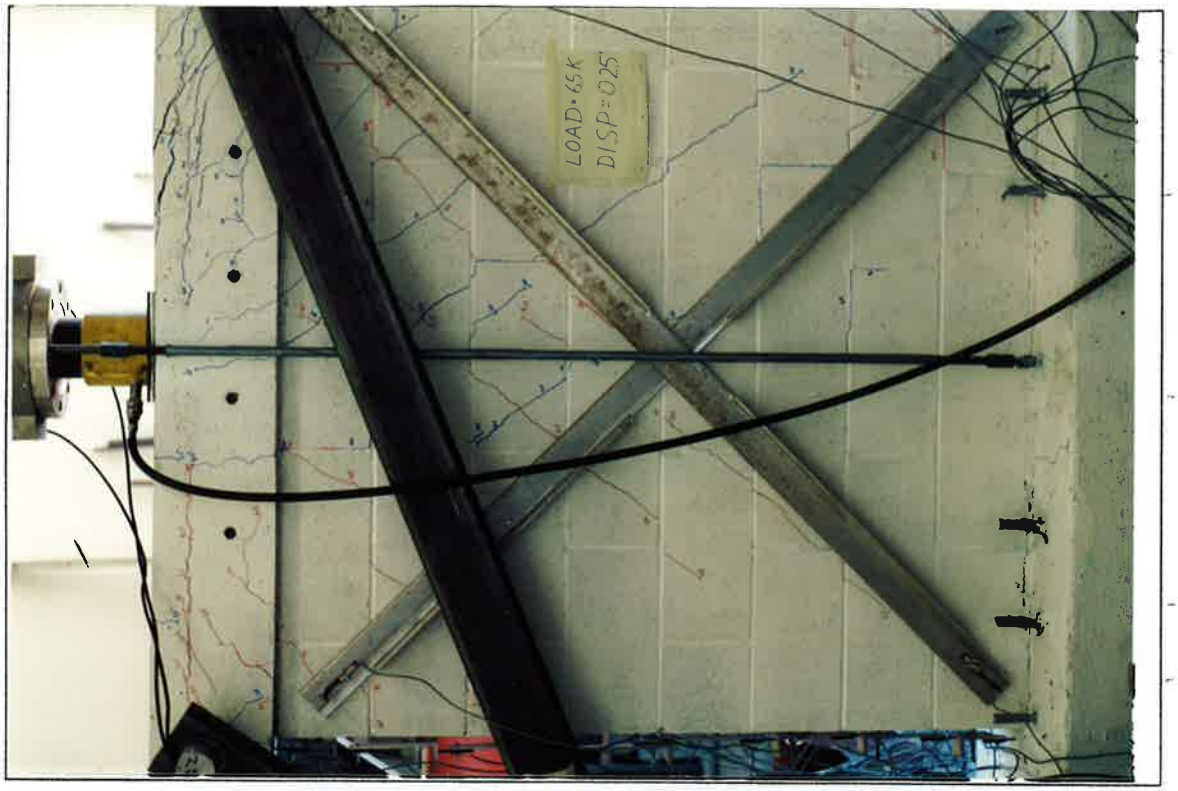

Photo B.5 Monolithic Wall At 289 kN (65 Kips) Lateral Load (North Face)

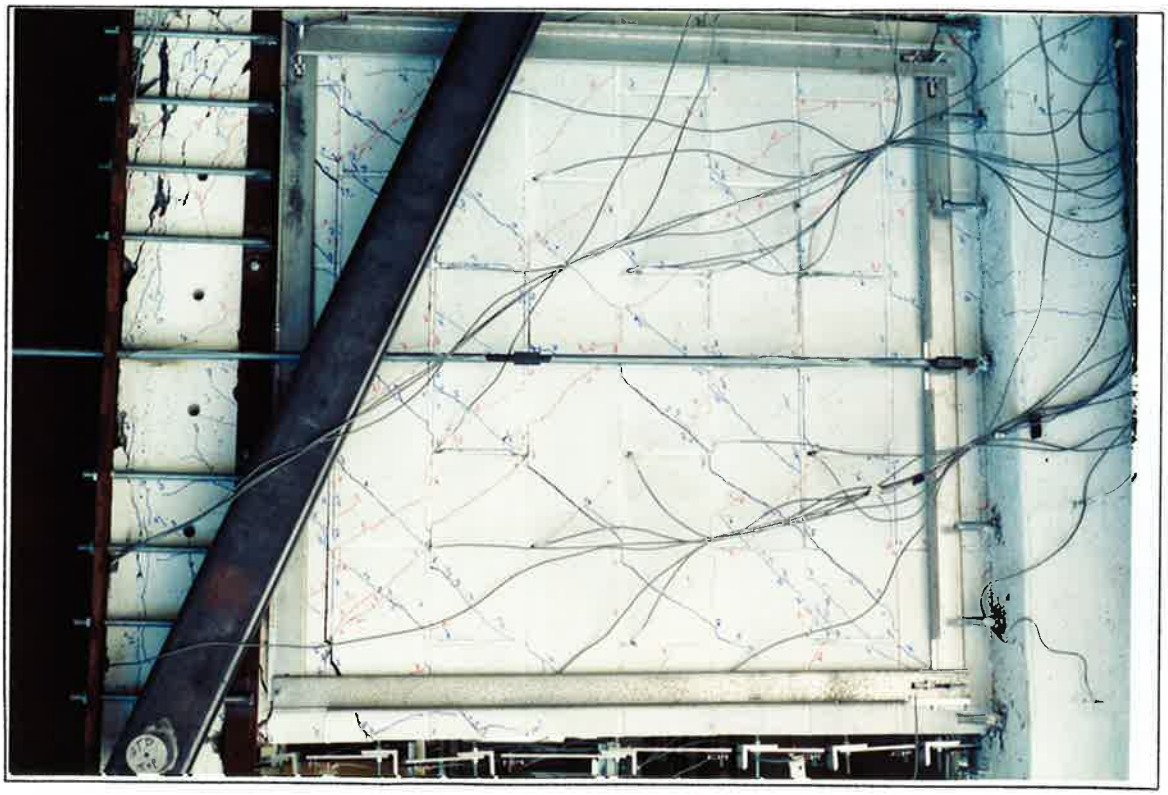

Photo B.6 Monolithic Wall South Face With Retrofitted Cap Beam

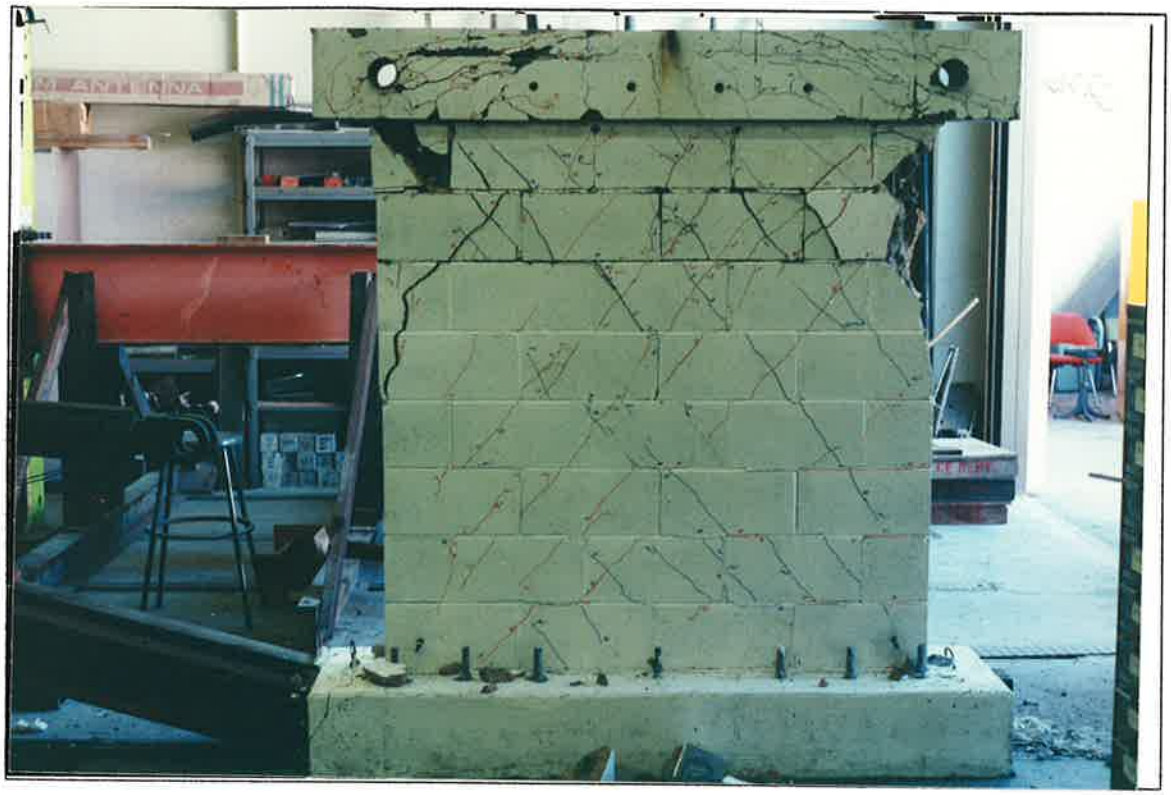

Photo B.7 Monolithic Wall North Face At Completion of Testing

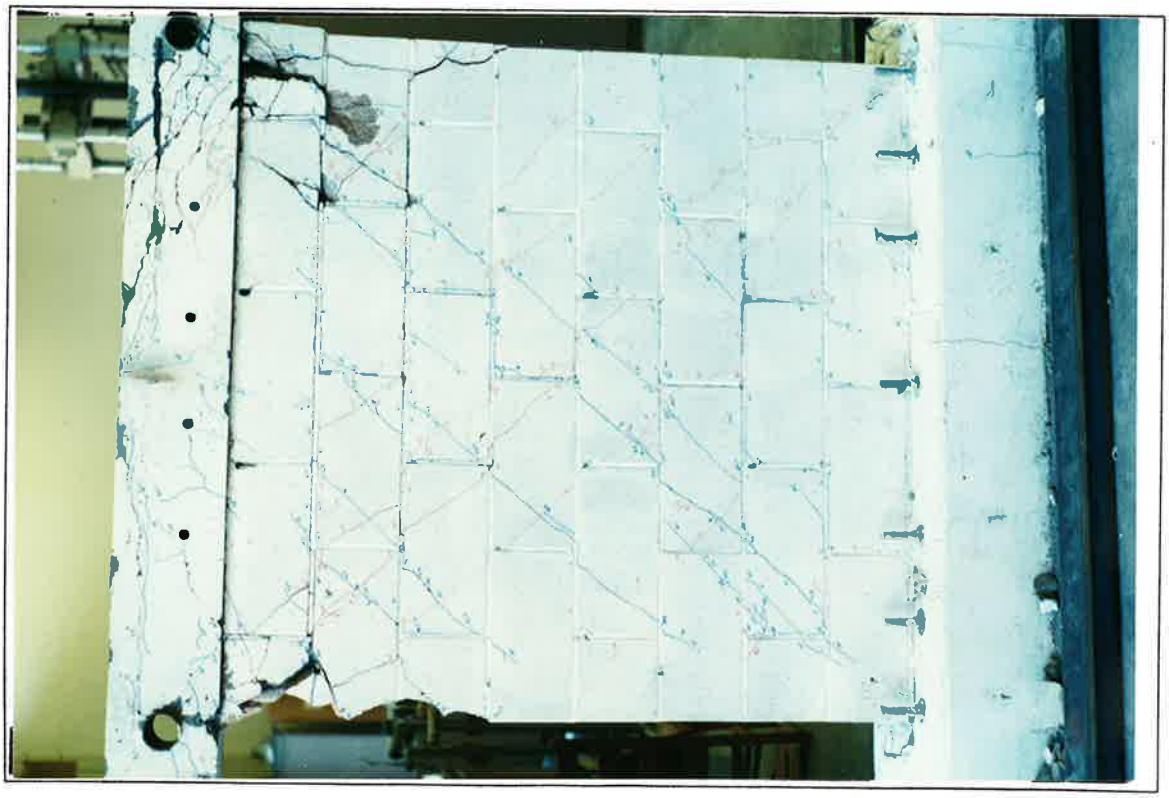

Photo B.8 Monolithic Wall South Face At Completion of Testing

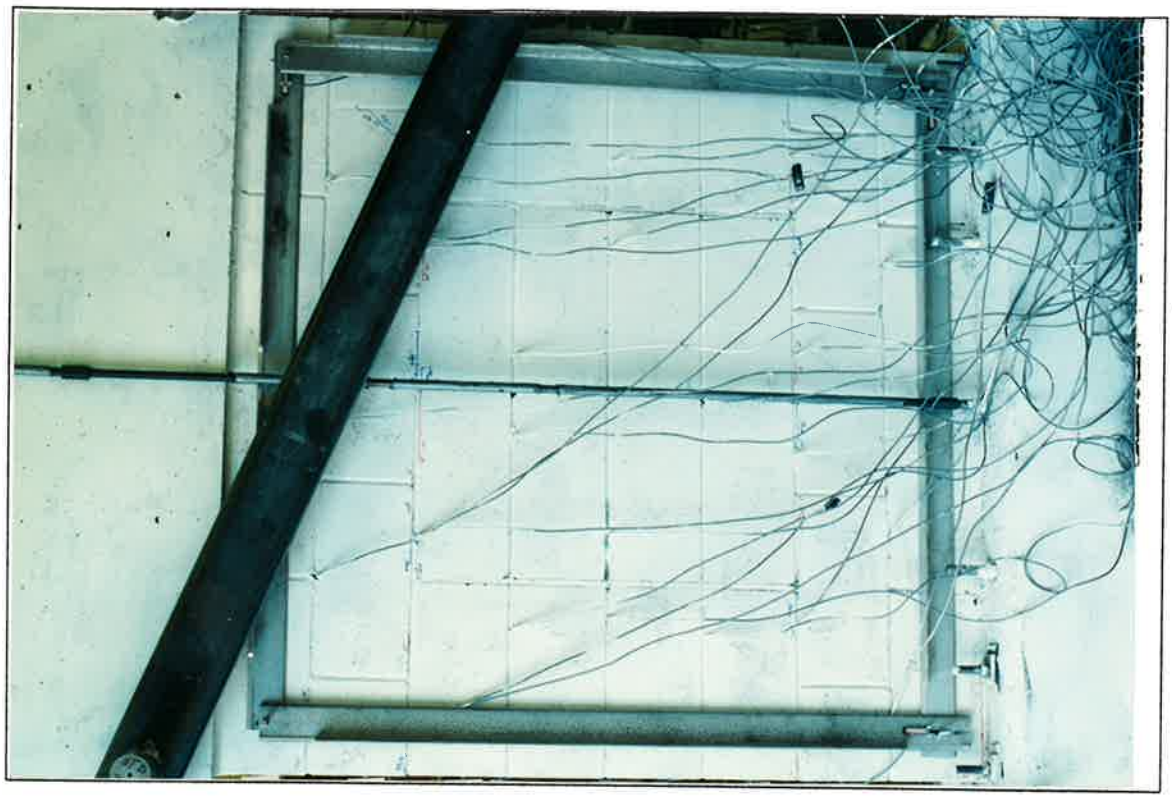

Photo B.9 Slitted Wall South Face At 133 kN (30 Kips) Lateral Load

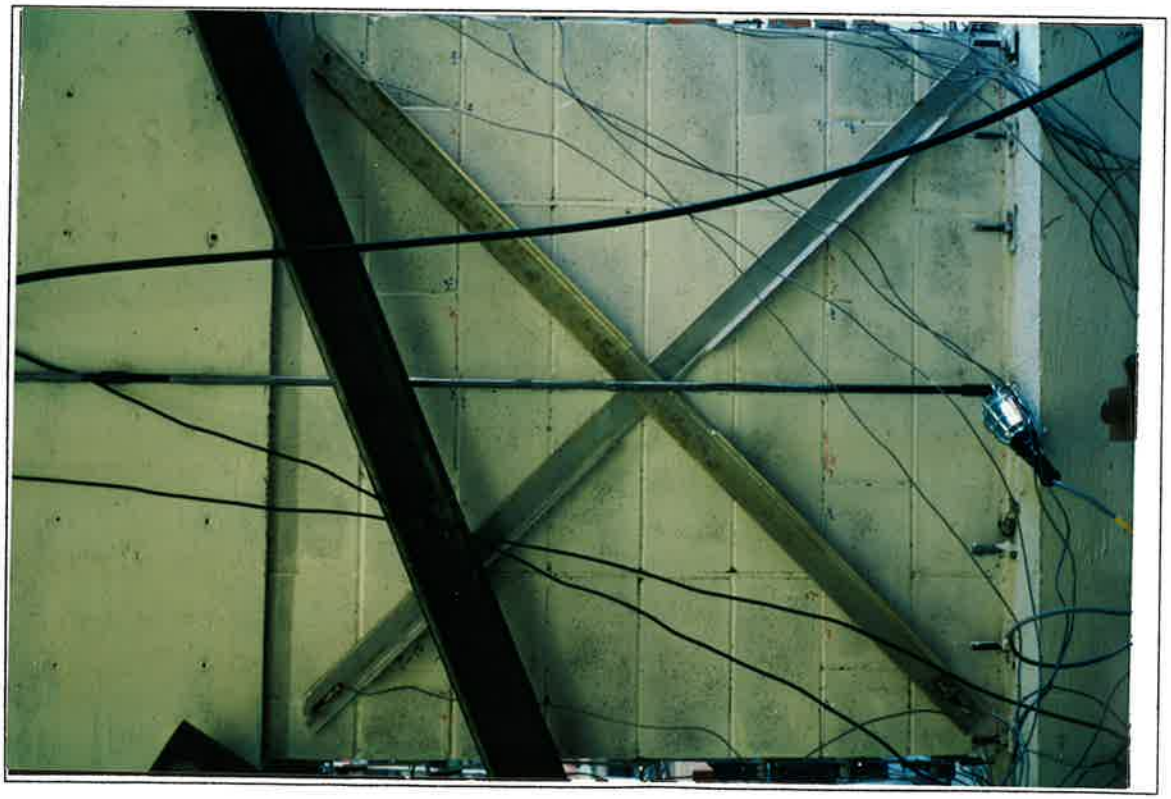

Photo B.10 Slitted Wall North Face At 133 kN (30 Kips) Lateral Load

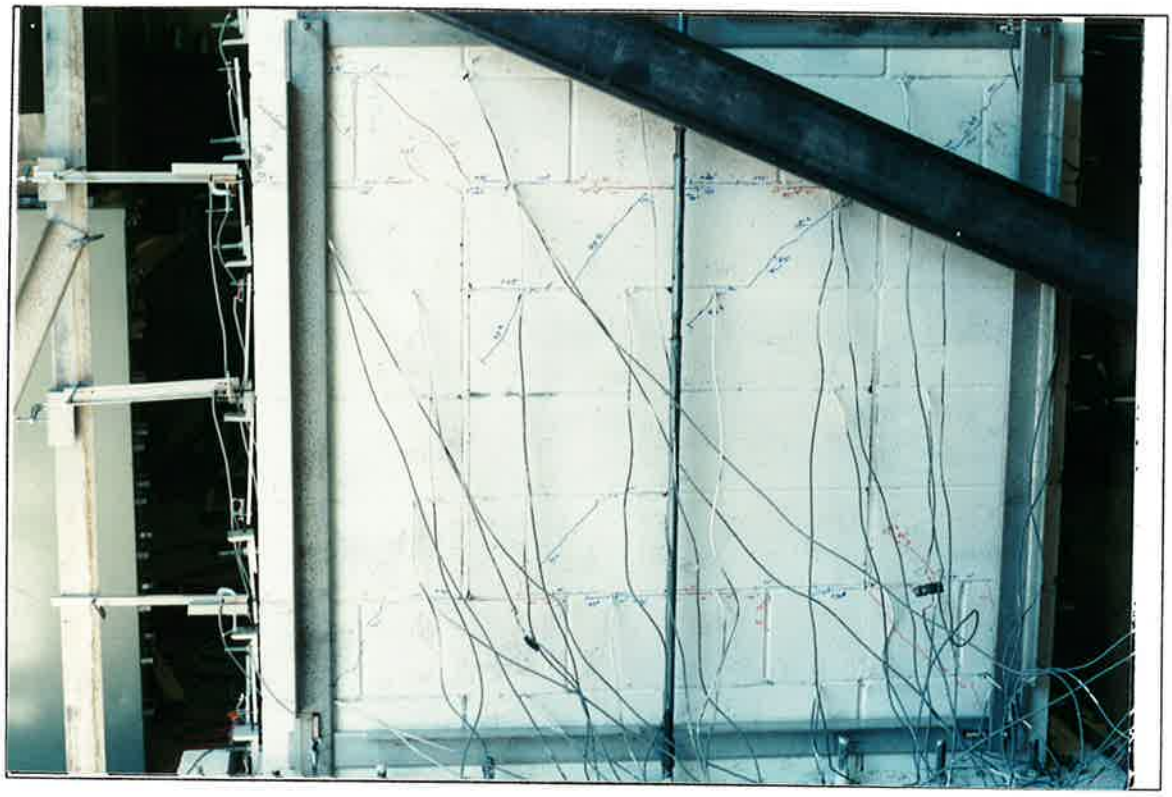

Photo B.11 Slitted Wall South Face At 200 kN (45 Kips) Lateral Load

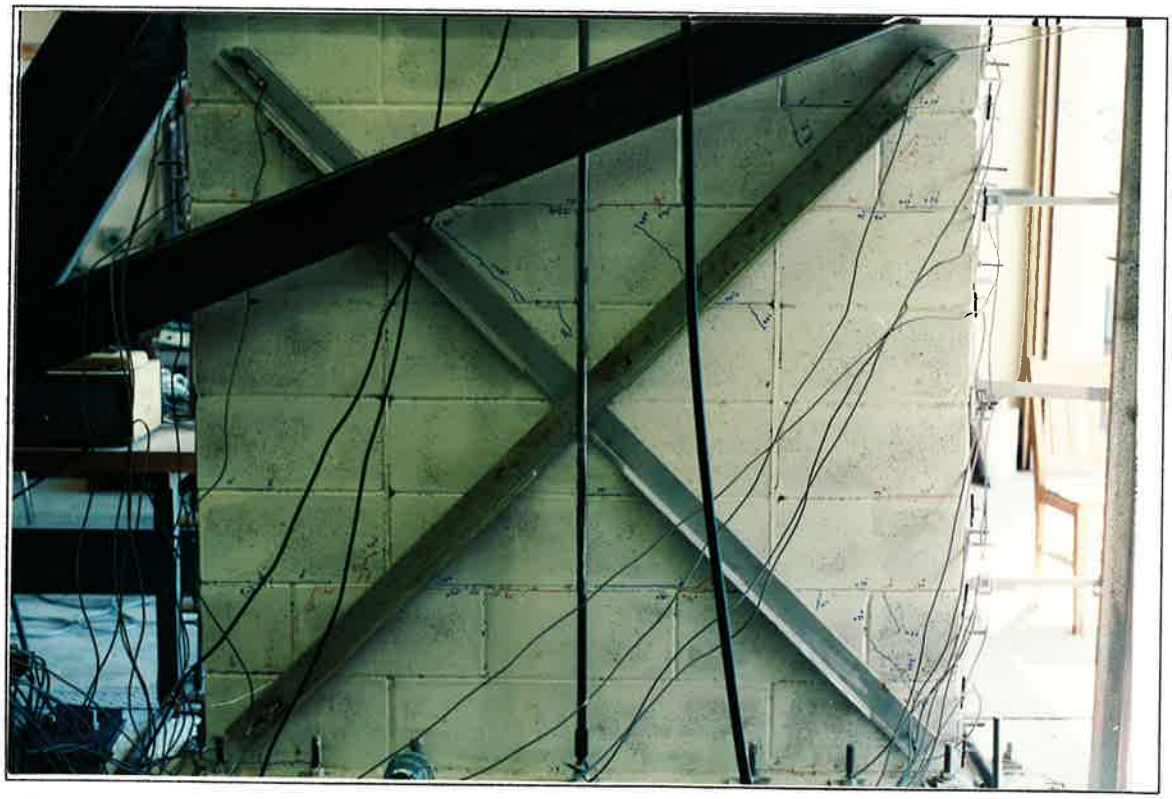

Photo B.12 Slitted Wall North Face At 200 kN (45 Kips) Lateral Load

Photo B.13 Slitted Wall South Face At 245 kN (55 Kips) Lateral Load

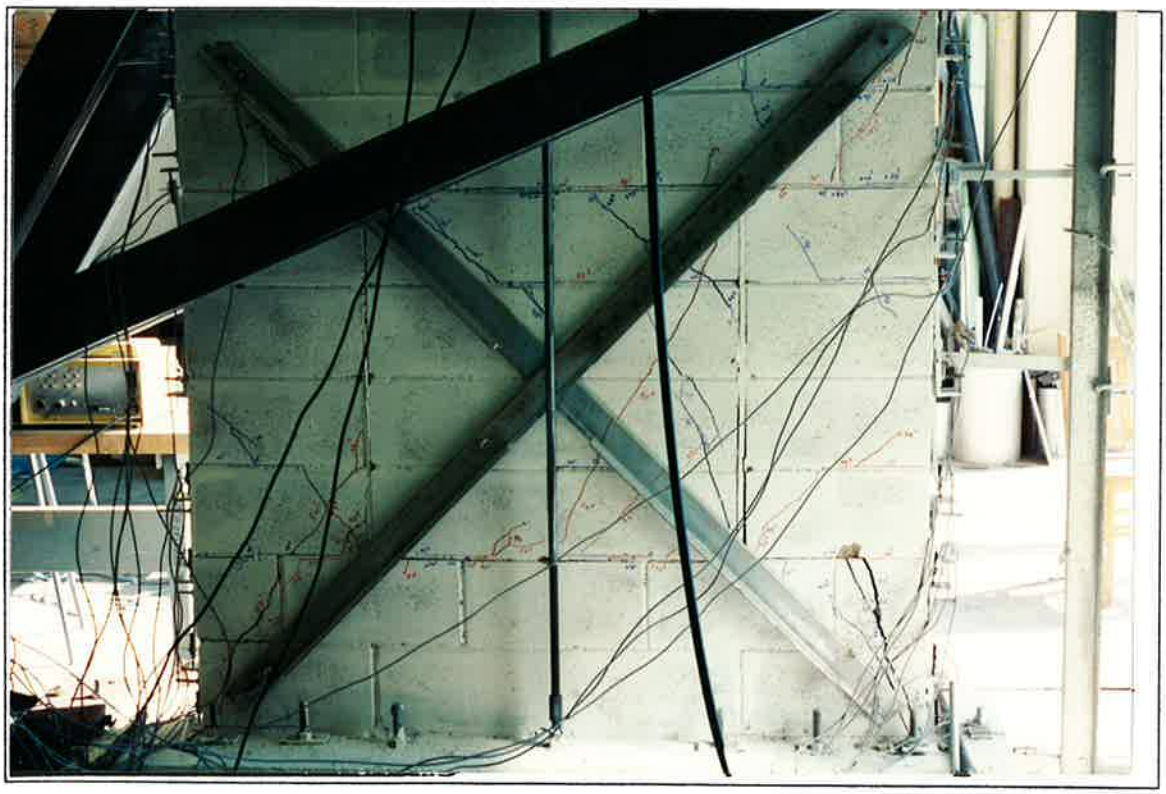

Photo B.14 Slitted Wall North Face At 245 kN (55 Kips) Lateral Load

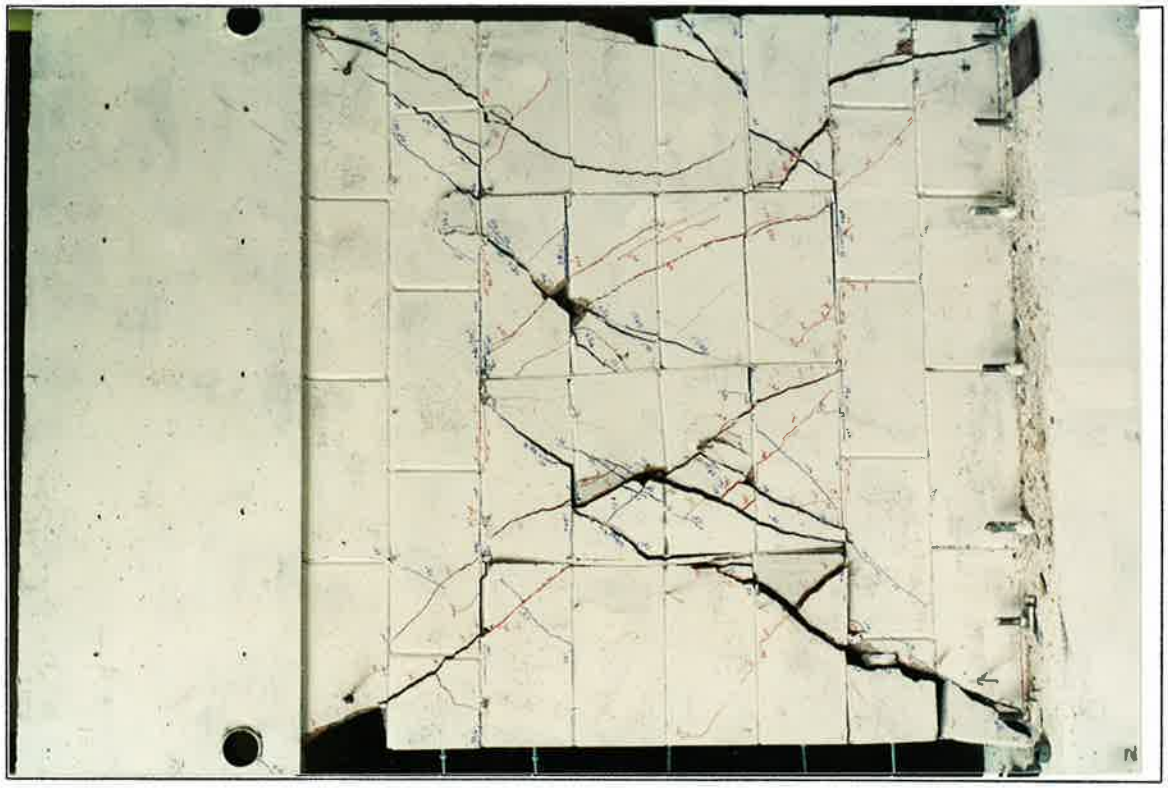

Photo B.15 Slitted Wall South Face At Completion of Testing

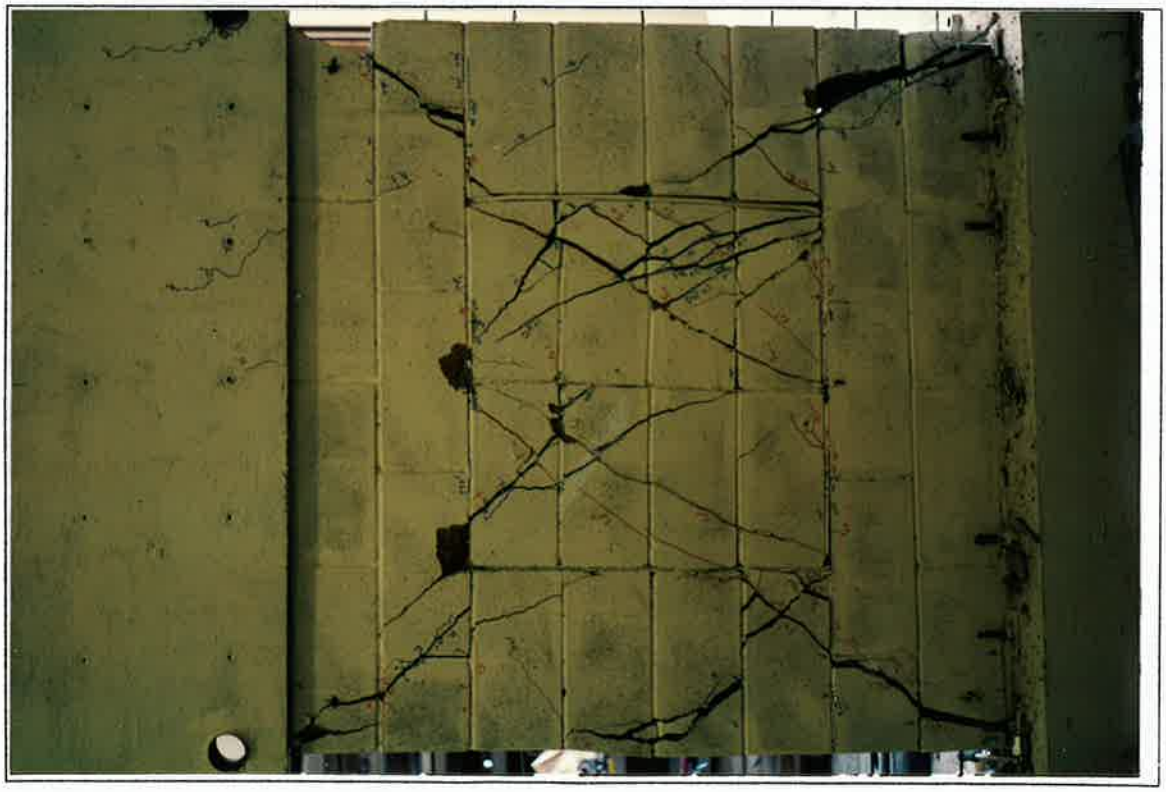

Photo B.16 Slitted Wall North Face At Completion of Testing